Calculation of V_{us} from lattice QCD

Junpei Kakazu

February 2019

Calculation of V_{us} from lattice QCD

Junpei Kakazu
Doctoral Program in Phyics

Submitted to the Graduate School of
Pure and Applied sciences
in Partial Fulfillment of Requirements
for the Degree of Doctor of Philosophy in
Science

at the
University of Tsukuba

Contents

Chapter 1

Introduction

A quark is fundamental constituent of matter, and a gluon carries strong force which is one of the four known forces. A Hadron is the composite particle which is made from two or more quarks stuck together by the gluon. There are two kind of hadron. The first is baryon, which is consist of odd numbers of quarks. The most known baryons are proton and neutron. The two baryons and are consist of up quark and down quark stuck together by strong force. The second is meson, which is consist of even numbers of quarks. The most known meson are pion, and the existence of the particle and its mass are predicted by H. Yukawa.

The physics of strong interaction is described by Quantum chromodynamics (QCD) since the hadron is consist of quark and gluon. In the small energy level, the strong decay constant becomes large, this is one of the property of QCD. Thus the analysis in this region with perturbative calculation fails. In order to solve the QCD in small energy scale with some mathematically well-defined way, lattice QCD is formulated as its regularized non-perturbative approach. Lattice QCD is the formulated QCD in a discretized Euclidian space-time by lattice spacing a corresponding to ultraviolet cut-off. Thus the theory is defined in a precise mathematical sense, and in finite space-time volume, the QCD could be considered as the field theory which is regularized by lattice spacing and finite volume. Lattice QCD could revert QCD in continuum space-time by the continuum limit of lattice spacing and the infinite space-time volume. Study of physical quantity with lattice QCD approach have a lots of success in hadronic measurements in small energy level. As one of the example of the physical quantity by Lattice QCD calculation, there is the study of mass spectra of hadrons [1]. Not just the success of the static quantity, Lattice QCD method is one of the most useful tool of the analyses of dynamical quark's physics. Form factor is the one of these quantities, which represents the correction derived from hadronic structure.

In the Standard Model of particle physics, quark is considered as a particle which has no spatial distribution, although hadron has some spatial distribution including quarks and gluon. The form factor of hadron is the dynamical quantity of deviation from point particle, and we could check the information of hadron's spatial distribution through the quantity. For example, the electromagnetic form factor of hadron is the quantity of deviation from charged point particle. We could check the quantity and obtain the information of the electromagnetic distribution of hadron and the regarding physical quantity, the mean square charge radius of hadron and the curvature. Form factor calculations with lattice QCD is the most precise theoretical approach in present [2]. Although the charge radius of pion is measured by 1% error in $\pi - e$ scattering experiment, present lattice QCD analyses determine the radius of pion from pion vector form factor by more than 4% error [2].

The uncertainties of the form factor in lattice QCD calculations come from the difference between the simulation and the reality. There are some origins of the uncertainties when lattice QCD result is reconciled with the reality. The first is the chiral extrapolation to the physical quark mass. Most of lattice QCD calculations are performed at heavier point than physical light quark masses and the result should be taken the physical limit. The second is the finite volume of the system. We could take into account the two kind of the origin of uncertainty from the finite volume. One is infinite volume. The actual calculations is finite, hence the result should be taken the limit. The other is the momentum interpolation (or extrapolation) to the target momentum transfer, usually zero momentum transfer. The accessible momentum in lattice calculation is the proportional to inverse the spatial extent of the system. The third is the the continuum extrapolation $a \to 0$. The system is discretized by a thus as we decrease a we have to increase the number of lattice point. Due to the two later reasons, the degree of propagators' matrix increases in proportional to the number of lattice point of the system in lattice QCD calculation. In other words, the calculation cost is the proportional to the system size, negative power of the masses, and therefore we need to compare and to contrast computational resource or suitable numerical result, in lattice QCD calculation. It is not readily to consider that the numerical result is reasonable, if the systematical uncertainties of lattice QCD calculations could not be suppressed substantially.

The Standard Model has some defectivenesses. One is that the Standard Model could not explain some phenomena, such as the oscillations of neutrino, the origin of masses, the imbalance of matter-antimatter, the strong CP problem, and the dark matter and dark energy. Other is that the Standard Model is inconsistent with general relativity in the condition like the space-time singularity such as the Big Bang and black hole event horizons. Theories of beyond the Standard Model include the extension of the Standard Model within supersymmetry or the explanations which are completely different from the Standard Model such as string theory and M theory. There are some probes for the detection of the signature of beyond the Standard Model, such as proton radius measurements and anomalous magnetic dipole moment of muon. The measurements of beyond the Standard Model need high precision , which provide stringent constraints of scenarios beyond the Standard Model.

The studies of weak semileptonic and leptonic decays of kaon have a long time and the measurements have provided. The "leptonic decay" means a decay caused by the weak interaction in which some pure pairs of lepton-neutrino are produced. The "semileptonic decay" means a decay in which some pairs of lepton-neutrino are produced in addition to some hadrons.

The semileptonic decay is related to that down-type quarks, down and strange quarks, decay into up quarks via charge current of weak interaction. The decay could be described by a superposition of down-type quarks' mass eigenstates. The Cabbibo-Kobayashi-Maskawa (CKM) matrix elements [4] is the unitary matrix which describes the coefficients of mixture of the mass eigenstates between up-type and down-type quarks.

Semileptonic decays of kaon decay into some pion(s) play an important role to determine V_{us}, which is one of the Cabbibo-Kobayashi-Maskawa (CKM) matrix elements to describe the mixing of the mass eigenstates between up and strange quarks. From the unitary condition of the up quark part in the CKM matrix, $\Delta_u \equiv |V_{ub}|^2 + |V_{us}|^2 + |V_{ub}|^2 - 1$ must be vanished in the standard model. Thus we could examine the existence of physics beyond the standard model by checking whether the Δ_u is vanished or remains.

We could determine the value of $|V_{us}|$ in the two different ways. One uses the form factor of the kaon semileptonic (K_{l3}) decay at zero momentum transfer. The other is the ratio of the meson decay

constants, f_K/f_π, which is related to the pure leptonic kaon (K_{l2}) decay It is not possible to determine $|V_{us}|$ only from the experiments, because in experimental results, for instance a branching ratio, $|V_{us}|$ is multiplied to the form factor or the decay constants. Thus some theoretical evaluations for the form factor and decay constants are necessary. The lattice QCD calculation is the most precise way to determine these quantities.

One phenomenological study for determination is the article by H. Leutwyler and M. Roos [5]. This approach is based on chiral perturbation theory (ChPT) [8–10] as an effective theory of strong interaction in low energy region. This effective theory relies on the property that QCD has chiral symmetry $U(N_f)_L \times U(N_f)_R$ in the massless limit of N_f flavor quarks. Spontaneous breaking of the chiral symmetry is bestowed by non-perturbative dynamics of QCD to the vector subgroup $SU(N_f)_V$. In ChPT, the singularity relating to Goldstone bosons' degrees of freedom occurred by spontaneous breaking of the chiral symmetry is considered. The expansion of ChPT is ordered in terms of quark masses or momentum square of Goldstone bosons. Most of previous studies of lattice calculations are performed at heavier than physical light quark masses, ChPT is generally invoked in the check of momentum transfer dependance of form factors and the chiral extrapolation to physical point.

The recent results of $|V_{us}|$ in PDG [3] are given by

$$|V_{us}| \quad = \quad \begin{cases} 0.2231(8) & (\text{form factor}) \\ 0.2253(7) & (\text{decay constant}) \\ 0.2256(8) & (\text{unitarity condition}). \end{cases}$$

The result from the form factor is estimated by combining the experimental value $|V_{us}|f_+(q^2=0) = 0.2165(4)$ in Ref. [28], and $f_+(0)$ in the FLAG's value [2]. The result from the decay constant ratio is estimated by using the experimental value of the K_{l2} decay [29], and f_K/f_π in the FLAG's value [2]. Another one is estimated by the unitarity condition $\Delta_u = 0$ using the most precise result of $|V_{ud}|$ [30] and ignoring $|V_{ub}|$ due to the small effect ($|V_{ub}| \approx O(10^{-3})$) in this estimation. In the $|V_{us}|$ estimations, there is difference between the value from the unitarity condition and that from the form factor by about 2σ.

The explorations of new physics require with highly precision. However, the $|V_{us}|$ values of the above from form factor and decay constant are the result of combinations experimental results and lattice calculations. and there are some uncertainties derived from lattice calculations in these values. It is still premature to conclude, however, that it is significant signal of new physics or not.

The enhances of computational power and improvements of simulation algorithms in recent years make it possible to perform large-scale dynamical simulations at physical masses of pion and kaon. In this work, to recognize the signature beyond the Standard Model we aim to determine of the semileptonic decay form factor by reducing the uncertainties of the chiral extrapolation and finite size effect in dynamical lattice QCD calculation with two light quarks and strange quark.

The details are as follows. First, meson three-point correlation functions with weak vector current and meson two-point functions on the four dimension hyper cube lattice whose number of grid point on the temporal and spatial extent is 128 are calculated by high performance computing system. The physical size of the lattice is 10.8 fm. Second, hadron matrix elements of semileptonic decay with the vector current are constructed by these correlation functions and then semileptonic decay form factors are defined by these matrix elements. Although the form factors are function of the momentum transfer, the accesible momenta are discrete and propotional to the inverse of the spatial extent on

the lattice. Third, we estimate the semileptonic form factor at zero momentum transfer by using monopole ansatz which is commonly used to measure in experiment and using the formulae of chiral perturbation theory. Fourth, $|V_{us}|$ is estimated by the combination of the semileptonic form factor at zero momentum transfer and experimental result and compared with other lattice QCD calculations and other results. Finally we find that our results are consistent with unitary condition of CKM, and the signals are unfavorable for new physics.

This article is composed as follows. The Cabbibo-Kobayashi-Maskawa (CKM) matrix elements as the fundamental parameters of the SM and their current status and the determination for one of the magnitude of the matrix elements are represented in chapter 2. Chapter 3 contains general structure of form factor and construction of form factor. In chapter 4, actual calculation methods of two-point and three-point function to obtain meson form factors, and some improvements for discretization effect will be represented in this chapter. In chapter 5, we present the brief of chiral perturbation theory (ChPT), and introduce of representation of the form factors on ChPT. In chapter 6, several results of the meson form factors and corresponding physical quantities by Lattice QCD calculations are shown and in chapter 7, we discuss about the result and future work to do for precise estimation.

Chapter 2

Cabbibo-Kobayashi-Maskawa Matrix

In this chapter, we present the Cabbibo-Kobayashi-Maskawa (CKM) matrix elements which are the fundamental parameters of the SM, the their current status and the determination for one of the magnitude of the matrix element of V_{us}.

2.1 Leptonic and semileptonic decay

The Cabbibo-Kobayashi-Maskawa (CKM) matrix [4, 6] is the unitary matrix which describes the matrix of the coefficients of mixture of the mass eigenstates between up-type and down-type quarks.

$$\begin{pmatrix} d' \\ s' \\ b' \end{pmatrix} = \begin{pmatrix} V_{ud} & V_{us} & V_{ub} \\ V_{cd} & V_{cs} & V_{cb} \\ V_{td} & V_{ts} & V_{tb} \end{pmatrix} \begin{pmatrix} d \\ s \\ b \end{pmatrix} = V_{CKM} \begin{pmatrix} d \\ s \\ b \end{pmatrix}, \tag{2.1.1}$$

where (d', s', b') represents weak eigenstate corresponding to up-type quarks in participate decay, (d, s, b) represents down-type quark mass eigenstate. The indices of the matrix element represent the mixture between up-type quarks (up, charm, top) and down-type quarks (down, strange, bottom). They appear from Yukawa interactions with Higgs condensate. The Lagrangian is given by

$$\mathcal{L} = -Y^d_{ij} \bar{Q^I_{L,i}} \phi d^I_{R,j} - Y^u_{ij} \bar{Q^I_{L,i}} \epsilon \phi u^I_{R,j} + h.c., \tag{2.1.2}$$

where $Y^{u,d}_{ij}$ are 3×3 complex matrices with quarks' generation labels i, j, Q^I_L are left-handed quark doublets, ϕ is the Higgs field and ϵ is the 2×2 antisymmetric tensor and d^I_R and u^I_R are right-handed down-type and up-type quark singlets, respectively. When ϕ acquires a vacuum expectation value (VEV), $< \phi >= (0, \frac{v}{\sqrt{2}})$, and then the equation (2.1.2) yields these quarks' mass terms.

The physical states are obtained by diagonalizing $Y^{u,d}_{ij}$ by combination unitary matrices and the VEV, $U^{u,d}_{L,R}$, as $M^{u,d} = U^{u,d}_L Y^{u,d} (U^{u,d}_R)^\dagger \frac{v}{\sqrt{2}}$. As a result, we obtain the charged weak current of $W^\pm$ boson to the physical u^i_L, d^j_L quarks with couplings, and then CKM matrix is given by the product of $U^{u,d}_{L,R}$; $V_{CKM} = U^u_L U^{d\dagger}_R$.

The CKM matrix could be parametrized by three quark mixing angles and KM complex phase [4]

(so-called *standard parametrization*). It is given by

$$\begin{pmatrix} c_{12}c_{13} & s_{12}c_{23} & s_{12}e^{-i\delta} \\ -s_{12}c_{23} - c_{12}s_{23}s_{13}e^{i\delta} & c_{12}s_{23} - s_{12}s_{23}s_{13}e^{-i\delta} & s_{23}c_{13} \\ s_{12}c_{23} - c_{12}c_{23}s_{13}e^{i\delta} & c_{12}s_{23} - s_{12}c_{23}s_{13}e^{-i\delta} & c_{23}c_{13} \end{pmatrix}, \tag{2.1.3}$$

where quark mixing angles $s_{ij} = sin\theta_{ij}, c_{ij} = cos\theta_{ij} (0 \leq \theta_{ij} \leq \frac{\pi}{2})$. The pathfinder of its idea was introduced by N. Cabibbo in two quarks' generations [6] and the extension to the three quarks' generations together KM complex phase $e^{i\delta}$. The development was introduced by M. Kobayashi and T. Maskawa [4]. The mechanism represents CP-violation in the quark mixture with flavor-changing weak interactions and it dominates CP-violation at electroweak scale, which is proved by the B-factories. (The other mechanisms of CP-violation, for example PMNS mechanism in the lepton mixture and the strong CP problem in the flavor-conserving strong interaction, will not be explained in this thesis)

In the frameworks of the SM, V_{CKM} must have unitarity $V_{CKM}V_{CKM}^{\dagger} = 1$. In this work, the target is $|V_{us}|$. Thus, in next section, we present the brief of up quark parts of the CKM matrix element, $|V_{ud}|$, $|V_{ub}|$ and $|V_{us}|$ in this review [3].

2.2 Brief of current status of the CKM matrix of up quark parts

The estimation of V_{us} requires the decay rates (or the combination) of the leptonic or semileptonic decay which are the decay emitting some pairs of lepton-neutrino. The "leptonic decay" means a decay caused by the weak interaction in which some pure pairs of lepton-neutrino are produced. The "semileptonic decay" means a decay in which some pairs of lepton-neutrino are produced in addition to some hadrons. (The "hadronic decay" means a decay in which some hadrons are purely produced, although the decay is not described in detail.) The analysis of these decay modes could provide the restriction of new physics scenarios : while within the Standard Model, all down-type quark transitions to up-type quarks with pair of lepton-neutrino ($d_i \to u_j l\nu$) are dominated by the same CKM coupling V_{jk} which is satisfied the unitarity condition $\Sigma_k |V_{jk}|^2 = 1$, and G_F is the same coupling that dominates muon decay, this is not necessarily true beyond the Standard Model. New bounds on violations of CKM unitarity and lepton universality and deviations from the $V-A$ structure translate into significant signals on various new physics scenarios. In other words, such tests may eventually turn up evidence of beyond the Standard Model.

In this work, the target is one of the Kaon semileptonic decay, $K \to \pi l\nu$ (so-called K_{l3}), and the matrix element corresponding to K_{l3} is calculated by lattice QCD. In this section, we present some determinations of $|V_{us}|$ in recent.

2.2.1 $|V_{us}|$

In this subsection, we present the determination of $|V_{us}|$ without the unitary condition of V_{CKM}. Leptonic and semileptonic kaon decays are used to obtain the determination of the magnitude of the element V_{us} in present. There are several reasons why the checks are particularly significant given as follows.

- There are the large amount of data of the leptonic and semileptonic kaon decays collected by several experiments.

- The hadronic matrix elements corresponding to the kaon decay could be calculated by Lattice QCD as nonperturbative approach.
- The detailed analyses of radiative corrections and isospin breaking effects perform within chiral perturbation theory (ChPT) (Chapter 5 in detail) as one of the QCD effective theory at low energy.

There are two traditional determinations of $|V_{us}|$ which are needed for some hadronic constants. One is from the ratio of leptonic decay rates of pion and of kaon. The ratio is written as

$$\frac{\Gamma(K \to l\nu)}{\Gamma(\pi \to l\nu)} = \frac{|V_{us}|^2}{|V_{ud}|^2}\frac{f_K^2}{f_\pi^2}\frac{m_K(1-m_l^2/m_K^2)^2}{m_\pi(1-m_l^2/m_\pi^2)^2}(1+\delta_{EM}), \tag{2.2.1}$$

where $l = e, \mu$ are the leptons, the neutrino ν is correspond to the leptons, m_l is the lepton mass, δ_{EM} is the effect of long-distance electromagnetic corrections, and f_K, f_π are the decay constant of kaon and pion, respectively. δ_{EM} depends only on the particle masses and this main uncertainty rely on models of the hadron structure. The masses and the decay rate could be obtained by experiments [27, 29] and δ_{EM} could be obtained by phenomenological approaches. Combining the equation (2.2.1) with values, the result is given by

$$\frac{|V_{us}|}{|V_{ud}|}\frac{f_K}{f_\pi} = 0.2760(4). \tag{2.2.2}$$

The $|V_{ud}|$ could be estimated by experiment (subsection 2.2.2). However, the ratio of decay constant should be restricted by other approach in order to obtain $|V_{us}|$. The ratio could be evaluated by lattice QCD simulations [2]. The average of these result is $f_K/f_\pi = 1.1933(29)$, and the combination $|V_{ud}|$ and the f_K/f_π reads to

$$|V_{us}| = 0.2253(7), \tag{2.2.3}$$

where the accuracy is restricted by the study of the ratio.

The other is from the semileptonic decay rates of kaon (K_{l3}). In this work, the corresponding hadronic matrix elements are calculated by lattice QCD. (The detail of form factor are to be mentioned latter 3) The K_{l3} decay rate is given by

$$\Gamma(K \to \pi l\nu) = \frac{G_F^2 m_K^5}{192\pi^3} C S_{EW}(1+\delta_{EM}+\delta_{SU(2)})^2 I|V_{us}|^2 f_+(q^2=0)^2, \tag{2.2.4}$$

where $f_+(q^2=0)$ is the vector form factor, as the function of momentum transfer, at the momentum transfer $q^2 = 0$, this is the same value the scalar form factor $f_0(q^2=0)$ at the momentum transfer $q^2 = 0$ (the momentum dependence is different from the vector form factor), S_{EW} is effect of short-distance electromagnetic corrections, δ_{EM} is the effect of long-distance electromagnetic corrections, $\delta_{SU(2)}$ is the effect of isospin breaking corrections, C is the square of Clebsch-Gordan coefficient which is given by $C = 1/2$ ($K^\pm \to \pi^0$), 1 ($K^0 \to \pi^-$), I is a phase space integral which depends on the

momentum transfer dependence of the form factors. The integral is given by

$$\begin{aligned} I &= \frac{1}{m_K^8}\int_{m_l^2}^{(m_K^2-m_\pi^2)} dq^2\lambda^{3/2}\left(1+\frac{m_l^2}{2q^2}\right)\left(1-\frac{m_l^2}{2q^2}\right)^2 \\ &\times \left(\tilde{f}_+(q^2)^2+\tilde{f}_0(q^2)^2\left(\frac{3m_l^2(m_K^2-m_\pi^2)^2}{(2q^2+m_l^2)\lambda}\right)\right), \\ \lambda &= (q^2-m_k^2-m_\pi^2)^2-4m_k^2m_\pi^2, \end{aligned} \tag{2.2.5}$$

where $\tilde{f}_+(q^2)=f_+(q^2)/f_+(0)$, $\tilde{f}_0(q^2)/f_0(0)$ is the normalized vector form factor and the normalized scalar form factor, respectively. The normalized form factors have the information of momentum dependence, for example slope of the form factors and these curvature, and the informations could be obtained as assumption of some parameterizations in experiment [29].

In the similar way as the decay constant ratio, combining the equation (2.2.1) with values, the result is given by

$$|V_{us}|f_+(q^2=0)=0.2165(4). \tag{2.2.6}$$

In this estimation, the average of decay mode of the five decay mode $K_L^0\to\pi e\nu$, $K_L^0\to\pi e\mu\nu$, $K^\pm\to\pi^0e^\pm\nu$, $K^\pm\to\pi^0\mu^\pm\nu$, and $K_L^0\to\pi e\nu$ is used. Similarly, the value of form factor should be restricted by other approach in order to obtain $|V_{us}|$. The value could be evaluated by lattice QCD simulations [2]. By using the average $f_+(q^2=0)=0.9704(32)$ and $|V_{us}|f_+(q^2=0)=0.2165(4)$, the result is given by

$$|V_{us}|=0.2231(8), \tag{2.2.7}$$

and the value from phenomenological approach [5] is in agreement with this value.

2.2.2 $|V_{ud}|$

In this subsection and next subsection, we present current status of the other parts of V_{CKM} corresponding to the determination of $|V_{us}|$ with the unitary condition. The most precise determination of $|V_{ud}|$ comes from the study of superallowed $J^P=0^+\to0^+$ nuclear beta decays, which are pure vector transitions. Taking the average the superallowed beta decays of the fourteen nuclei most precise determinations [30] yields $|V_{ud}|=0.97420(21)$. The error is dominated by theoretical uncertainties from nuclear Coulomb distortion effect and radiative corrections. A precise determination of $|V_{ud}|$ is also obtained from the measurement of the neutron lifetime. The interest in this measurement is that the determination of $|V_{ud}|$ is very clean theoretically, because it is a pure vector transition (without axial vector transition) and is free from nuclear's structure uncertainties.

2.2.3 $|V_{ub}|$

To obtain $|V_{ub}|$ from exclusive decays which are the semileptonic decays with specific hadronic final state, the form factors have to be known. The $B\to\pi l\nu^-$ branching ratio is now known to 5%. Lattice QCD calculations of the $B\to\pi l\nu^-$ form factor are available for the high momentum transfer q^2 region ($q^2>16$ or $18\mathrm{GeV}^2$). A fit to the experimental partial rates and lattice QCD results versus q^2 yields $|V_{ub}|=(3.70\pm0.10\pm0.12)\times10^{-3}$.

The determination of $|V_{ub}|$ from inclusive decays which are the semileptonic decays with hadronic final states including up quark $B \to X_u l\nu^-$ (X_i : hadron including i flavor quark) is complicated due to large $B \to X_c l\nu^-$ backgrounds. In most regions of phase space in which the charm background is kinematically forbidden, the hadronic physics enters via unknown nonperturbative functions, so-called shape functions. The inclusive decay shape functions need to calculate not only leading order but also model-dependent subleading order, to obtain $|V_{ub}|$ The large and pure pairs of B meson samples at the B factories permit the selection of $B \to X_u l\nu^-$ decays in events where the other B meson is fully reconstructed. With this full reconstruction tag method, the four-momenta of both the leptonic and the signals of hadronic final states can be measured. The signals could give access to a wider kinematic region, because of improved purity of signal. The result estimated from inclusive $B \to X_u l\nu^-$ decay is given by $|V_{ub}| = (4.49 \pm 0.16^{+0.16}_{-0.17} \pm 0.17) \times 10^{-3}$, where the first error is experimental, the second one comes from the model dependence quoted by the individual measurements, and the third one is an additional one estimated. The uncertainties in extracting $|V_{ub}|$ from inclusive and exclusive decays have a large deviation. The result combined the two determinations is given by $|V_{ub}| = (3.94 \pm 0.36) \times 10^{-3}$

The combination of the unitary condition of V_{CKM} and the two magnitudes of the matrix element, $|V_{ud}|, |V_{ub}|$ yields $|V_{us}|$. However $|V_{ub}|$ is too small to affect the $|V_{us}|$ and could be ignored $|V_{ub}|$ in the estimation (although including the value, the $|V_{us}|$ varies by $O(10^{-5})$). Thus the result is given by

$$|V_{us}| = 0.2256(8). \tag{2.2.8}$$

The result of unitary condition lies in the framework of the SM, thus checking the deviation from the result of the SM could provide signals of beyond the SM. Comparing the results among three determinations of $|V_{us}|$, the results of decay constant ratio and from unitary condition are consistent and the difference about 2σ between the determinations without unitary condition occurs.

Chapter 3

Meson form factors

In this chapter, we represent general structure of form factor and construction of form factor by using the meson two-point functions and the three-point functions with vector current.

3.1 General strcuture of form factors

The matrix element of the vector current operator V_μ between two spin-0 particles could be written, by imposing Lorentz invariance, in the most general form as

$$\langle Y(\vec{p'})\,|V_\mu|\,X(\vec{p})\rangle = (p'+p)_\mu f + (p'-p)_\mu g, \tag{3.1.1}$$

where p', p are the four-momenta of initial state and final state of particle $X,\ Y$, respectively and f, g are form factors as scalar functions. The form factors is the functions of the combination of kinematic variables, $p^2,\ p'^2,\ p,\ p',\ (p+p')^2,\ (p-p')^2$. Only three of the variables are linearly independent and we choose p'^2, p^2 and momentum transfer $q^2 = -(p'-p)^2$ as the arguments of the functions.

The hermiticity of the current, which provides restrictions of f and g.

$$\begin{aligned}\langle Y(\vec{p'})\,|V_\mu|\,X(\vec{p})\rangle &= \langle Y(\vec{p'})\left|(V_\mu)^\dagger\right|X(\vec{p})\rangle = (\langle X(\vec{p})\,|V_\mu|\,Y(\vec{p'})\rangle)^* \\ &= (p'+p)_\mu f(p'^2,p^2,q^2) + (p'-p)_\mu g(p'^2,p^2,q^2) \\ &= (p'+p)_\mu f^*(p^2,p'^2,q^2) - (p'-p)_\mu g^*(p^2,p'^2,q^2),\end{aligned} \tag{3.1.2}$$

and the ward identity of vector current, which provides more restrictions by using X meson propagators $\Delta_X(p^2)$,

$$\Delta_Y^{-1}(p'^2) - \Delta_X^{-1}(p^2) = q_\mu\langle Y(\vec{p'})\,|V_\mu|\,X(\vec{p})\rangle = (p'^2-p^2)f - q^2 g. \tag{3.1.3}$$

In particular, the relation apply to on-shell meson with $X = Y$, for example pion electromagnetic form factor, and show that g vanishes. In on-shell mesons with $X \neq Y$ and q^2 is small, the relation yields

$$\Delta_Y^{-1}(p'^2) - \Delta_X^{-1}(p^2) = (m_Y^2 - m_X^2)\left(f - \frac{q^2}{m_Y^2-m_X^2}g\right), \tag{3.1.4}$$

the new form factor is defined by $h = f - \frac{q^2}{m_Y^2-m_X^2}g$, and at $q^2 = 0$ f equals h. The above discussions

are general. And the "exact" conservation of the vector current, for example electromagnetic current, in on-shell condition of both state of $X = Y$ boson yields

$$0 = q_\mu \langle X(\vec{p'}) \left| V_\mu \right| X(\vec{p}) \rangle = (p'^2 - p^2) f - q^2 g, \tag{3.1.5}$$

thus for general q^2 and on-shell condition $p^2 = p'^2 = m_X^2$, g must vanish.

However, in this work (and in actual fact), the strange mass is different from the light quark (up or down) mass, and the vector current with strangeness violating is used in the works of semileptonic form factors

The "partial" conservation of the vector current with strangeness violating $V_\mu = \bar{s}\gamma_\mu u$ with the deviation between strange mass m_s and light quark (up or down) mass m_l is given by,

$$\partial_\mu \bar{s}\gamma_\mu u = i(m_s - m_l)\bar{s}u, \tag{3.1.6}$$

where, $\bar{s}u$ $(= S)$ is scalar current with strangeness violating.

Combining the "partial conservation" and the relations,

$$\begin{aligned} q_\mu \langle Y(\vec{p'}) \left| V_\mu \right| X(\vec{p}) \rangle &= (m_s - m_l) \langle Y(\vec{p'}) \left| S \right| X(\vec{p}) \rangle \\ \rightarrow (m_Y^2 - m_X^2) h &= (m_s - m_l) \langle Y(\vec{p'}) \left| S \right| X(\vec{p}) \rangle, \end{aligned} \tag{3.1.7}$$

and the relation shows that the form factor h is given by scalar current in proportion to the mass deviations.

In the following discussions of semileptonic form factors, "*vector form factors*" are defined by the functions of q^2, $f = f_+(q^2), g = f_-(q^2)$ from the vector current, and "*scalar form factor*" is defined by the functions of q^2, $h = f_0(q^2)$. The scalar form factor could be rewritten by linear combination of vector form factors,

$$f_+(q^2) + \frac{-q^2}{m_Y^2 - m_X^2} f_-(q^2) = f_0(q^2). \tag{3.1.8}$$

3.2 Construction of form factor

In order to obtain the form factors, we calculate the meson three-point functions $C_\mu'^{XY}(\vec{p'}, \vec{p}, t; t_f, t_i)$ with the vector current V_μ and X meson interpolator O_X given by

$$\tilde{C}_\mu^{XY}(\vec{p'}, \vec{p}, t; t_f, t_i) = \langle 0 | O_Y(\vec{p'}, t_f) V_\mu(\vec{q}, t) O_X^\dagger(\vec{p}, t_i) | 0 \rangle \tag{3.2.1}$$

$$= \frac{Z_Y(\vec{p'}) Z_X(\vec{p})}{4 E_Y(\vec{p'}) E_X(\vec{p})} \frac{1}{Z_V} \langle Y(\vec{p'}) \left| V_\mu \right| X(\vec{p}) \rangle e^{-E_Y(\vec{p'})(t_f - t)} e^{-E_X(\vec{p})(t - t_i)} + \cdots, \tag{3.2.2}$$

where Z_V is the renormalization factor of the vector current (detailed in the section t4.1), $\vec{p}, t_i$ are the momentum and the time of the source operator, respectively, and $\vec{p'}, t_f$ are the momentum and the time of the sink operator, respectively, $X, Y = \pi, K$, and $t_i < t < t_f$. $E_X(\vec{p})$ and $Z_X(\vec{p})$ are evaluated from the meson two-point functions given by

$$C^X(\vec{p}, t, t_i) = \langle 0 | O_X(\vec{p}, t) O_X^\dagger(\vec{p}, t_i) | 0 \rangle = \frac{|Z_X(\vec{p})|^2}{2 E_X(\vec{p})} (e^{-E_X(\vec{p})|t - t_i|} + e^{-E_X(\vec{p})(T - |t - t_i|)}) + \cdots, \tag{3.2.3}$$

with the periodic boundary condition in the temporal direction. The terms of the dots $(\cdots)$ are contributions of excited states. The meson masses, m_π and m_K, are obtained from a single exponential fit to each two-point function. Their energies are determined by the equation $E_X(\vec{p}) = \sqrt{m_X^2 + \vec{p}^2}$ using the fit result of m_X.

To simplify in our calculation, we fix $\vec{p'} = \vec{0}$, $t_f - t_i$ =constant (in actual $t_f - t_i = 36$), the three-point function in the temporal region $t_i < t < t_f$ is written as

$$\begin{aligned} & C_\mu^{XY}(\vec{p},t) \equiv \tilde{C}_\mu^{XY}(\vec{0},\vec{p},t;t_f,t_i) = \langle 0|O_Y(\vec{0},t_f)V_\mu(\vec{q},t)O_X^\dagger(\vec{p},t_i)|0\rangle \\ = & \frac{Z_Y(\vec{0})Z_X(\vec{p})}{4E_Y(\vec{0})E_X(\vec{p})}\frac{1}{Z_V}\langle Y(\vec{0})\,|V_\mu|\,X(\vec{p})\rangle e^{-m_Y(t_f-t)}e^{-E_X(\vec{p})(t-t_i)} + \cdots, \end{aligned} \tag{3.2.4}$$

in the following. When pion and kaon electromagnetic form factor are extracted, we construct the ratio $R(q,t)$ by using the meson three-point function and the two-point function

$$R_X(q,t) = \frac{2m_X Z_V C_4^{XX}(\vec{p},t)}{(m_X + E_X(\vec{p}))Z_X(\vec{0})Z_X(\vec{p})}e^{E_X(\vec{p})(t-t_i)} \to f_X(q^2), (X = \pi,\ K). \tag{3.2.5}$$

When semileptonic form factors are extracted, we construct the ratio $d_i(q,t)$ (i=1,2,3) by using the meson three-point function whose source meson has non zero momentum and the two-point function.

$$d_1(q,t) = \frac{C_4^{XY}(\vec{0},t)C_4^{YX}(\vec{0},t)}{C_4^{YY}(\vec{0},t)C_4^{XX}(\vec{0},t)} \to \frac{(m_Y+m_X)^2}{4m_Y m_X}(f_0(q^2_{max}))^2, \tag{3.2.6}$$

$$d_2(q,t) = \frac{C_4^{XY}(\vec{p},t)C^X(\vec{p},t,t_i)}{C_4^{XY}(\vec{0},t)C^X(\vec{p},t,t_i)} \to \left(\frac{E_X(\vec{p})+m_Y}{m_X+m_Y} + \frac{E_X(\vec{p})-m_Y}{m_X+m_Y}\xi(q^2)\right)\frac{f_+(q^2)}{f_0(q^2_{max})}, \tag{3.2.7}$$

$$d_3(q,t) = \frac{C_i^{XY}(\vec{p},t)C_4^{YY}(\vec{p},t)}{C_i^{YY}(\vec{p},t)C_4^{XY}(\vec{p},t)} \to \frac{(E_Y(\vec{p})+m_Y)(1-\xi(q^2))}{E_X(p)+m_Y+(m_Y-E_X(p))\xi(q^2)}, \tag{3.2.8}$$

where $\xi(q^2)$ is given by the ratio of vector form factors,

$$\xi(q^2) = \frac{f_-(q^2)}{f_+(q^2)}. \tag{3.2.9}$$

Chapter 4

Calculation of correlation functions

In this chapter, we present calculation methods of two-point and three-point function to obtain meson form factors, and some improvements for discretization effect in the calculations.

4.1 Calculation of meson three-point functions

We compute two-point and three-point function to obtain meson form factors. The meson two-point function and three-point function which obtains bare vector current with periodic boundary condition in temporal direction are the below formulae. When $t_i \leq t \leq t_f$,

$$\begin{aligned}\tilde{C}_{\mu}^{XY}(\vec{p'},\vec{p},t;t_f,t_i) &= \langle 0|O_Y(\vec{p'},t_f)V_\mu(\vec{q},t)O_X^\dagger(\vec{p},t_i)|0\rangle \\ &= \frac{Z_Y(\vec{P'})Z_X(\vec{P})}{4E_Y(\vec{P'})E_X(\vec{p})}\frac{1}{Z_V}\langle Y(\vec{p'})\,|V_\mu|\,X(\vec{p})\rangle e^{-E_Y(\vec{p'})(t_f-t)}e^{-E_X(\vec{p})(t-t_i)}+\cdots,\end{aligned}$$

$O_X = \bar{q}\gamma_5 q$ is a local pseudoscalar operator of $X = \pi,\ K$ meson (pion or kaon). Z_X is given as $Z_\pi(\vec{p}) = \langle 0|\, O_X(\vec{0},0)\,|X(\vec{p})\rangle$. The term of $(\cdots)$ is contribution of excited states. The vector current is defined by weak vector current $V_\mu = \bar{s}\gamma_\mu u$ when $X \neq Y$, and by electromagnetic current $V_\mu = \sum_{f=u,d,s} Q_f \bar{q}_f \gamma_\mu q_f$ when $X = Y$ We assume that the correlation functions is dominated by the lightest state, and contribution of excited states is not estimated. We make the quantities $R(q,t)$ and $d_{1,2,3}(q,t)$ which is combined of three-point function, two-point function and definition of meson form factors (in Chapter 3). Fixing the source time slice $t_i = 0$, the quantities $R(q,t)$ and $d_{1,2,3}(q,t)$ have current time t dependence, though we can extract meson form factors without t dependance from $R(q,t)$ and $d_{1,2,3}(q,t)$ when current-sink temporal separation is large enough and current-source temporal separation is large enough too ($0 \ll t \ll t_f$). When $\vec{p'} = \vec{0}$, is the matching factor by which the bare lattice current needs to be multiplied in order to obtain the renormalized current.

The connected three-point function with vector current could be written by using quark propagator D^{-1}

$$\tilde{C}_{\mu}^{XY,\ conn}(\vec{0},\vec{p},t;t_f,t_i) = \sum_{\vec{x},\vec{y},\vec{z}} e^{i\vec{p}_i\cdot\vec{x}+i\vec{q}\cdot\vec{z}} tr\left[\gamma_5 D^{-1}(z,x)\gamma_\mu D^{-1}(x,y)\gamma_5 D^{-1}(y,z)\right], \tag{4.1.1}$$

where is $\vec{x},\vec{y}$ are the spatial position of the source operator of meson, the sink operator of meson, respectively and $\vec{z}$ the position of vector current.

The connected three-point function is consist of three quark propagators. In actual calculation,

the connected three-point function is calculated in the follow steps

1. quark propagator with source momentum $\vec{p}_i = \vec{0}$ which is correspond to red (number 1) line in the Fig. 4.1 is calculated by using random wall source.

2. quark propagator with sink 3 momentum $\vec{p}_f = \vec{0}$ which is correspond to green (number 2) line in the Fig. 4.1 is calculated by using sequential source Σ, which is given by

$$\Sigma(x, z) = \sum_{\vec{y}} D^{-1}(x, y)\gamma_5 D^{-1}(y, z), \tag{4.1.2}$$

   and then $C_\mu^{XY,\ conn}$ is rewritten as

$$\tilde{C}_\mu^{XY,\ conn}(\vec{0}, \vec{p}, t; t_f, t_i) = \sum_{\vec{x},\vec{y},\vec{z}} e^{i\vec{p}\cdot\vec{x}+i\vec{q}\cdot\vec{z}} tr\left[\gamma_5 D^{-1}(z, x)\gamma_\mu \Sigma(x, z)\right]. \tag{4.1.3}$$

3. quark propagator with source 3 momentum $\vec{p}_i \neq \vec{0}$which is correspond to blue (number 3) line in the Fig. 4.1.

The three quark propagators are calculated in periodic boundary condition of temporal direction, in addition, the quark propagator with source momentum $\vec{p}_i = \vec{0}$ is calculated in anti periodic boundary condition. This is because the wrapping around effect as described latter could be suppressed.

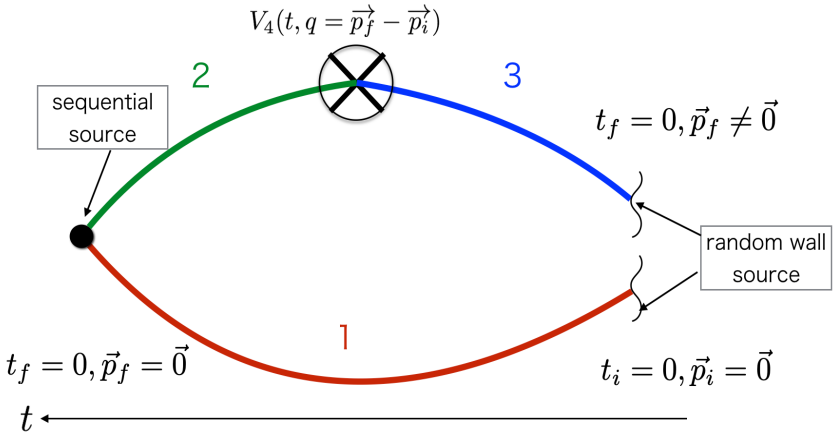

Figure 4.1: Diagram of connected three-point function

In actual calculation of quark propagator with source momentum of this work, we use the random source as described latter.

4.2 Random wall source

Quark propagator is given by using external source η_{AB} and Dirac operator matrix D_{AB}^{-1}

$$S_{AC}(x; t_i) \equiv \sum_{\vec{y}} \sum_{B} D_{AB}^{-1}(x; t_i, \vec{y})\eta_{BC}(\vec{y}, t_i), \tag{4.2.1}$$

where, A, B, C represent the indices of color and spinor.

Introducing point source $\eta_{BC}(\overrightarrow{y}, t_i) = \delta(\overrightarrow{y} - \overrightarrow{x}_0)\delta_{BC}$, quark propagator can be solved

$$\begin{aligned} S_{AC}(x; t_i) &= \sum_{\overrightarrow{y}} \sum_{B} D^{-1}_{AB}(x; t_i, \overrightarrow{y})\delta(\overrightarrow{y} - \overrightarrow{x}_0)\delta_{BC} \\ &= D^{-1}_{AC}(x; t_i, \overrightarrow{x}_0). \end{aligned} \tag{4.2.2}$$

However, the propagators need to be solved at some point in space-time for all the indices, and the numbers of the index are 12 (number of color and spinor 3×4). In other words, The equation of propagator represents 12 equations of the indices of color and spinor at certain point.

In this work, the order of the propagator matrix is about 3.2 billions (12×128^4), and to solve the propagator by using point source is spent the expensive computational cost (budget and time). Thus we need to reduce the computational cost, random wall source $D_{BA}S_{AC} = \eta_{BC}(\overrightarrow{y}, t_i)\eta_{BC}(\overrightarrow{y}, t_i) \in \mathbb{Z}(2) \otimes \mathbb{Z}(2)$, is introduced. Doing not fail to discriminate color indices from spinor indices by using the source is able to compute by 1/12 cost of the point source [14].

There are some kinds of random source, for instance

$$\eta_{B0}(\overrightarrow{y}, t_i) = \left\{ \frac{\pm 1 \pm i}{\sqrt{2}} \right\} \in \mathbb{Z}(2) \otimes \mathbb{Z}(2), \tag{4.2.3}$$

and

$$\eta_{B0}(\overrightarrow{y}, t_i) = \{ \pm 1, \pm i \} \in \mathbb{Z}(4). \tag{4.2.4}$$

When $N \to \infty$, the source η is satisfied

$$\frac{1}{N} \sum_{j=0}^{N} \eta^j_{A0}(\overrightarrow{x}, t_i)\eta^{\dagger j}_{0B}(\overrightarrow{y}, t_i) \to \delta(\overrightarrow{x} - \overrightarrow{y})\delta_{AB}. \tag{4.2.5}$$

The quark propagator is written by

$$S_{AC}(x; t_i) = \frac{1}{N} \sum_{j=1}^{N} \sum_{\overrightarrow{y}} \sum_{B} D^{-1}_{AB}(x; t_i, \overrightarrow{y})\eta^{\dagger j}_{BC}(\overrightarrow{y}, t_i), \tag{4.2.6}$$

and therefore the propagator of pion is given by using the quark propagators

$$
\begin{aligned}
& C^{\pi}(\vec{p}, t, t_i = 0) \\
= & \sum_{\overrightarrow{x}} e^{-i\vec{p}\cdot\vec{x}} \mathrm{tr}\left[\gamma^5 S(x; \overrightarrow{y}, t)\gamma^5 (\gamma^5 S(x; \overrightarrow{y}, t)\gamma^5)^{\dagger}\right] \\
= & \sum_{j=0}^{N} \sum_{\overrightarrow{x}} e^{-i\vec{p}\cdot\vec{x}} \sum_{\overrightarrow{z}} \sum_{B,B'} \left[\gamma^5 D^{-1}_{AB}(x; t, \overrightarrow{y})\eta^j_{BC}(\overrightarrow{y}, t)\gamma^5 (\gamma^5 D^{-1}_{AB'}(x; t, \overrightarrow{z})\eta^j_{B'C}(\overrightarrow{z}, t)\gamma^5)^{\dagger}\right] \\
= & \sum_{\overrightarrow{x}} e^{-i\vec{p}\cdot\vec{x}} \sum_{\overrightarrow{z}} \sum_{B,B'} \left[\sum_{j=1}^{N} \frac{1}{N} \eta^j_{BC}(\overrightarrow{y}, t)\eta^{\dagger j}_{CB'}(\overrightarrow{z}, t)\gamma^5 D^{-1}_{AB}(x; t, \overrightarrow{y})\gamma^5 (\gamma^5 D^{-1}_{AB'}(x; t, \overrightarrow{z})\gamma^5)^{\dagger}\right] \\
\to & \sum_{\overrightarrow{x}} e^{-i\vec{p}\cdot\vec{x}} \sum_{\overrightarrow{z}} \sum_{B,B'} \left[\delta(\overrightarrow{y} - \overrightarrow{z})\delta_{BB'}\gamma^5 D^{-1}(x; \overrightarrow{y}, t)\gamma^5 (\gamma^5 D^{-1}_{AB'}(x; \overrightarrow{y}, t)\gamma^5)^{\dagger}\right] \\
= & \sum_{\overrightarrow{x}} e^{-i\vec{p}\cdot\vec{x}} \sum_{B} \left[\gamma^5 D^{-1}_{AB}(x; \overrightarrow{y}, t)\gamma^5 (\gamma^5 D^{-1}_{AB}(x; \overrightarrow{y}, t)\gamma^5)^{\dagger}\right]. \qquad (4.2.7)
\end{aligned}
$$

the three-point functions could be calculated as the same procedure.

4.3 $O(a)$ improvement

Introducing the QCD action on lattice we have to discretize derivative terms in the continuum action. It is point out that some discretization effect must appear. After calculation by lattice QCD, the result have to be take the continuum limit $a \to 0$ due to the adjustment to reality. However, performing the continuum limit is the nontrivial task. Thus we have to deal with the discretization effects, for example, by including them in the extrapolation $a \to 0$

In particular, Adding some extra terms to the Wilson fermion action and matching their coefficients appropriately, which could reduce the discretization error from $O(a)$ to $O(a^2)$.

4.3.1 In a toy model

Let us begin the discussion with the improvement of action. We consider the central difference $f'(x)$ for some dimensionless function f of single variable.

$$
f'(x) \to \frac{f(x+a) - f(x-a)}{2a} (\equiv \hat{\partial} f(x)) = f'(x) + a^2 C^{(2)}(x) + a^4 C^{(4)}(x) + O(a^6), \qquad (4.3.1)
$$

where, $C^{(n)}$ is the correction terms of $O(a^n)$, and $\hat{\partial}_\mu$ is central difference operator. only even power of a and odd derivative of $f(x)$ could appear on the right-hand side. Combining the Taylor expansion

$$
f(x \pm a) = f(x) \pm a f'(x) + \frac{a^2}{2} f''(x) \pm \frac{a^3}{6} f'''(x) + O(a^4), \qquad (4.3.2)
$$

we can identify the leading correction coefficient $C^{(2)}(x)$

$$
C^{(2)}(x) = \frac{1}{6} f'''(x). \qquad (4.3.3)
$$

The strategy for improvement is to add to the left-hand side of the central derivative an extra discretized term such that the correction terms on the right-hand side are canceled up to the required

order.

For improvement of $O(a^2)$ we use the ansatz with an extra discretized term $D^{(3)}[f](x) = f'''(x) + O(a^2)$.

$$\frac{f(x+a) - f(x-a)}{2a} + ca^2 D^{(3)}[f](x) = f'(x) + O(a^4). \tag{4.3.4}$$

Combining the Taylor expansion (4.3.2) again, we can identify

$$D^{(3)}[f](x) = \frac{f(x+2a) - f(x+a) + f(x-a) - f(x-2a)}{2a^3}, \; c = \frac{1}{6}, \tag{4.3.5}$$

and $O(a^2)$ improvement is done. In lattice QCD, the determination of coefficients is complicated and more involved, this is why QCD has the nonlinear property and need to be renormalized. Thus the determination must be done by perturbative or nonperturbative approach.

The approach to improve is known as *Symanzik improvement program* [15–18].

4.3.2 Improvement of lattice QCD Lagrangian

Let us apply the strategy to improvement of the action of lattice QCD. We start on the lattice with the gauge action and Wilson fermion action

$$\begin{aligned} S_{wilson} &= -\sum_{n,\mu\neq\nu} \beta tr\left[U^\dagger_{n,\mu} U_{n+\hat{\mu},\nu} U^\dagger_{n+\hat{\nu},\mu} U^\dagger_{n,\nu}\right] \\ &+ a^4 \sum_n \bar{\psi}_n \left[\sum_\mu \gamma_\mu \left(\frac{U_{n,\mu}\psi_{n+\hat{\mu}} - U^\dagger_{n,\mu}\psi_{n-\hat{\mu}}}{2a}\right) + m\psi_n\right], \end{aligned} \tag{4.3.6}$$

where $\beta = 6/g^2$. Typically, the gauge part of discretization effects is $O(a)$ and the fermion part of discretization effects is $O(a^2)$. The correction terms should be ordered according to their dimension and have the symmetries of the QCD action. We could write the effective action in the form with correction terms of Lagrangian

$$S_{eff} = \int d^4x \left(L^{(0)}(x) + aL^{(1)}(x) + a^2 L^{(2)}(x) + O(a^3)\right), \tag{4.3.7}$$

where, $\int d^4x L^{(0)}(x)$ is the usual QCD action and the mass dimension of the correction terms $L^{(k)}(x), k \geq 1$ is $k+4$. Requiring the symmetries of the lattice action, one may show that the leading correction term $L^{(1)}(x)$ could be written as a linear combination of the following five-dimensional operators

$$\begin{aligned} L^{(1)}_1 &= \bar{\psi}\sigma_{\mu\nu}F_{\mu\nu}\psi, \\ L^{(1)}_2 &= \bar{\psi}(\overleftarrow{D}_\mu\overleftarrow{D}_\mu + \overrightarrow{D}_\mu\overrightarrow{D}_\mu)\psi, \\ L^{(1)}_3 &= mtr[F_{\mu\nu}F_{\mu\nu}], \\ L^{(1)}_4 &= m\bar{\psi}\gamma_\mu(\overrightarrow{D}_\mu - \overleftarrow{D}_\mu)\psi, \\ L^{(1)}_5 &= m^2\bar{\psi}\psi, \end{aligned} \tag{4.3.8}$$

where, $\sigma_{\mu\nu} = [\sigma_\mu, \sigma_\mu]/2i$ and m is quark mass. By using the equation of motion of field $(\gamma_\mu D_\mu + m)\psi = 0$ gives rise to the two relations, $L^{(1)}_1 - L^{(1)}_2 + 2L^{(1)}_5 = L^{(1)}_4 + 2L^{(1)}_5 = 0$, to reduce the terms. The relations may be used to vanish the terms $L^{(1)}_2$ and $L^{(1)}_4$, and some factors of the terms $L^{(1)}_3$ and $L^{(1)}_5$

are already present in original action, such that they can be accounted for by a redefinition of the bare parameters m, β. Thus for $O(a)$ improvement of the Wilson lattice action, $L_1^{(1)}$ might be added to the original action

$$S_{imp} = S_{wilson} + \frac{c_{sw}}{2} a^5 \sum_{n\in\Lambda} \sum_{\mu<\nu} \bar{\psi}\sigma_{\mu\nu}\widehat{F}_{\mu\nu}\psi, \tag{4.3.9}$$

where discretized field tensor as a combination terms of plaquettes $\widehat{F}$ (it is conventional but not unique choice) is given by

$$\widehat{F}_{\mu\nu} = \frac{-i}{8a^2}(Q_{\mu\nu} - Q_{\mu\nu}), \tag{4.3.10}$$

$$Q_{\mu\nu} = U_{\mu\nu} + U_{\nu\mu} + U_{-\mu-\nu} + U_{-\nu\mu}, \tag{4.3.11}$$

$$U_{\mu\nu} = \exp(-ia^2 F_{\mu\nu} + O(a^3)), \tag{4.3.12}$$

and c_{sw} is the real coefficient as $Sheikholeslami - Wohlert\ coefficient$ [19].

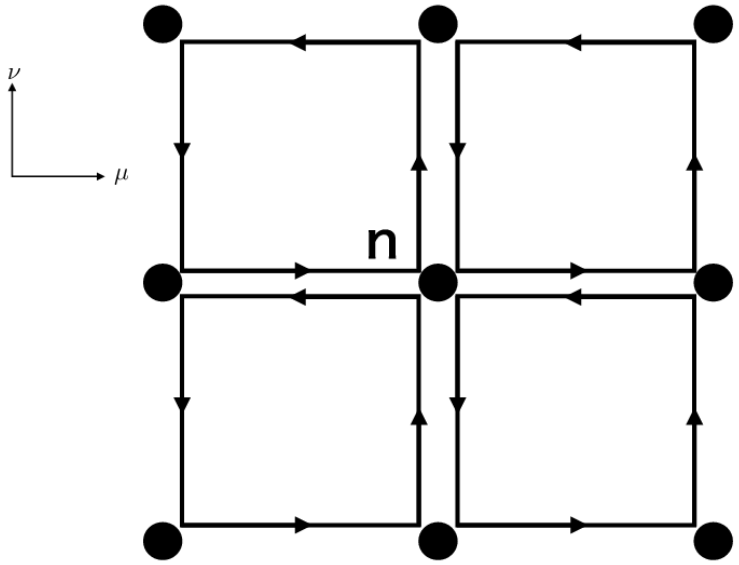

Figure 4.2: Illustration of $Q_{\mu\nu}(n)$. This is the sum of plaquettes $U_{\mu\nu}(n)$ on μ-ν plane

The visualization of the plaquettes' sum $Q_{\mu\nu}(n)$ on μ-ν plane in Fig.4.2 is the shape like a clover leaf. The correction term is often referred to as *clover term* or *clover improvement*.

4.3.3 Improvement of interpolators

In this work, the vector current is needed to calculate the hadronic matrix elements which are necessary to obtain the meson form factors. Thus, in order to achieve a full $O(a)$ improvement, it is necessary not just for Lagrangian on lattice also for the interpolator to be improved. We start with isovector

current V_μ^a and isoaxialvector current A_μ^a

$$V_\mu^a(n) = \frac{1}{2}\bar{\psi}(n)\gamma_\mu\tau^a\psi(n), \tag{4.3.13}$$

$$A_\mu^a(n) = \frac{1}{2}\bar{\psi}(n)\gamma_5\gamma_\mu\tau^a\psi(n), \tag{4.3.14}$$

where τ^a is the a-th components of Pauli matrix, and the current with correction term could be written by

$$V_\mu^a(n) = V_\mu^{a,(0)}(n) + aV_\mu^{a,(1)}(n) + O(a^2), A_\mu^a(n) = A_\mu^{a,(0)}(n) + aA_\mu^{a,(1)}(n) + O(a^2). \tag{4.3.15}$$

After the continuum limit, the currents with the corrections (4.3.15) become the original current (4.3.13) Ones may show that the leading correction term $V_\mu^{a,(1)}(x)$ or $A_\mu^{a,(1)}(x)$ could be written as a linear combination of the following four-dimensional operators of the vector current

$$\begin{aligned} V_{\mu,1}^{a,(1)} &= \frac{1}{2}\bar{\psi}\sigma_{\mu\nu}(\overleftarrow{D}_\nu - \overrightarrow{D}_\nu)\tau^a\psi, \\ V_{\mu,2}^{a,(1)} &= \frac{m}{2}\bar{\psi}\gamma_\mu\tau^a\psi, \\ V_{\mu,3}^{a,(1)} &= \frac{1}{2}\partial_\nu(\bar{\psi}\sigma_{\mu\nu}\tau^a\psi), \end{aligned} \tag{4.3.16}$$

and the following four-dimensional operators of the axialvector current

$$\begin{aligned} A_{\mu,1}^{a,(1)} &= \frac{1}{2}\bar{\psi}\gamma_5\sigma_{\mu\nu}(\overleftarrow{D}_\nu - \overrightarrow{D}_\nu)\tau^a\psi, \\ A_{\mu,2}^{a,(1)} &= \frac{m}{2}\bar{\psi}\gamma_5\gamma_\mu\tau^a\psi, \\ A_{\mu,3}^{a,(1)} &= \frac{1}{2}\partial_\mu(\bar{\psi}\gamma_5\tau^a\psi), \end{aligned} \tag{4.3.17}$$

although, as for the improvement of the lattice action we could apply the equation of motion of field $(\gamma_\mu D_\mu + m)\psi = 0$, $V_1^{a,(1)}$ ($A_1^{a,(1)}$) could be rewritten by linear combination of $V_2^{a,(1)}$ and $V_3^{a,(1)}$ ($A_2^{a,(1)}$ and $A_3^{a,(1)}$), and then the part of $V_2^{a,(1)}$ ($A_2^{a,(1)}$) is included in the original vector current. Thus for $O(a)$ improvement of the (axial)vector current, $V_3^{a,(1)}(A_3^{a,(1)})$ might be added to the original current

$$V_\mu^{a,\ imp}(n) = V_\mu^{a,(0)}(n) + ac_V\hat{\partial}_\nu T_{\mu\nu}^a(n) + O(a^2), \tag{4.3.18}$$

$$A_\mu^{a,\ imp}(n) = A_\mu^{a,(0)}(n) + ac_A\hat{\partial}_\mu P^a(n) + O(a^2), \tag{4.3.19}$$

where, tensor current $T_{\mu\nu}^a = \bar{\psi}\sigma_{\mu\nu}\tau^a\psi$ and pseudoscalar current $P^a = \bar{\psi}\gamma_\mu\tau^a\psi$.

For the full $O(a)$ improvement of correlation functions, we need to determine the c_{sw}, c_V and c_A. There are several determinations of the coefficients [19–22], and the value of c_A is very small [23] under the same parameters and ways of improvement with the ones of the configuration in this work (see [32] and Chapter 6). Thus c_V in this work is considered small thanks to the similar improvement.

4.4 Gauge field smearing

When aiming for correlation functions, one is mainly interested in long-distance behaviors. On the other hand, The short-distance behaviors of the gauge field are violent. In order to improve the signal of the correlation functions in short-distance, the techniques *smoothing* or *smearing* the gauge field

are often used either only in the time slices or even in space and time. When smoothing or smearing the gauge field, the traditional technique is updating the link valuables by local average over short path connection of the link end points. The technique is a gauge covariant procedure and not needed to fix the gauge.

When operators or propagators in the correlations are constructed by using the smeared configurations, the signals of the correlation functions in long-distance behaviors should not be affected in the continuum limit. Smearing algorithms are all averaging products of links along certain paths connecting the endpoints of the link. In SU(3) case, the updated links have to be the projection of average to an SU(3) matrix.

The two combined methods of smearing the gauge field is used in this work. One is the "*APE smearing*" [24], which is averaging over the original link U_μ and over six "*staples*" in four dimensional space $C_{\mu\nu}(n)$ connecting its endpoints in four dimensional space,

$$V_\mu(n) = (1-\alpha)U_\mu + \frac{\alpha}{6}\sum_{\nu\neq\mu} C_{\mu\nu}(n), \tag{4.4.1}$$

$$C_{\mu\nu}(n) = U_\nu(n)U_\mu(n+\hat{\nu})U_\nu(n+\hat{\mu})^\dagger + U_\nu(n-\hat{\nu})U_\mu(n-\hat{\nu})^\dagger U_\nu(n-\hat{\nu}+\hat{\mu})), \tag{4.4.2}$$

where the real parameter α is tuned depending on the gauge coupling constant. The projection of sum to SU(3) is done by maximizing of real part of $tr[XV_\mu^\dagger]$ and by using X as updated link.

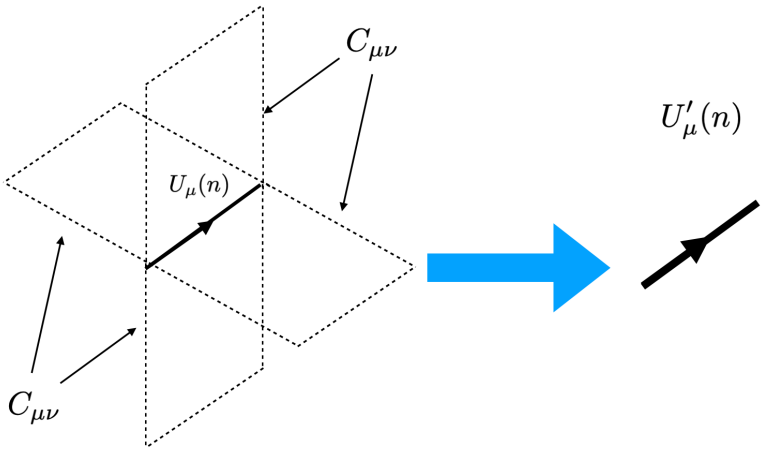

Figure 4.3: Illustration of APE smearing of gauge field. Solid oriented line presents original link variable U_μ, and dashed line staples represent $C_{\mu\nu}$. After the projection, the new link $X = U'_\nu(n)$ (heavier oriented line) could be obtained.

The other is "*stout smearing*" [25]. The method is the perpendicular way to project, updating the new link after a smearing algorithm by

$$U'_\mu(n) = \exp(iQ_\mu(n))U_\mu(n), \tag{4.4.3}$$

where, Q_μ is constructed from staples $C_{\mu\nu}$

$$Q_\mu(n) = \frac{i}{2}\left(\Omega_\mu(n)^\dagger - \Omega_\mu(n) - \frac{1}{3}tr[\Omega_\mu(n)^\dagger - \Omega_\mu(n)]\mathbf{1}_{3\times 3}\right), \tag{4.4.4}$$

$$\Omega_\mu(n) = \left(\sum_{\nu\neq\mu}\rho_{\mu\nu}C_{\mu\nu}(n)\right)U_\mu(n)^\dagger, \tag{4.4.5}$$

where $\rho_{\mu\nu}$ is the tunable real parameter. The advantage of stout smearing is that the new link $U'_\mu(n)$ is differentiable with respect to the link, which is a benefit in applications in the hybrid Monte Carlo method for dynamical fermions in this works.

The process such gauge field smearing could be iterated. The smearing involve not just neighboring links but also extends over larger distance, and we should pay to attention smearing effect in asymptotic behaviors with strong interactions of the propagators.

4.5 Wrapping around effect

When pion mass is heavy, the pion electromagnetic form factor is extracted by fitting plateau of $R(q,t)$ as constant. We could obtain the form factors when one pion from source to current and the other pion from sink to current (left side of the Fig. 4.4). While pion mass is light, current time dependence appears in $R(q,t)$. We should not only take usual form factor but also other effect into account; this is " pion wrapping around effect (2 pions effect) ". This effect is derived from periodic boundary condition in temporal direction (this is similar to the situation of Ref. [35]). If pion mass is light, pion which goes beyond the temporal boundary from sink (source) is not damped enough by $\exp(-E_\pi \times t)$, Therefore pion remains on source (sink), and the propagation to the current could be considered 2 pions propagation after merging other pion (right side of the Fig. 4.4). The effect does not appear in Dirichlet boundary condition.

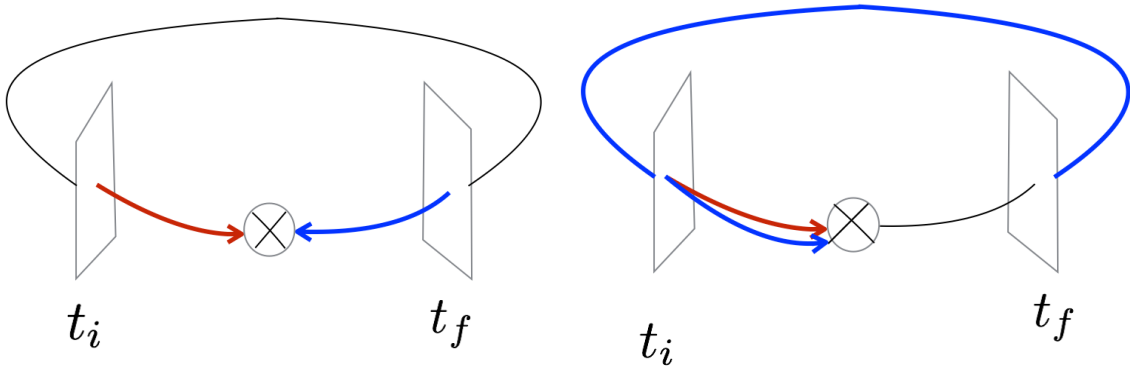

Figure 4.4: Diagrams of pion propagation in periodic boundary condition. Red arrow is the pion which propagates from source (t_i). Blue arrow is the pion which propagates from sink (t_f). The left panel is the diagram of usual form factor. Each pion goes to current without 2-pion propagation. The right panel is the diagram of pion wrapping around effect.

Thus, we assume this fit form of $R(q,t)$,

$$f_0 + f_1 \times \frac{e^{-E_{2\pi}\times t}e^{-E_\pi\times(T-t_f)} - e^{-E_{2\pi}\times(t_f-t)}e^{-m_\pi\times(T-t_f)}}{e^{-E_\pi\times t}e^{-m_\pi\times(t_f-t)}}, \tag{4.5.1}$$

if $(t_i =)0 < t < t_f$. $E_{2\pi} = E_\pi + m_\pi + \Delta E$. ΔE is finite size effect of 2 pions. There are 2 free fit parameters; f_0 is the quantity of form factor and f_1 is the quantity which is derived from the matrix element $\langle \pi\pi | V_\mu | 0 \rangle$. The relative minus sign in the second term of (6.3.2) is derived from the switching local pion operator across gamma matrix γ_μ of current from other local pion operator in three-point function. However thanks to large box calculation, we assume that the finite size effect is negligible.

In the calculations of three-point functions, not only the calculations with two quark propagators in the same (anti)periodic boundary conditions of temporal direction, but also the calculations with quark propagator with source momentum $\vec{p_i} = \vec{0}$ (number 1 propagator corresponding the red line in the Fig.4.1) in anti-periodic boundary conditions of temporal direction is performed. And then the result of these two calculations combined for suppressing the wrapping around effect.

The discussion could be extended not only effect of two other mesons, for example kaon, but two alternating mesons, for example combination of kaon and pion, such as semileptonic form factor analysis. However other meson mass is heavier than pion mass, thus the wrapping around effects might be small due to the meson temporal propagation damping by $\exp(-m_X t)$, where m_X is X meson.

Chapter 5

Chiral perturbation theory

In this chapter, we present the brief of chiral perturbation theory (ChPT), which is effective theory of low energy QCD formulated by S. Weinberg [8] and developed by J. Gassor and H. Leutwyler [9–11]. The idea of ChPT is to expand by some energy parameter *i.e.* quark mass and momentum of Goldstone boson in the low energy level. In this work, we use the idea to obtain the form factors as functions of momentum transfer.

5.1 The ideas of ChPT

The QCD Lagrangian for the number N_f of quarks, is given by

$$\mathcal{L}^{QCD} = \Sigma_f \bar{\psi}_f (i\not{D} - M)\psi_f - \frac{1}{4} Tr(F_{\mu\nu}F^{\mu\nu}), f = (u, d, s \cdots), \tag{5.1.1}$$

where $\not{D}$ is the covariant derivative ($D_\mu = \partial_\mu - igT^a/2A^a_\mu$) dotted Dirac matrix γ_μ with the strong coupling constant g, the generator of color $SU(3)$ $T^a, (a = 1, \ldots, 8)$ and gluon field A^a. M is the quark mass matrix $M = diag(m_u, m_d, m_s, \cdots)$ and gluon field strength is given by $F^a_{\mu\nu} = \partial_\mu A^a_\nu \partial_\nu A^a_\mu + gf_{abc}A^b_\mu A^c_\nu$ with the structure constant of $SU(3)$ f_{abc}. Low energy experiments are performed with states of hadron while $\mathcal{L}^{QCD}$ describes the quark and gluon dynamics. In addition, the coupling constant g at low energy, in the covariant derivative and the field strength, is not appropriate for a perturbative expansion. Thus, some effective field theory is helpful.

The chirality is defined by the eigenvalue ± 1 of γ_5. The γ_5 is described by chiral representation,

$$\gamma_5 = \begin{pmatrix} 1 & 0 \\ 0 & -1 \end{pmatrix} = i\gamma_0\gamma_1\gamma_2\gamma_3, \tag{5.1.2}$$

and the eigenstate is defined by two-component spinors ξ, ζ,

$$\psi = \begin{pmatrix} \xi \\ \zeta \end{pmatrix} = \begin{pmatrix} \xi \\ 0 \end{pmatrix} + \begin{pmatrix} 0 \\ \zeta \end{pmatrix} \equiv \psi_R + \psi_L, \tag{5.1.3}$$

where ψ_L is the left-handed spinor and ψ_R is the right-handed spinor. The projection operators are defined by using γ_5,

$$P_L = \frac{1}{2}(1 - \gamma_5), P_R = \frac{1}{2}(1 + \gamma_5), \tag{5.1.4}$$

The operators P_L, P_R could decompose the eigenstate into ψ_L, ψ_R, respectively. The hermitian eigenstate of ψ_L, ψ_R

$$\bar{\psi}_L = \psi_\dagger P_L \gamma_0 = \bar{\psi} P_R, \bar{\psi}_R = \psi_\dagger P_R \gamma_0 = \bar{\psi} P_L, \tag{5.1.5}$$

The mass term $\bar{\psi}\psi$ and the kinetic term $\bar{\psi}\gamma_\mu\psi$ of the QCD Lagrangian (5.1.1) could be rewritten by those spinors.

$$\begin{aligned}
\bar{\psi}\psi &= \bar{\psi}_R\psi_R + \bar{\psi}_R\psi_L + \bar{\psi}_L\psi_R + \bar{\psi}_L\psi_L, \\
&= \bar{\psi}P_L P_R\psi + \bar{\psi}P_L P_L\psi + \bar{\psi}P_R P_R\psi + \bar{\psi}P_R P_L\psi, \\
&= \bar{\psi}_R\psi_L + \bar{\psi}_L\psi_R, \qquad (5.1.6) \\
\bar{\psi}\gamma_\mu\psi &= \bar{\psi}_R\gamma_\mu\psi_R + \bar{\psi}_L\gamma_\mu\psi_L. \qquad (5.1.7)
\end{aligned}$$

Thus, the QCD Lagrangian could be described as follow.

$$\mathcal{L}^{QCD} = \Sigma_f \left(\bar{\psi}_{R,f} i\not{D}\psi_{R,f} + \bar{\psi}_{L,f} i\not{D} + m_f(\psi_{L,f}\bar{\psi}_{R,f}\psi_{L,f} + \bar{\psi}_{L,f}\psi_{R,f})\right) - \frac{1}{4}Tr(F_{\mu\nu}F^{\mu\nu}). \tag{5.1.8}$$

The kinetic terms in (5.1.8) are decomposed into left-handed components and right-handed components. However, The mass terms in (5.1.8) are mixed these components. In the massless limit of quarks, the Lagrangian is invariant under a global $U(N_f)_L \times U(N_f)_R = SU(N_f)_L \times SU(N_f)_R \times U(1)_L \times U(1)_R$ transformation.

$$(\psi_L, \psi_R) \to (V_L\psi_L, V_R\psi_R), (V_L \in U(N_f)_L, V_R \in U(N_f)_R), \tag{5.1.9}$$

and more specifically, the massless limit of quarks under $SU(N_f)_L \times SU(N_f)_R$ transformation is so called *chiral limit*. The transformations could be described as follows

$$(\psi_L, \psi_R) \to (U_L\psi_L, U_R\psi_R), \tag{5.1.10}$$

$$U_L = \exp\left[i\sum_{a=1}\theta_L^a\frac{t^a}{2}\right] \in SU(N_f)_L, U_R = \exp\left[i\sum_{a=1}\theta_R^a\frac{t^a}{2}\right] \in SU(N_f)_R, \tag{5.1.11}$$

where t_a is the generator of $SU(N_f)$ and h_{abc} is structure constant, which satisfy

$$[t_a, t_b] = ih_{abc}t_c, Tr(t_a t_b) = 2\delta_{ab}. \tag{5.1.12}$$

In chiral limit, a Lagrangian is invariant under the transformations, this Lagrangian has *chiralsymmetry*. Considering the QCD Lagrangian is in chiral limit,

$$\mathcal{L}^{QCD_0} = \Sigma_f \left(\bar{\psi}_{R,f} i\not{D}\psi_{R,f} + \bar{\psi}_{L,f} i\not{D})\right) - \frac{1}{4}Tr(F_{\mu\nu}F^{\mu\nu}). \tag{5.1.13}$$

the noethor currents and charges which have $SU(N_f)_L \times SU(N_f)_R$ symmetry is as follows

$$L_\mu^a = \bar{\psi}_L i\gamma_\mu\frac{t^a}{2}\psi_L, Q_L^a = \int d^3x L_0^a, \tag{5.1.14}$$

$$R_\mu^a = \bar{\psi}_R i\gamma_\mu\frac{t^a}{2}\psi_R, Q_R^a = \int d^3x R_0^a. \tag{5.1.15}$$

These charges satisfies $SU(N_f)_L \times SU(N_f)_R$ algebra,

$$[Q_L^a, Q_L^b] = ih_{abc}Q_L^c, [Q_R^a, Q_R^b] = ih_{abc}Q_R^c, [Q_L^a, Q_R^b] = 0. \tag{5.1.16}$$

These chiral transformation could be rewritten by introducing vector transformation $V = L + R$ and axial vector transformation $A = L - R$. The symmetry group could be rewritten as $U(N_f)_L \times U(N_f)_R \to SU(N_f)_V \times SU(N_f)_A \times U(1)_V \times U(1)_A$. The baryon number conservation is introduced by the $U(1)_V$ symmetry. The $U(1)_A$ is not a symmetry of quantum theory in full order due to anomaly of vector current divergence. $SU(N_f)_V \times SU(N_f)_A$ transformations are described as follows

$$\psi \to V\psi, \psi \to A\psi, \tag{5.1.17}$$

$$U_V = \exp\left[i\sum_{a=1} \theta_V^a \frac{t^a}{2}\right], U_A = \exp\left[i\sum_{a=1} \gamma_5 \theta_A^a \frac{t^a}{2}\right]. \tag{5.1.18}$$

The vector current V_μ^a and axial vector current A_μ^a are presented as

$$V_\mu^a = R_\mu^a + L_\mu^a = \bar{\psi} i\gamma_\mu \frac{t^a}{2}\psi, \tag{5.1.19}$$

$$R_\mu^a = R_\mu^a - L_\mu^a = \bar{\psi} i\gamma_5\gamma_\mu \frac{t^a}{2}\psi, \tag{5.1.20}$$

and then the corresponding noether charges are rewritten by (5.1.14)

$$Q_V^a = Q_R^a + Q_L^a, Q_A^a = Q_R^a - Q_L^a. \tag{5.1.21}$$

The commutative relations are presented as follows

$$[Q_V^a, Q_V^b] = ih_{abc}Q_V^c,\ [Q_A^a, Q_A^b] = ih_{abc}Q_V^c,\ [Q_V^a, Q_A^b] = ih_{abc}Q_A^c. \tag{5.1.22}$$

The relations shows that the vector transformation is closed, However the axial vector transformation is not algebraic closed. In other words the axial vector transformation is not group.

For Heisenberg equations of QCD hamiltonian H^{QCD},

$$[H^{QCD}, Q_V^b] = 0,\ [H^{QCD}, Q_A^b] = 0. \tag{5.1.23}$$

The hamiltonian has some symmetries under the vector transformation and the axial vector transformation, thus spectra of some hadron mass might have some effects of the symmetry. Considering the isospin symmetry ($SU(2)_V$), in the case of meson, the charged pion mass $m_{\pi^\pm} = 0.13957$ GeV and neutral pion mass $m_{\pi^0} = 0.134977$ GeV are degenerated approximately. Similarly, in the case of baryon, the proton mass $m_p = 0.93827$ GeV and the neutron mass $m_n = 0.93957$ GeV are degenerated approximately too. However, Considering the axial transformation (like parity transformation), in the case of meson, the nearest partner of pion ($J^P = 0^-$) is a_0 ($J^P = 0^+$). the mass of the $m_{a_0} = 0.980$ GeV. Thus, we consider that the experimental results is not reflected the symmetry under the axial vector transformation. The fact indicates that the symmetry under the axial vector transformation breaks.

The $N_f^2 - 1$ axial charge generate $N_f^2 - 1$ massless Goldstone boson, which could be considered the three pions for $N_f = 2$ and, the three pions, the four kaons and single eta meson for $N_f = 3$. The

quark mass is performed as perturbation of ChPT, and therefore the quark masses clearly break the symmetry, these Goldstone boson are not massless. The effective Lagrangian is built so that it respects the symmetries of the QCD Lagrangian, for instance $SU(N_f)_L \times SU(N_f)_R$, charge conjugation, parity, time reversal and Lorentz invariance, and describes the dynamics of the Goldstone bosons at low energy.

The Goldstone bosons are written in terms of a unitary matrix of fields U (specific form in later) that transforms under the chiral symmetry group transformation $SU(N_f)_L \times SU(N_f)_R$ as

$$U \to U_L U U_R^\dagger. \tag{5.1.24}$$

The effective Lagrangian $\mathcal{L}^{Ch}$ is introduced so that it has $SU(N_f)_L \times SU(N_f)_R$ symmetry and is expanded in terms of powers of derivatives of the goldstone bosons' field matrix U

$$\mathcal{L}^{eff}(U, \partial U, \partial^2 U, \cdots) = \sum_{n=1} \mathcal{L}_{2n}. \tag{5.1.25}$$

The index $2i$ in L_{2i} stands for the number of derivatives of U. Only even powers of derivatives could occur in the Lagrangian. This is because the Lagrangian has Lorentz invariance in other words the Lagrangian is supporsed to be a Lorentz scalar. The quark masses which clearly break the symmetry are introduced in such a method, that the mass term in the effective Lagrangian has chiral symmetry. The behavior under $SU(N_f)_L \times SU(N_f)_R$ chiral transformation of the quark mass matrix M is assumed to be

$$M \to U_L M U_R^\dagger. \tag{5.1.26}$$

The mass terms in(5.1.1) is $SU(N_f)_L \times SU(N_f)_R$ chiral transformation and then the chiral symmetry in the effective theory is broken in the same mechanism as in QCD.

More general form of the QCD Lagrangian in the assumption of external sources is given by

$$\mathcal{L}^{QCD,ext} = \Sigma_f \bar{\psi}_f (i \not{D}) \psi_f - \frac{1}{4} Tr(F_{\mu\nu} F^{\mu\nu}) + \Sigma_f \bar{\psi}_f (i \not{\psi} + \frac{\not{\psi}^{(s)}}{3} + \gamma_5 \not{\phi}) \psi_f + \Sigma_f \bar{\psi}_f (s - i\gamma_5 p) \psi_f, \tag{5.1.27}$$

where the $v_\mu^{(s)}$ is singlet vector current, the $v_\mu = v_\mu^a \frac{\lambda^a}{2}$ are vector currents, the $a_\mu = a_\mu^a \frac{\lambda^a}{2}$ are axial vector currents, the $s_\mu = s^a \frac{\lambda^a}{2}$ are scalar currents, the $p_\mu = p^a \frac{\lambda^a}{2}$ are pseudoscalar currents, and $\lambda^a, (a = 1, \ldots, 8)$ are the 3×3 matrices . The QCD Lagrangian (5.1.1) in $N_f = 3$ is reconstructed from (5.1.27) by fixing $v_\mu^{(s)} = v_\mu = a_\mu = p = 0$, $s = M$. The global chiral symmetry group is $SU(N_f)_L \times SU(N_f)_R \times U(1)_V$, which could be promoted to a local one by introducing the appropriate transformation behavior of the external sources. $\mathcal{L}^{QCD,ext}$ in terms of left-handed and right-handed currents with the help of

$$v_\mu = \frac{(r_\mu + l_\mu)}{2}, a_\mu = \frac{(r_\mu - l_\mu)}{2}, \tag{5.1.28}$$

$$\bar{\psi}(s - i\gamma_5 p)\psi = \bar{\psi}_L (s - i\gamma_5 p)\psi_R + \bar{\psi}_R (s - i\gamma_5 p)\psi_L, \tag{5.1.29}$$

is rewritten as without flavor index

$$\begin{aligned}\mathcal{L}^{QCD,ext} &= \bar{\psi}(i\not{D})\psi - \frac{1}{4}Tr(F_{\mu\nu}F^{\mu\nu}) \\ &+ \bar{\psi}_L(\not{l} + \frac{\not{v}^{(s)}}{3})\psi_R + \bar{\psi}_R(\not{r} + \frac{\not{v}^{(s)}}{3})\psi_L \\ &+ \bar{\psi}_L(s - i\gamma_5 p)\psi_R + \bar{\psi}_R(s - i\gamma_5 p)\psi_L. \end{aligned} \tag{5.1.30}$$

The quarks and external fields locally transform as

$$\begin{aligned}\psi_L &\to \exp(-i\alpha(x))V_L(x)\psi_L, \\ \psi_R &\to \exp(-i\alpha(x))V_R(x)\psi_R, \\ l_\mu &\to V_L(x)l_\mu V_L^\dagger(x) + iV_L(x)\partial_\mu V_L^\dagger(x), \\ r_\mu &\to V_R(x)r_\mu V_R^\dagger(x) + iV_R(x)\partial_\mu V_R^\dagger(x), \\ v_\mu^{(s)} &\to v_\mu^{(s)} - \partial_\mu\alpha(x), \\ s + ip &\to V_R(x)(s + ip)V_L^\dagger(x), \\ s - ip &\to V_L(x)(s - ip)V_R^\dagger(x), \end{aligned}$$

where $V_R(x), V_L(x)$ are the matrices which represent local $SU(3)$ transformations, $\alpha(x)$ is a parameter. (5.1.30) is invariant under these local transformations. In order to embed the local symmetry into the effective Lagrangian $\mathcal{L}^{eff}(U, \partial U, \partial^2 U, \cdots; v, a, s, p)$, a covariant derivative D_μ, left-handed field strength tensor $f_{\mu\nu}^L$, right-handed field strength tensor $f_{\mu\nu}^R$ will be introduced

$$\begin{aligned}\partial_\mu U \to D_\mu U &= \partial_\mu U - i(r_\mu U - U l_\mu), \\ f_{\mu\nu}^L &= \partial_\mu l_\nu - \partial_\nu l_\mu - i[l_\mu, l_\nu], \\ f_{\mu\nu}^R &= \partial_\mu r_\nu - \partial_\nu r_\mu - i[r_\mu, r_\nu]. \end{aligned} \tag{5.1.31}$$

According to the power counting scheme,

$$\begin{aligned} U &: O(p^0), \\ \partial_\mu, D_\mu U, r_\mu, l_\mu &: O(p^1), \\ s, p, f_{\mu\nu}^L, f_{\mu\nu}^R &: O(p^2), \end{aligned} \tag{5.1.32}$$

the Lagrangian could be expanded. The generating functional with the QCD Lagrangian $Z_{QCD}(v, a, s, p)$ in the low energy regime is defined by

$$e^{iZ^{QCD}(v,a,s,p)} = \int \mathcal{D}\psi\mathcal{D}\bar{\psi}\mathcal{D}A_\mu^a \exp\left(i\int d^4x \mathcal{L}^{QCD}(\psi, \bar{\psi}, A_\mu^a, v, a, s, p)\right). \tag{5.1.33}$$

It could be approximated by a sequence of effective generating functionals $Z^{eff}(v, a, s, p)$.

$$Z^{eff}(v, a, s, p) = Z_2^{eff} + Z_4^{eff} + \cdots, \tag{5.1.34}$$

which is expanded corresponding to (5.1.25)

Introducing ξ with the (pseudo)scalar external fields

$$\chi = 2B_0(s + ip), \tag{5.1.35}$$

the lowest order of chiral effective Lagrangian $\mathcal{L}_2$ could be constructed including an explicit symmetry breaking mass term and the components (5.1.32), and then this is given as

$$\mathcal{L}_2 = \frac{F_0^2}{4} tr[D_\mu U (D^\mu U)^\dagger] + \frac{F_0^2}{4} tr[\chi U^\dagger + U\chi^\dagger], \tag{5.1.36}$$

with the field matrix U. The parameters F_0, B_0 should be determined by other approaches. And the higher order of chiral effective Lagrangian $\mathcal{L}_{2n}$ could be constructed too.

5.2 Higher order Lagrangian

The Goldstone bosons' field matrix of $U \in SU(3)$ and quark mass matrix M are defined by

$$U(x) = \exp\left(\frac{\sqrt{2}i}{F_0}\phi(x)\right), \phi(x) = \begin{pmatrix} \frac{1}{\sqrt{2}}\pi^0 + \frac{1}{\sqrt{6}}\eta & \pi^+ & K^+ \\ \pi^- & \frac{-1}{\sqrt{2}}\pi^0 + \frac{1}{\sqrt{6}}\eta & K^0 \\ K^- & \bar{K^0} & \frac{-2}{\sqrt{6}}\eta \end{pmatrix},$$
$$M = diag(m_u, m_d, m_s). \tag{5.2.1}$$

The masses of meson in the isospin limit $m_u = m_d$ to the lowest order in the quark mass are given by

$$m_\pi^2 = 2B_0 m_u, m_K^2 = B_0(m_u + m_s), m_\eta^2 = \frac{2B_0}{3}(m_u + 2m_s). \tag{5.2.2}$$

In the reality, we know that isospin symmetry slightly breaks in the strong interaction. The neutral and charged pion mass are equal up to the leading order in the quark mass

$$m_{\pi^0}^2 = m_{\pi^\pm}^2 = B_0(m_u + m_d). \tag{5.2.3}$$

And, the isospin symmetry breaking effect is occured by electromagnetic interactions being of the order $O((m_u + m_d)^2)$.

The $SU(3)$ chiral effective Lagrangian could be expanded until $O(p^6)$ without pure external field terms

$$\mathcal{L}^{SU(3)} = \mathcal{L}_2 + \mathcal{L}_4 + \mathcal{L}_6 + \cdots = \mathcal{L}_2 + \sum_{n=1}^{10} O_i L_i + \sum_{n=1}^{94} P_i C_i + \cdots . \tag{5.2.4}$$

There are coefficients which are scale-dependent values L_i, C_i in the Lagrangian of the higher orders as effective coupling constants. These are so-called *Low Energy Constants* (LEC) of NLO and NNLO, respectively (Discussion about the LECs of NNLO in Ref. [12, 13]). The $O(p^4)$ order of $SU(3)$ chiral

effective Lagrangian $\mathcal{L}_4$ could be constructed the components (5.1.32),

$$\begin{aligned}
\mathcal{L}_4^{SU(3)} &= L_1(tr[D_\mu U(D^\mu U)^\dagger])^2 + L_2 tr[D_\mu U(D^\nu U)^\dagger] tr[D^\mu U(D^\nu U)^\dagger] \\
&+ L_3 tr[D_\mu U(D^\mu U)^\dagger D_\nu U(D^\nu U)^\dagger] + L_4 tr[D_\mu U(D^\mu U)^\dagger] tr[D^\nu U(D^\nu U)^\dagger] \\
&+ L_5 tr[D_\mu U(D^\mu U)^\dagger(\chi U^\dagger + U\chi^\dagger)] + L_6(tr[(\chi U^\dagger + U\chi^\dagger)])^2 \\
&+ L_7(tr[(\chi U^\dagger - U\chi^\dagger)])^2 + L_8 tr[\chi U^\dagger \chi U^\dagger + U\chi^\dagger U\chi^\dagger] \\
&+ -iL_9(tr[f_{\mu\nu}^R D^\mu U(D^\nu U)^\dagger + f_{\mu\nu}^L (D^\mu U)^\dagger D^\nu U]) + L_{10} tr[U f_{\mu\nu}^L U^\dagger f^{R,\mu\nu}] \\
&+ H_1 tr[f_{\mu\nu}^R f^{R,\mu\nu} + f_{\mu\nu}^L f^{L,\mu\nu}] + H_2 tr[\chi\chi^\dagger]. \qquad (5.2.5)
\end{aligned}$$

The LECs $L_i, (i = 1, \cdots, 10)$ could be obtained phenomenologically. H_1 and H_2 are effective coupling constants for pure external fields (no Goldstone boson fields), and therefore they are physically irrelevant.

If we use the SU(2) representation of U which represents the fields of Goldstone bosons. The $SU(2)$ chiral effective Lagrangian could be expanded until $O(p^6)$ without pure external field terms

$$\mathcal{L}^{SU(2)} = \mathcal{L}_2 + \mathcal{L}_4 + \mathcal{L}_6 + \cdots = \mathcal{L}_2 + \sum_{n=1}^{7} O_i l_i + \sum_{n=1}^{57} P_i c_i + \cdots . \qquad (5.2.6)$$

The $O(p^4)$ order of $SU(2)$ chiral effective Lagrangian $\mathcal{L}_4$ could be constructed by the components (5.1.32). The Lagrangian was formulated by Gassor and Leutwyler [9].

$$\begin{aligned}
&\mathcal{L}_4^{GL,SU(2)} = \frac{l_1}{4}(tr[D_\mu U(D^\mu U)^\dagger])^2 + \frac{l_2}{2} tr[D_\mu U(D^\nu U)^\dagger] tr[D^\mu U(D^\nu U)^\dagger] \\
&+ \frac{l_3}{16}(tr[(\chi U^\dagger + U\chi^\dagger)])^2 + \frac{l_4}{4} tr[D_\mu U(D^\mu \chi)^\dagger + D_\mu \chi (D^\mu U)^\dagger] \\
&+ l_5\left(tr[U f_{\mu\nu}^L U^\dagger f^{R,\mu\nu}] - \frac{1}{2} tr[f_{\mu\nu}^R f^{R,\mu\nu} + f_{\mu\nu}^L f^{L,\mu\nu}]\right) \\
&+ i\frac{l_6}{2}(tr[f_{\mu\nu}^R D^\mu U(D^\nu U)^\dagger - f_{\mu\nu}^L (D^\mu U)^\dagger D^\nu U]) \\
&- \frac{l_7}{16}(tr[(\chi U^\dagger - U\chi^\dagger)])^2 + \frac{h_1 + h_3}{4} tr[\chi\chi^\dagger] - 2h_2 tr[f_{\mu\nu}^R f^{R,\mu\nu} + f_{\mu\nu}^L f^{L,\mu\nu}] \\
&+ \frac{h_1 - h_3}{16}\left((tr[(\chi U^\dagger - U\chi^\dagger)])^2 + (tr[(\chi U^\dagger + U\chi^\dagger)])^2 - 2tr[\chi U^\dagger \chi U^\dagger + U\chi^\dagger U\chi^\dagger]\right), \qquad (5.2.7)
\end{aligned}$$

where

$$U(x) = \exp\left(\frac{\sqrt{2}i}{F_0}\phi(x)\right), \phi(x) = \begin{pmatrix} \frac{1}{\sqrt{2}}\pi^0 & \pi^+ \\ \pi^- & \frac{-1}{\sqrt{2}}\pi^0 \end{pmatrix},$$
$$M = diag(m_u, m_d). \qquad (5.2.8)$$

The LECs $l_i, (i = 1, \cdots, 7)$ could be obtained phenomenologically. The constants h_1, h_2 and h_3 are contact terms which depend on the conventions used to specify the time ordered product, they do not appear in observable quantities.

5.3 Meson form factors

In this work, it is sufficient for construction semileptonic form factors to set

$$l_\mu = \frac{g_2}{\sqrt{2}} \begin{pmatrix} 0 & V_{ud}W_\mu^+ & V_{us}W_\mu^+ \\ V_{ud}^* W_\mu^- & 0 & 0 \\ V_{us}^* W_\mu^- & 0 & 0 \end{pmatrix}, r_\mu = 0, s = diag(m_l, m_l, m_s), \tag{5.3.1}$$

where g_2 is the weak coupling constant, corresponding to the Fermi decay constant $g^2/8m_W^2 = G_F/\sqrt{2}$. and for construction electromagnetic form factors to set

$$l_\mu = r_\mu = eA_\mu diag\left(\frac{2}{3}, -\frac{1}{3}, -\frac{1}{3}\right),\ s = diag(m_l, m_l, m_s). \tag{5.3.2}$$

where e is the electric charge, A_μ is classical photon field.

The result of the form factors could be separable by chiral order.

$$f(q^2) = f^{(2)}(q^2) + f^{(4)}(q^2) + \cdots . \tag{5.3.3}$$

The $O(p^2)$ of the semileptonic form factors are given by the current conservation.

$$f_+^{(2)}(q^2) = f_0^{(2)}(q^2) = 1,\ f_0^{(2)}(q^2). \tag{5.3.4}$$

After calculation of tree level and one loop corrections which contribute to the semileptonic form factors (The diagrams of 5.1), the $O(p^4)$ of the semileptonic form factors are given by,

$$\begin{aligned} f_+^{(4)}(q^2) &= -2\frac{q^2}{f_0^2}L_9 + \frac{3}{8f_0^2}(\bar{A}(m_\eta^2) + \bar{A}(m_\pi^2) + 2\bar{A}(m_K^2)) \\ &+ \frac{3}{2f_0^2}(\bar{B}_{22}(m_\pi^2, m_K^2, q^2) + \bar{B}_{22}(m_K^2, m_\eta^2, q^2)), \end{aligned} \tag{5.3.5}$$

$$\begin{aligned} f_-^{(4)}(q^2) &= -2\frac{(m_K^2 - m_\pi^2)}{f_0^2}L_9 + 4\frac{(m_K^2 - m_\pi^2)}{f_0^2}L_5 + \\ &+ \frac{1}{f_0^2}(1/2\bar{A}(m_\eta^2) - 5/12\bar{A}(m_\pi^2) + 7/12\bar{A}(m_K^2) \\ &+ \bar{B}(m_\pi^2, m_K^2, q^2, \mu)(-m_\pi^2/12 - 5m_K^2/12 - 5q^2/12) \\ &+ \bar{B}(m_K^2, m_\eta^2, q^2, \mu)(m_\pi^2/12 - 7m_K^2/12 - q^2/4) \\ &+ \bar{B}_1(m_\pi^2, m_K^2, q^2, \mu)(-7m_\pi^2/12 - 19m_K^2/12 - 5q^2/12) \\ &+ \bar{B}_1(m_K^2, m_\eta^2, q^2, \mu)(-1m_\pi^2/12 + 23m_K^2/12 + q^2/4) \\ &+ \bar{B}_{21}(m_\pi^2, m_K^2, q^2, \mu)(3m_\pi^2/2 - 3m_K^2/2 + 5q^2/6) \\ &+ \bar{B}_{21}(m_K^2, m_\eta^2, q^2, \mu)(3m_\pi^2/2 - 3m_K^2/2 + q^2/2) \\ &+ \bar{B}_{22}(m_\pi^2, m_K^2, q^2, \mu)(-5/6) \\ &+ \bar{B}_{22}(m_K^2, m_\eta^2, q^2, \mu)(-1/2)), \end{aligned} \tag{5.3.6}$$

where, A, B_{ij} are loop integrals in appendix A, f_0 is decay constant in the chiral limit and m_x^2 is the square of X meson ($X = \pi, K, \eta$).

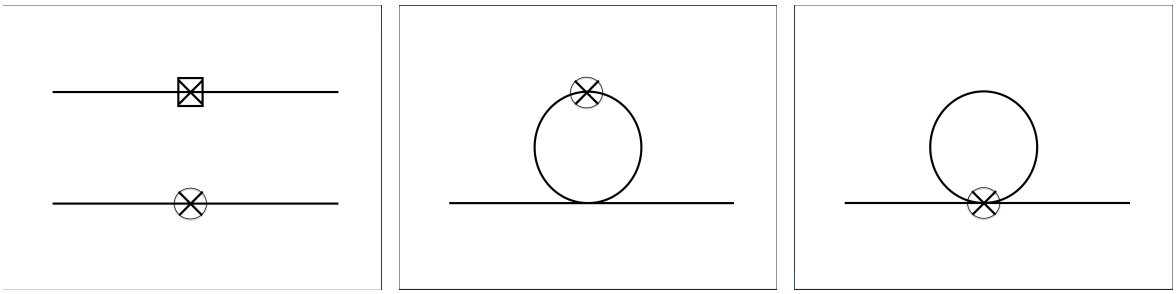

Figure 5.1: Diagrams of of tree level (the left panel) and one loop correction (the two right panels) which contribute to the semileptonic form factors. The circle with cross represents a vertex inserting weak vector current from $\mathcal{L}_2$ and, the square with cross represents a vertex inserting weak vector current from $\mathcal{L}_4$.

The result of $f_{+,0}(q^2=0)$ in $O(p^4)$ analysis is trivial (because of loop integrals of the $O(p^4)$ forms), and therefore we must introduce the some terms of NNLO.

The contribution on $O(p^6)$ of ChPT is given by

$$f_{+,0}^{(6)}(q^2) = f_{+,0}^{C_i,(6)}(t) + f_{+,0}^{L_i,(6)}(t) + (\textit{loop contribution}), \tag{5.3.7}$$

where the term $f^{C_i,(6)}$ is the contribution of LEC of $\mathcal{L}_6$, C_i, the terms $f^{L_i,(6)}$ is the contribution of LEC of $\mathcal{L}_4$, L_i and the term "loop contribution" depends on the irreducible two-loop integrals and reducible ones.

The terms of $O(p^6)$ which depend on only LECs of $\mathcal{L}_6$, C_i is given by

$$\begin{aligned}
f_+^{C,(6)}(q^2) &= \frac{1}{f_0^4}\left[-8(m_\pi^2-m_K^2)^2(C_{12}+C_{34})\right. \\
&+ (-q^2)\{-4m_\pi^2(2C_{12}+4C_{13}+C_{64}+C_{65}+C_{90}) \\
&+ -4m_K^2(2C_{12}+4C_{13}+2C_{63}+2C_{64}+C_{90})\} \\
&+ \left. 4(-q^2)^2(C_{88}+C_{90})\,\right], \qquad (5.3.8)\\
f_-^{C,(6)}(q^2) &= -\frac{(m_\pi^2-m_K^2)}{f_0^4} \\
&\times [\,4m_\pi^2(6C_{12}-4C_{13}+2C_{15}+4C_{17}+2C_{34}+C_{64}+C_{65}+C_{90}) \\
&+ 4m_K^2(6C_{12}+8C_{13}+2C_{14}+4C_{15}+2C_{34}+C_{63}+2C_{64}+C_{90}) \\
&+ 4(-q^2)(-2C_{12}+C_{88}-C_{90})\,]\,. \qquad (5.3.9)
\end{aligned}$$

At $q^2=0$, the parts proportional to $(m_\pi^2-m_K^2)^2$ in $f_{+,0}(0)$ represent the effect of strangeness violating and the breakdown of chiral symmetry, and the linear contribution of $(m_K^2-m_\pi^2)\propto(m_s-m_l)$ (see the Eq.(5.2.2)) vanishes, which is known as "*Ademollo-Gatto thorem*" (see Appendix B and Ref. [5, 50]).

However, it is unstable for using the forms as it is to analyze the momentum dependence of form factors, and the mixture the linear term of $-q^2$ in the NLO form and the one in the NNLO contribution complicates to determine the LECs. Thus we will introduce the analytic term as follows in this work

$$f_{+,0}^{(6)}(q^2) = c_0^{+,0} + c_2^{+,0}(-q^2)^2. \tag{5.3.10}$$

Chapter 6

Results

In this chapter, the results of lattice calculations are shown.

6.1 Set up

We use the configuration generated at the physical point, $m_\pi = 0.135$ GeV, on the large volume corresponding to $La = Ta = 10.8$ fm ($L = T = 128$, $a = 0.084$fm), which is a part of the PACS10 configuration [32]. The configurations were generated by using $N_f = 2+1$ non-perturbative Wilson clover quark action with six stout smearing link [33] (smearing parameter $\rho_{\mu\nu} = \rho = 0.1$) and the improvement coefficient $c_{SW} = 1.11$, and the Iwasaki gauge action [34] at $\beta = 1.82$. The hopping parameters of degenerated light quarks and strange quark are $(\kappa_{ud}, \kappa_s) = (0.126117, 0.124902)$, respectively.

In our form factor calculation, we use 20 configurations in total. We adopt 8 positions of the source time $t_i = 0, 16, 32, 48, 64, 72, 96, 112$ per configuration, and 4 choices of the temporal axis thanks to the hypercube lattice. In the calculation of meson two-point functions and three-point functions, we use $\mathbb{Z}(2) \otimes \mathbb{Z}(2)$ random wall source spread in the spatial sites, and also color and spin spaces [37]. The number of the random source is one in each t_i. The three-point function is calculated by the sequence described in Chapter 4.1 at the sink time slice t_f, where the sink meson momentum is fixed to zero. We choose the temporal separation between the source and sink as $|t_f - t_i| = 36$ (≈ 3.0 fm).

For the constant fits of the quantities $R^X(q,t)$ and $d_{1,2,3}(q,t)$ explained in the above, we use the fit range of $t = 15 - 21$ when $t_i = 0$. We calculate the three-point function of $X, Y (= \pi, K)$ mesons $C_\mu^{XY}(\vec{p}, t)$ with vector currents V_μ, when $X \neq Y$, V_μ is weak vector current of strangeness violating, or when $X = Y$, V_μ is electromagnetic current. We also calculate two-point function of $X (= \pi, K)$ meson $C^X(\vec{p}, t)$ with the momentum $\vec{p} = (2\pi/L)\vec{n}$ of $|\vec{n}|^2 \leq 6$ without the twisted boundary condition which is used to obtain arbitrary momentum of valence quarks (of quark propagators) in previous studies, where $\vec{n}$ is an integer vector. And the number of direction of $\vec{n}$ and the components (of permutations or flipping sign) are chosen as follows (Table 6.1).

$\vert\vec{n}^2\vert = n$	# of direction	$\vec{n}$= ...
$n = 0$	1 (full)	$\vec{n} = (0, 0, 0)$
$n = 1$	6 (full)	$\vec{n} = (1, 0, 0)$
$n = 2$	12 (full)	$\vec{n} = (1, 1, 0)$
$n = 3$	8 (full)	$\vec{n} = (1, 1, 1)$
$n = 4$	6 (full)	$\vec{n} = (2, 0, 0)$
$n = 5$	9	$\vec{n} = (2, 1, 0)$
$n = 6$	9	$\vec{n} = (2, 1, 1)$

Table 6.1: the integer vector which we choose in this work. "(full)" means the full directions which we can take by permutations or flipping sign.

The one elimination jackknife method is employed to estimate the statistical errors.

6.2 Meson two-point and three-point functions

The two-point and three-point functions of mesons we calculate are as follows

$$\begin{aligned} C^X(\vec{p}, t) &= \langle 0|O_X(\vec{p}, t)O_X^\dagger(\vec{p}, 0)|0\rangle, \\ C_\mu^{XY}(\vec{p}, t) &= \langle 0|O_Y(\vec{0}, 36)V_\mu(\vec{q}, t)O_X^\dagger(\vec{p}, 0)|0\rangle, \end{aligned}$$

where the interpolators $O_X^\dagger$, $V_\mu(\vec{q}, t)$ are

$$\begin{aligned} O_\pi^\dagger &= \bar{d}\gamma_5 u, \\ O_K^\dagger &= \bar{s}\gamma_5 u, \\ V_\mu &= \begin{cases} \bar{s}\gamma_\mu u & X \neq Y, \\ \sum_{f=u,d,s} Q_f \bar{\psi}_f \gamma_\mu \psi_f & X = Y. \end{cases} \end{aligned}$$

These functions are needed to construct meson form factors. Because of calculation in $N_f = 2 + 1$, up and down quarks are degenerated.

In the section, the lines in the figures of the results which are colored and the fit forms for effective mass are following the patterns below.

- Periodic Boundary Condition (PBC)(black line) effective mass :fit by $f(t) = A(e^{-m\times t} + e^{-m\times(T-t)})$.
- Anti-PBC(APBC)(red line) effective mass : fit by $f(t) = A(e^{-m\times t} - e^{-m\times(T-t)})$.
- PBC+APBC(P+AP)(green line) effective mass :fit by $f(t) = A(e^{-m\times t} + e^{-m\times(2T-t)})$.

where, A is the parameter as an amplitude of two-point functions. In the result of two-point functions, the PBC means the results in the calculation with two quark propagators in the same (anti)periodic boundary conditions of temporal direction, the APBC means the results of the calculation with quark propagators of two alternating periodic boundary conditions of temporal direction, and the P+AP means the result in the combination of the two calculations.

In the result of three-point functions, the PBC means the results of calculation with two quark propagators in the same (anti)periodic boundary conditions of temporal direction, the APBC means the results of calculation with quark propagator with source momentum $\vec{p}_i = \vec{0}$ (number 1 propagator

corresponding the red line in the Figure 4.1) in anti-periodic boundary conditions of temporal direction, and the P+AP means the result of the combination these two calculations.

The effective mass $m(t)$ is defined by

$$m(t) = ln\frac{C^X(\vec{0}, t, t_i = 0)}{C^X(\vec{0}, t+1, t_i = 0)}. \tag{6.2.1}$$

The two-point function is dominated by the energy of ground state. The effective masses become constant and its curves flatten at the energy of ground state or its mass. In order to obtain the mass of ground state, we solve the equation for m at each time

$$\frac{C^X(\vec{0}, t, t_i = 0)}{C^X(\vec{0}, t+1, t_i = 0)} = \frac{f(t)}{f(t+1)}. \tag{6.2.2}$$

For example, in PBC, the equation is given by

$$\frac{C^X(\vec{0}, t, t_i = 0)}{C^X(\vec{0}, t+1, t_i = 0)} = \frac{\cosh(m(t - \frac{T}{2}))}{\cosh(m(t+1-\frac{T}{2}))}, \tag{6.2.3}$$

and then the mass is extracted from the effective mass plateau.

6.2.1 Two-point functions

Pion two-point functions : $C^{\pi}(\vec{p}, t, t_i = 0)$

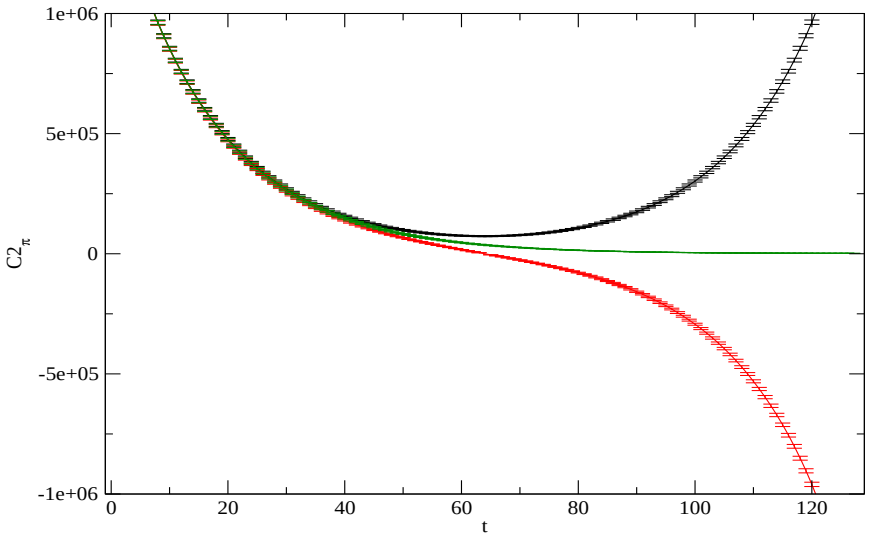

Figure 6.1: pion two-point function of $n = 0$

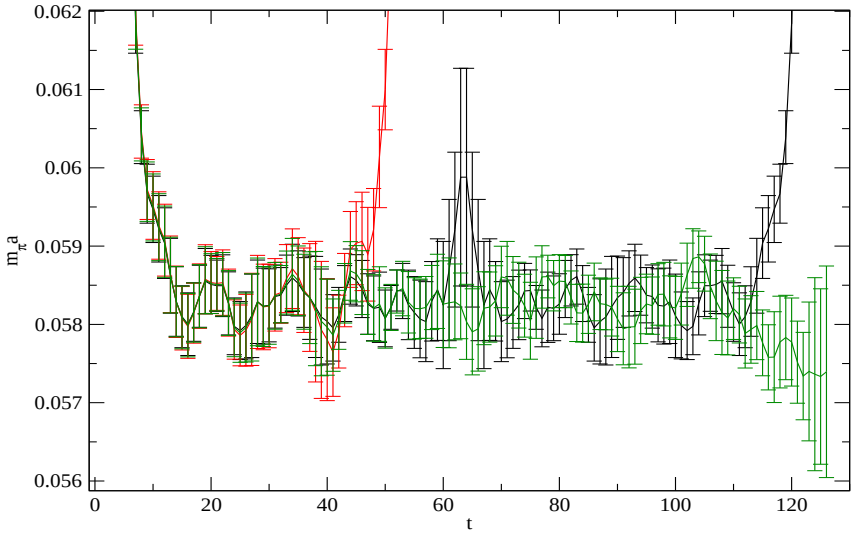

Figure 6.2: time dependence of pion effective mass m by lattice unit

The table of pion masses are as follows

	m_π	m_π(GeV)	$\chi^2/d.o.f$
$PBC(t = 20 - 64)$	0.058289(350)	0.13598(82)	6.75×10^{-4}
$APBC(t = 20 - 63)$	0.058322(347)	0.13607(81)	2.21×10^{-3}
$P + AP(t = 20 - 110)$	0.058294(328)	0.13600(76)	7.82×10^{-4}
$m_{\pi_0}(PDG2018)$	0.1349770(5) GeV	$m_{\pi_\pm}(PDG2018)$	0.13957061(24) GeV

Table 6.2: comparison with pion masses of various conditions and experimental values from PDG [3]. $(t = \cdots)$ means the fit range of the effective mass

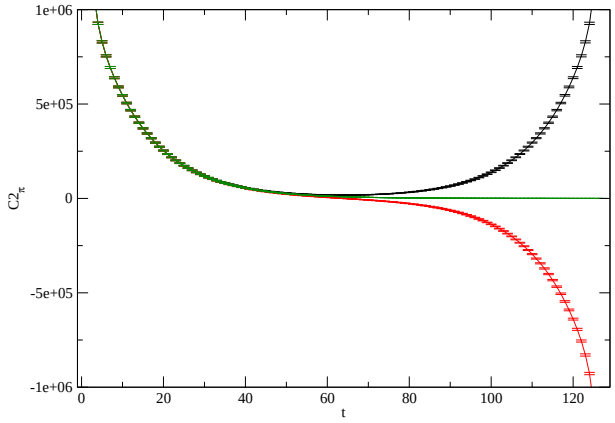

Figure 6.3: pion two-point function of $n = 1$

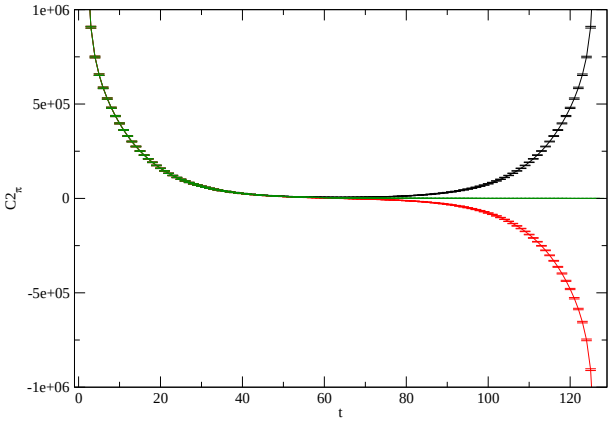

Figure 6.4: pion two-point function of $n = 2$

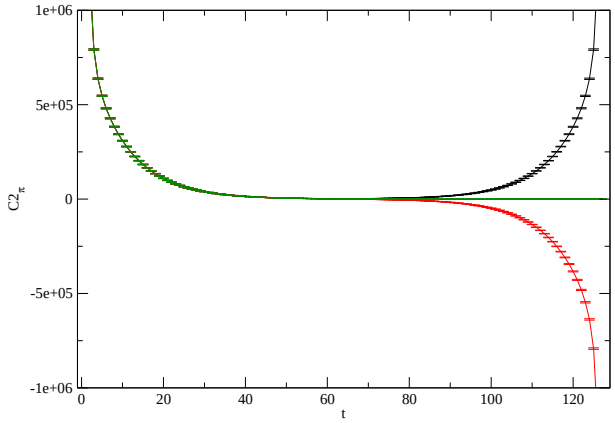

Figure 6.5: pion two-point function of $n = 3$

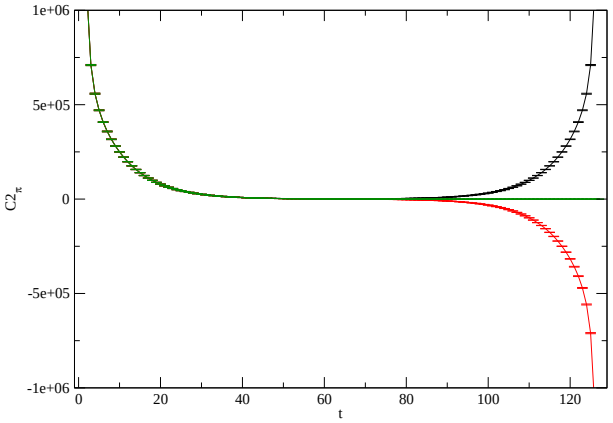

Figure 6.6: pion two-point function of $n = 4$

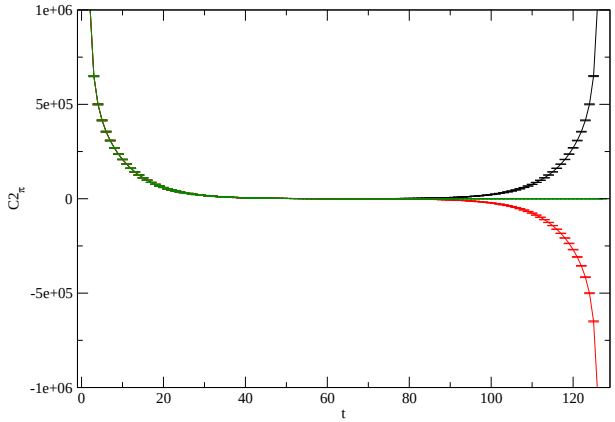

Figure 6.7: pion two-point function of $n = 5$

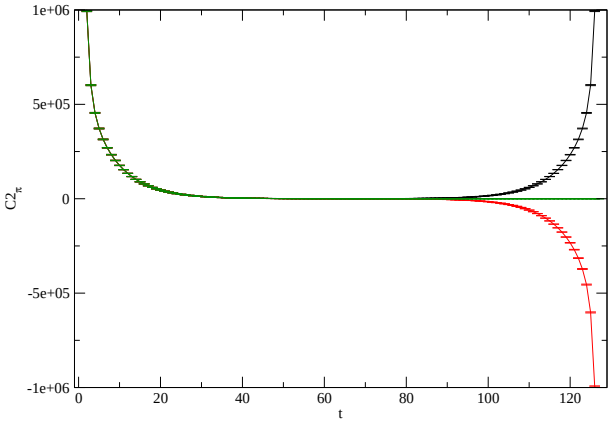

Figure 6.8: pion two-point function of $n = 6$

Kaon two-point functions : $C^K(\vec{p}, t)$

The analysis of Kaon two-point functions could be done in the same way as the pion's one.

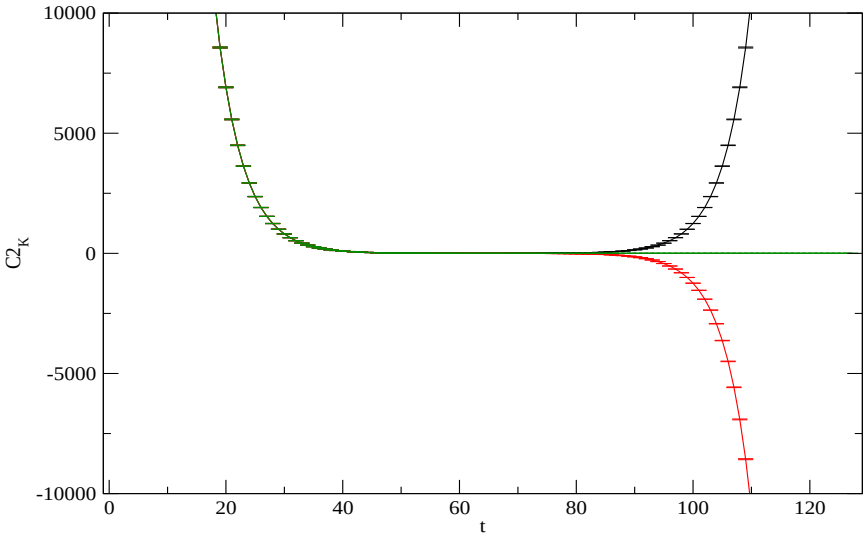

Figure 6.9: kaon two-point function of $n = 0$

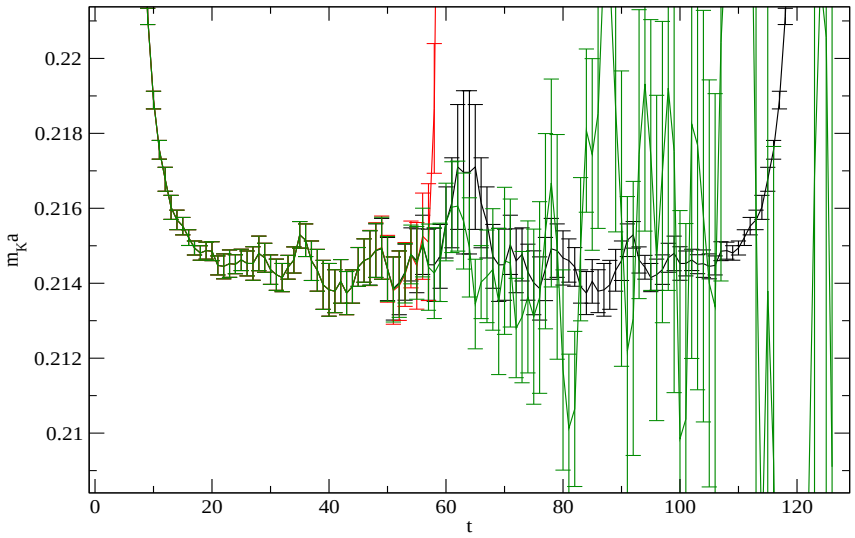

Figure 6.10: time dependence of kaon effective mass $m(t)$ by lattice unit

	m_K	m_K(GeV)	$\chi^2/d.o.f$
$PBC(t = 16 - 64)$	0.21449(110)	0.50041(26)	0.11
$APBC(t = 16 - 63)$	0.21448(109)	0.50038(25)	0.12
$P + AP(t = 16 - 80)$	0.21449(132)	0.50040(31)	0.10
$m_{K_0}(PDG2018)$	0.497611(13) GeV	$m_{K_\pm}(PDG2018)$	0.493677(16) GeV

Table 6.3: comparison with kaon masses of various conditions and experimental values from PDG [3]. $(t = \cdots)$ means the fit range of the effective mass

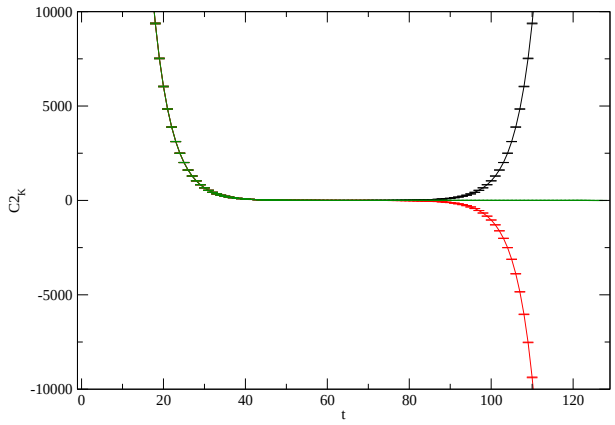

Figure 6.11: kaon two-point function of $n = 1$

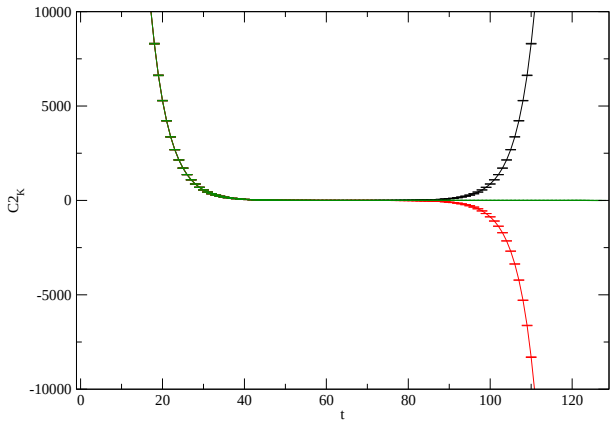

Figure 6.12: kaon two-point function of $n = 2$

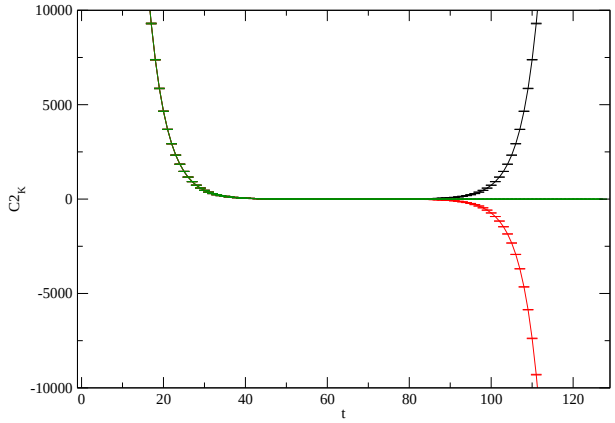

Figure 6.13: kaon two-point function of $n = 3$

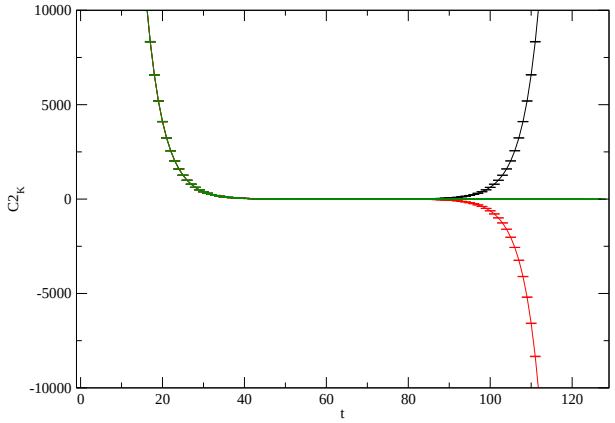

Figure 6.14: kaon two-point function of $n = 4$

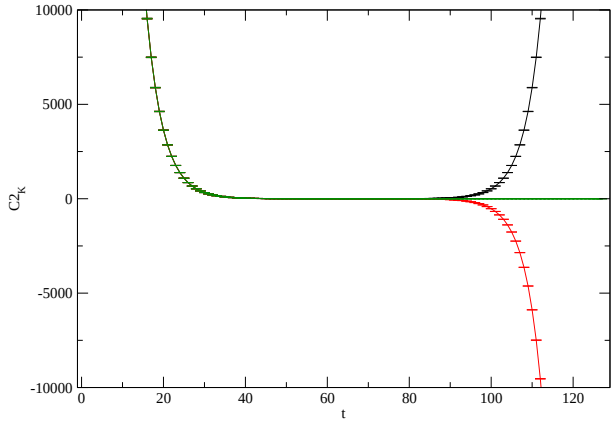

Figure 6.15: kaon two-point function of $n = 5$

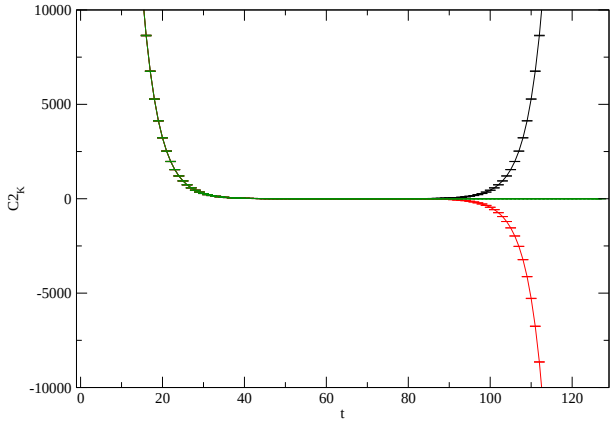

Figure 6.16: kaon two-point function of $n = 6$

The Fig.6.1 and the Fig.6.9 show that the periodicity of the two-point function in P+AP might be twice larger than PBC's one and the plateau in effective mass curve might be extended in the Fig. 6.2 and the Fig. 6.10. However effective mass curve of kaon is noisy in the region $t \geq 80$. The tendency of the two-point function is similar to the two-point functions with non zero momenta and kaon's one. From this effective mass analysis, The pion mass in this work is consistent with experimental value. The kaon mass in this work is slightly higher than experimental value. In the analysis of form factors as follows, we will use the mass of P+AP obtained from these analyses and input energies of mesons are constructed by $E_X = \sqrt{m_X^2 + (\frac{2\pi}{L})^2}$ and the masses.

6.2.2 Three-point functions

Pion three-point functions : $C_4^{\pi\pi}(\vec{p}, t)$

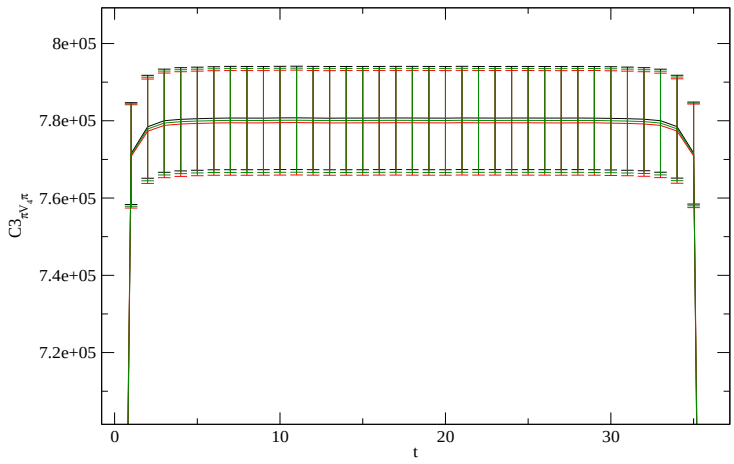

Figure 6.17: pion three-point function of $n = 0$

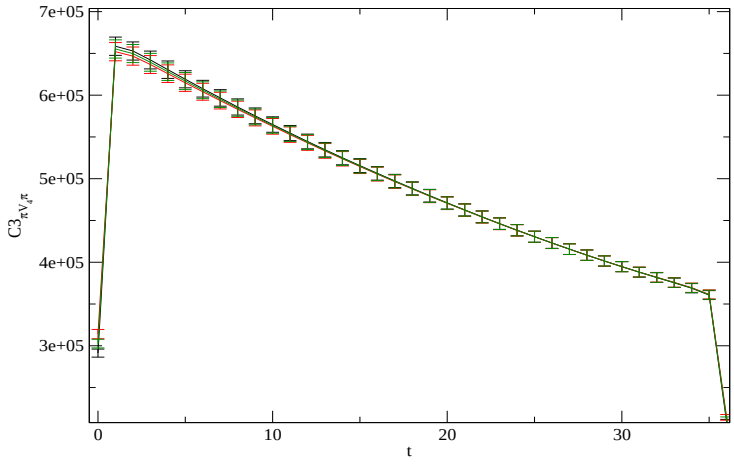

Figure 6.18: pion three-point function of $n = 1$

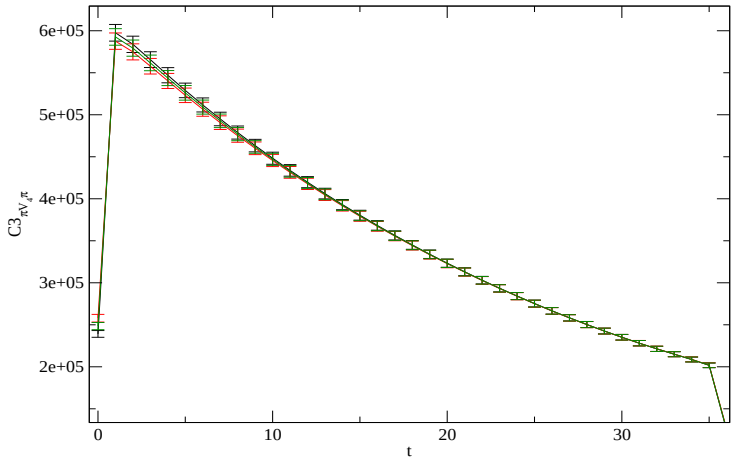

Figure 6.19: pion three-point function of $n = 2$

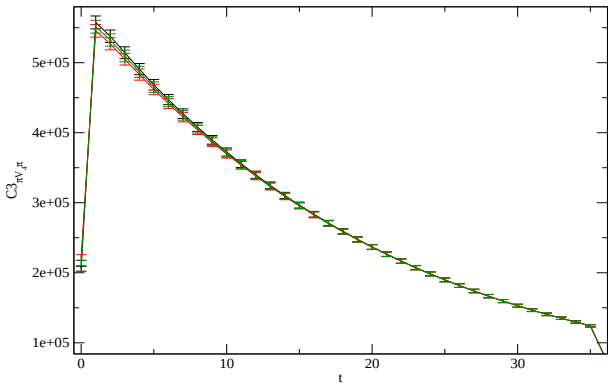

Figure 6.20: pion three-point function of $n = 3$

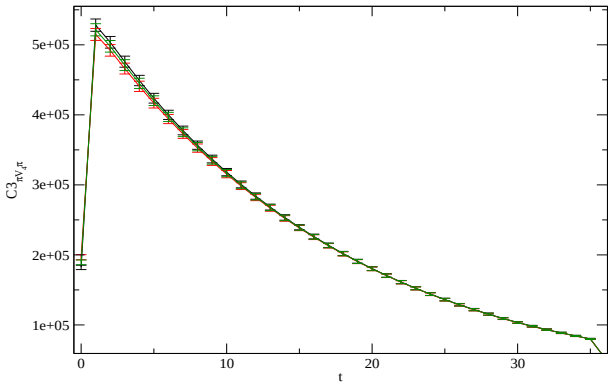

Figure 6.21: pion three-point function of $n = 4$

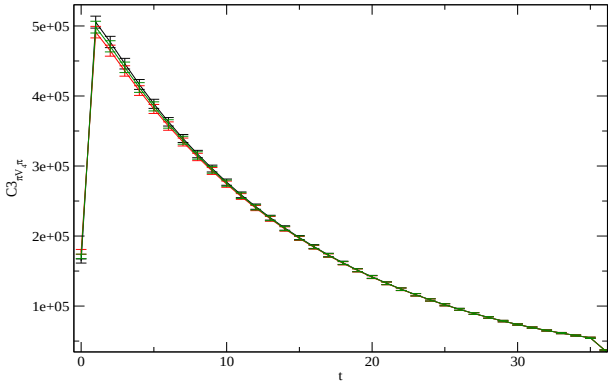

Figure 6.22: pion three-point function of $n = 5$

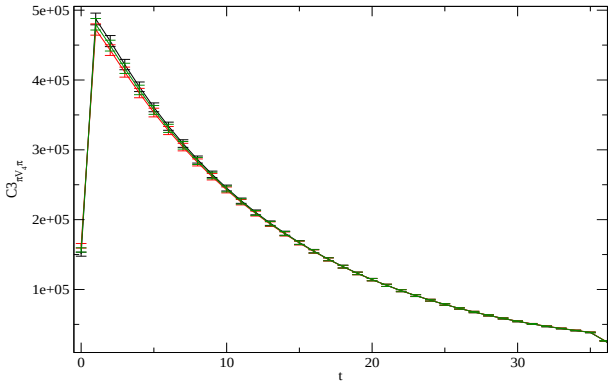

Figure 6.23: pion three-point function of $n = 6$

Pion three-point functions : $C_i^{\pi\pi}(\vec{p}, t)$

Three-point function of V_i is normalized by i-th component of source momentum

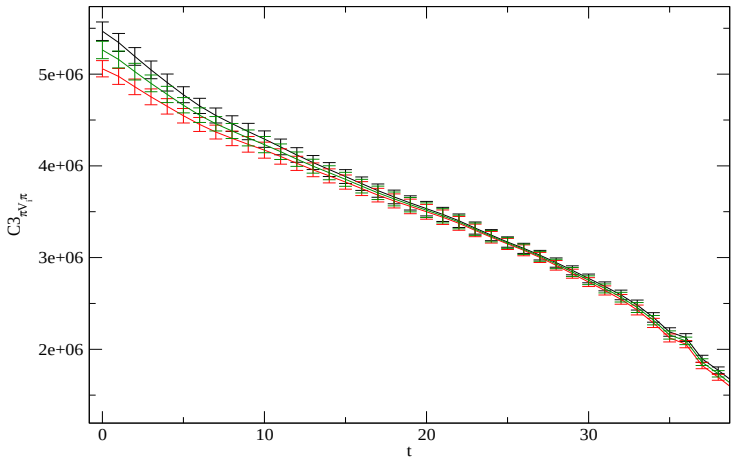

Figure 6.24: pion three-point function of $n = 1$

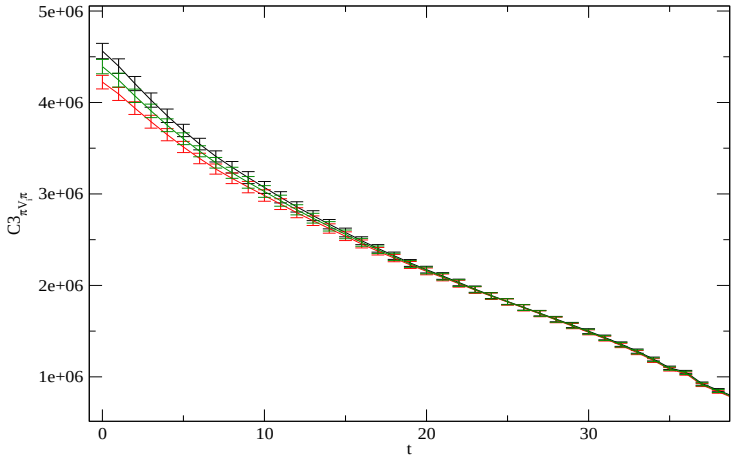

Figure 6.25: pion three-point function of $n = 2$

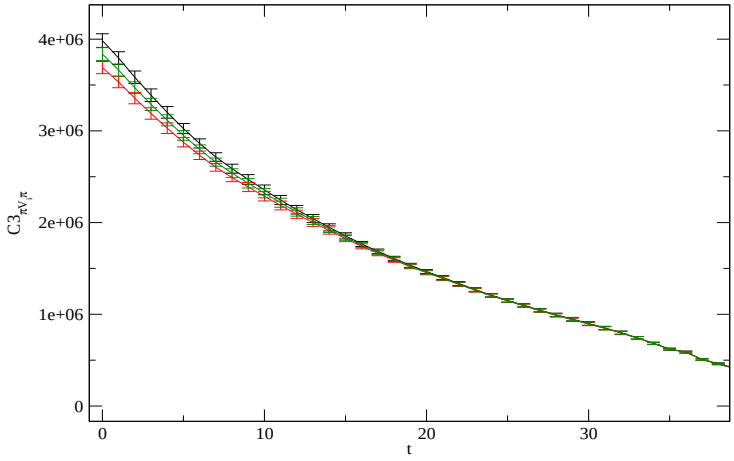

Figure 6.26: pion three-point function of $n = 3$

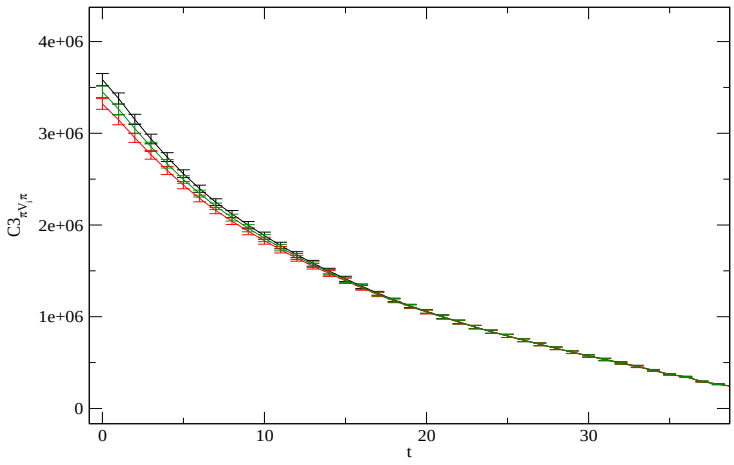

Figure 6.27: pion three-point function of $n = 4$

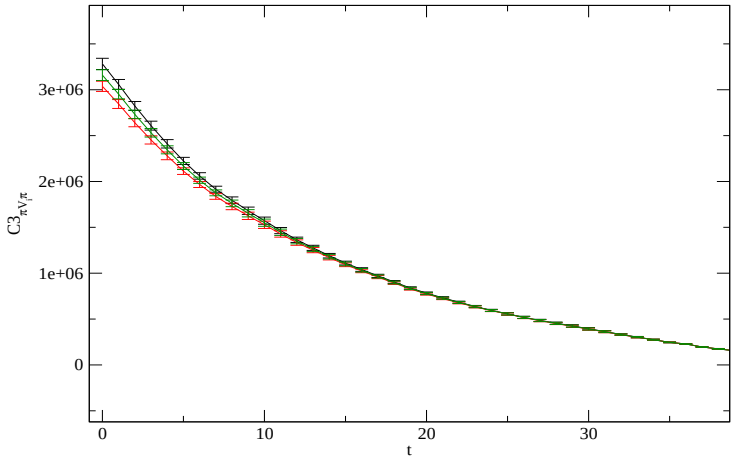

Figure 6.28: pion three-point function of $n = 5$

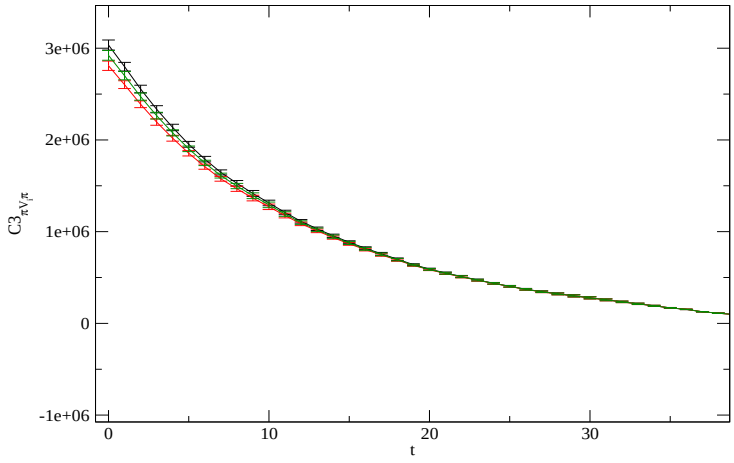

Figure 6.29: pion three-point function of $n = 6$

Kaon three-point functions : $C_4^{KK}(\vec{p}, t)$

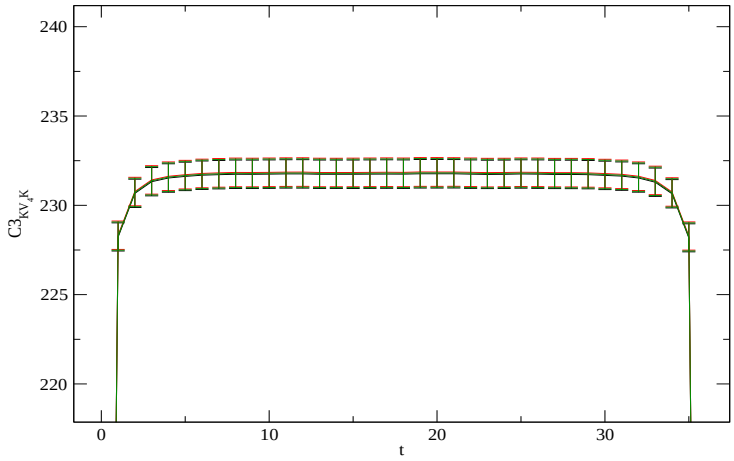

Figure 6.30: kaon three-point function of $n = 0$

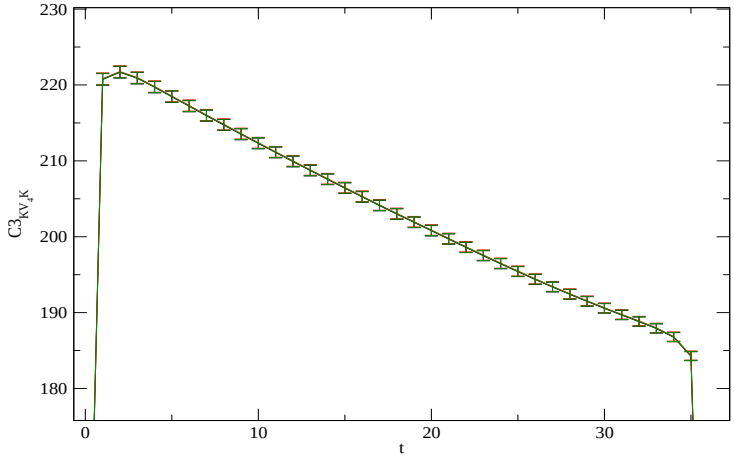

Figure 6.31: kaon three-point function of $n = 1$

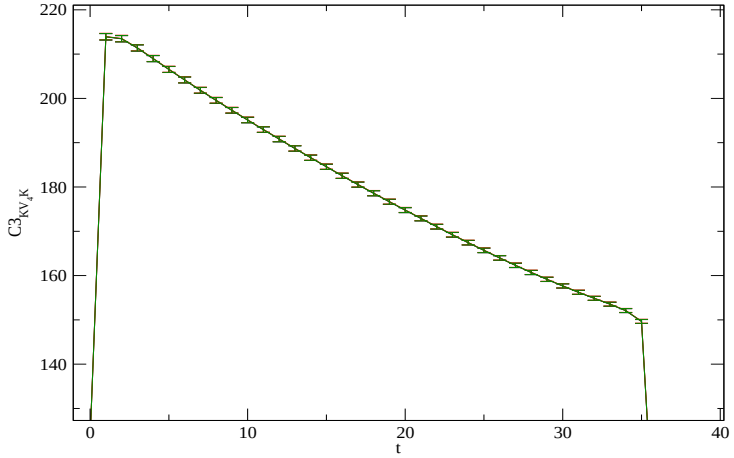

Figure 6.32: kaon three-point function of $n = 2$

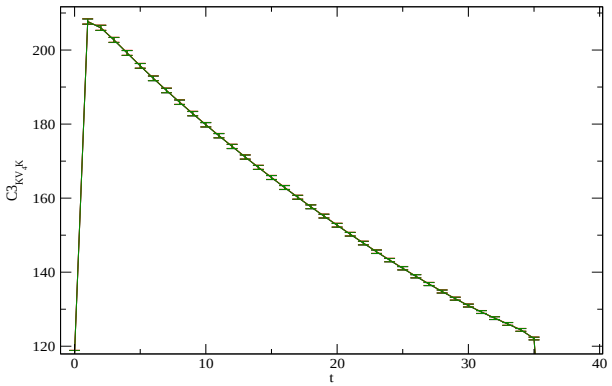

Figure 6.33: kaon three-point function of $n = 3$

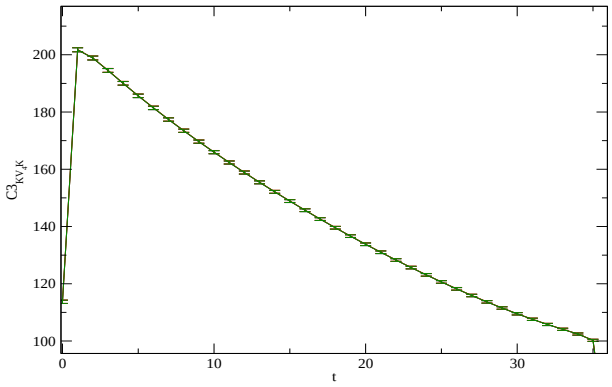

Figure 6.34: kaon three-point function of $n = 4$

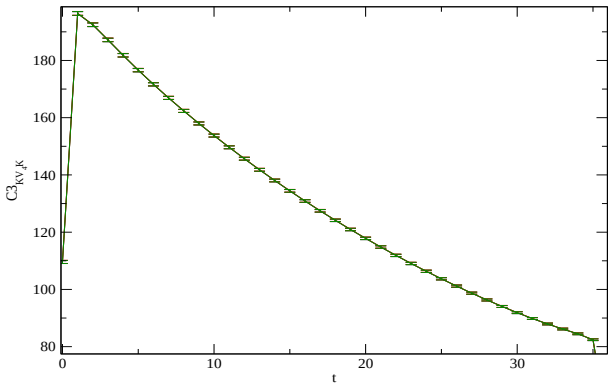

Figure 6.35: kaon three-point function of $n = 5$

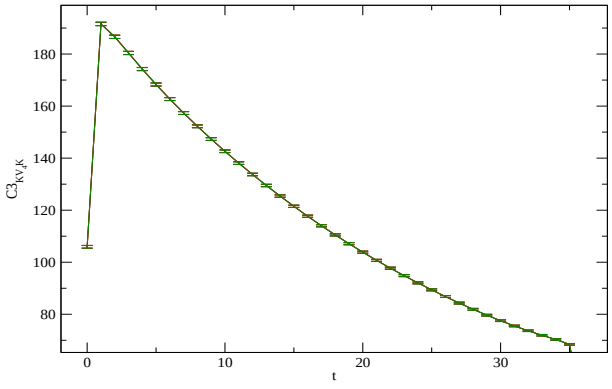

Figure 6.36: kaon three-point function of $n = 6$

Kaon three-point functions : $C_i^{KK}(\vec{p}, t)$

Three-point function of V_i is normalized by i-th component of source momentum

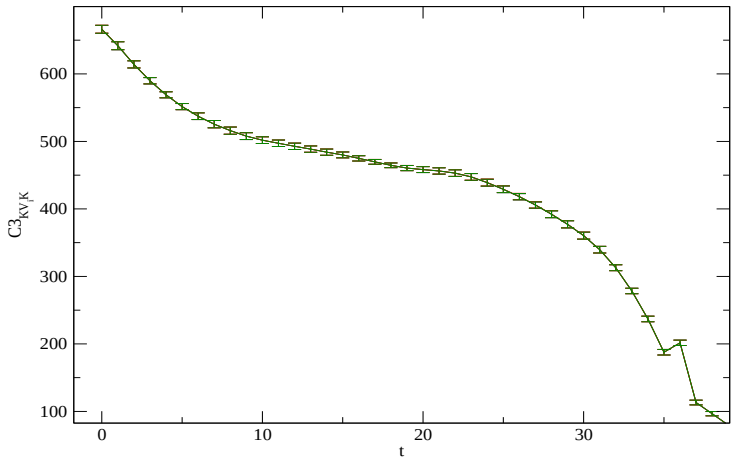

Figure 6.37: kaon three-point function of $n = 1$

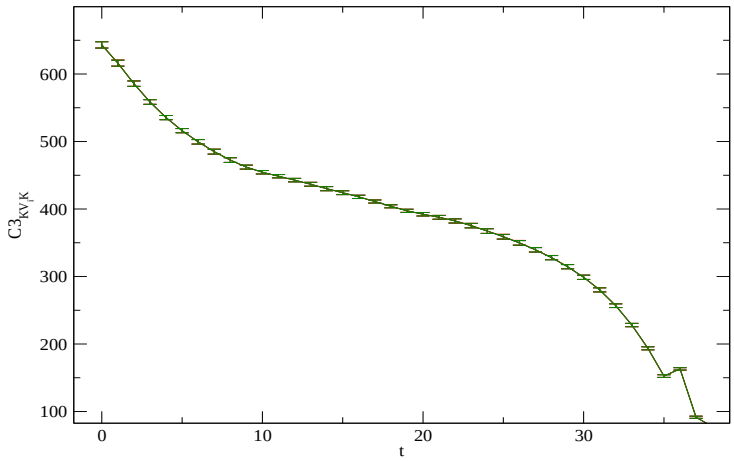

Figure 6.38: kaon three-point function of $n = 2$

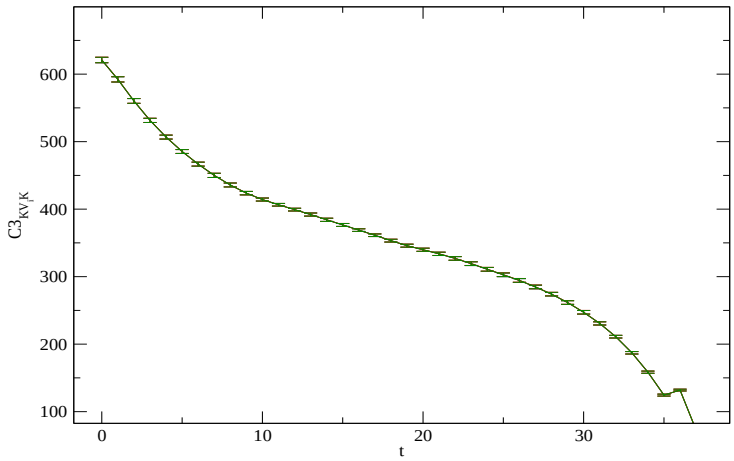

Figure 6.39: kaon three-point function of $n = 3$

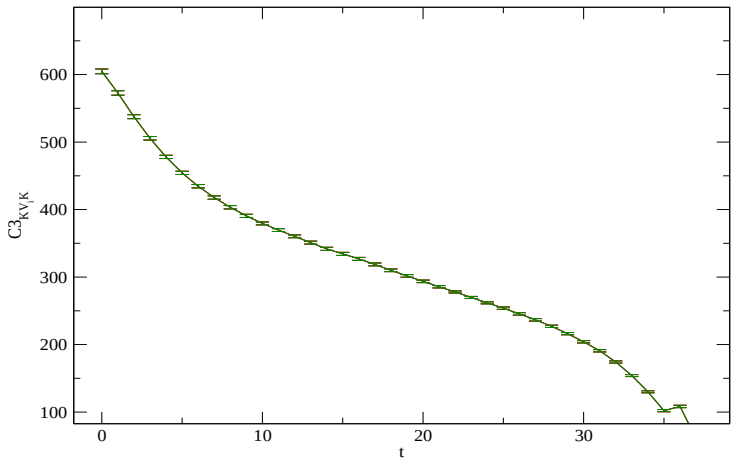

Figure 6.40: kaon three-point function of $n = 4$

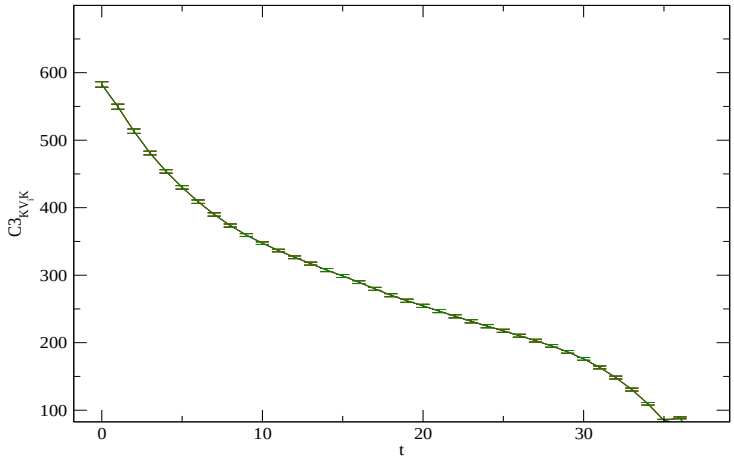

Figure 6.41: kaon three-point function of $n = 5$

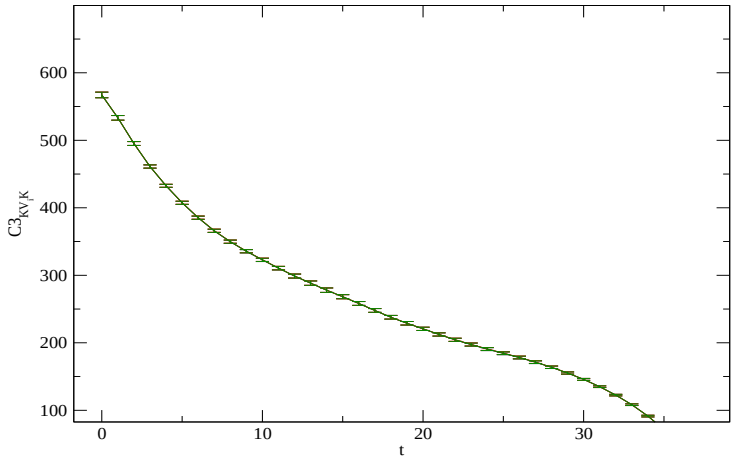

Figure 6.42: kaon three-point function of $n = 6$

Three-point functions : $C_4^{\pi K}(\vec{p}, t)$

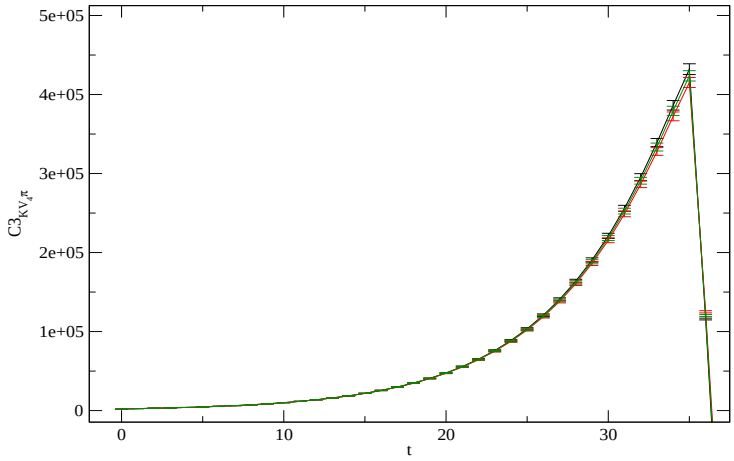

Figure 6.43: kaon three-point function of $n = 0$

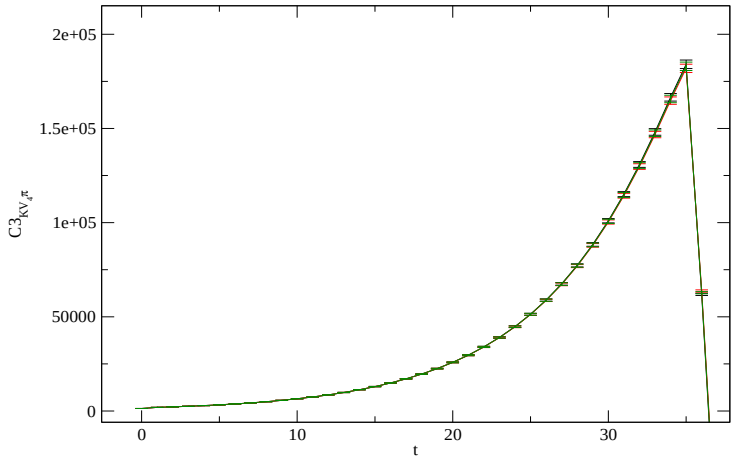

Figure 6.44: three-point function of $n = 1$

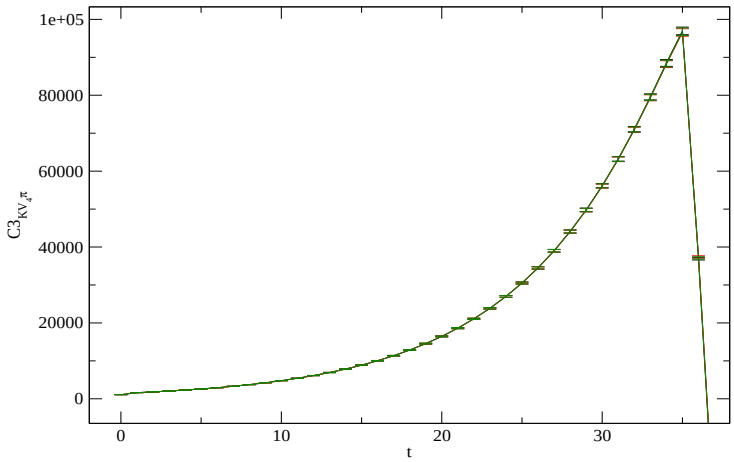

Figure 6.45: three-point function of $n = 2$

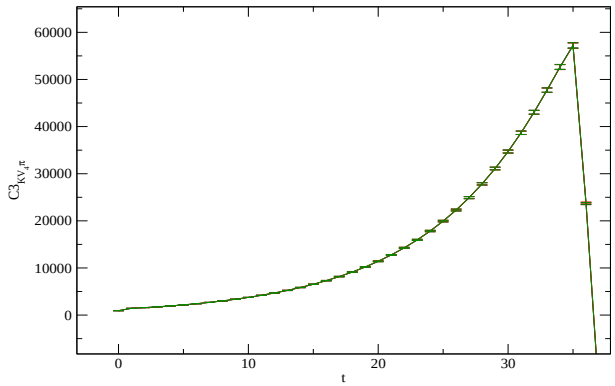

Figure 6.46: three-point function of $n = 3$

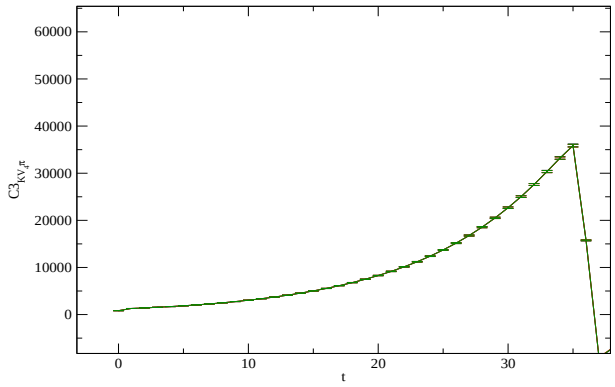

Figure 6.47: three-point function of $n = 4$

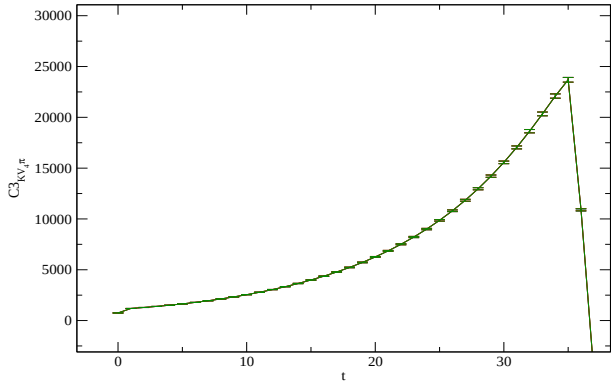

Figure 6.48: three-point function of $n = 5$

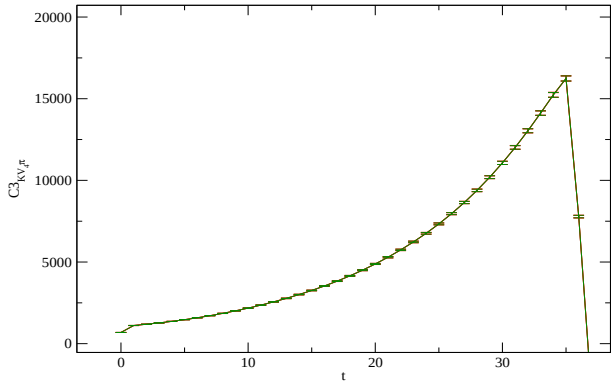

Figure 6.49: three-point function of $n = 6$

Three-point functions : $C_i^{\pi K}(\vec{p}, t)$

Three-point function of V_i is normalized by i-th component of source momentum

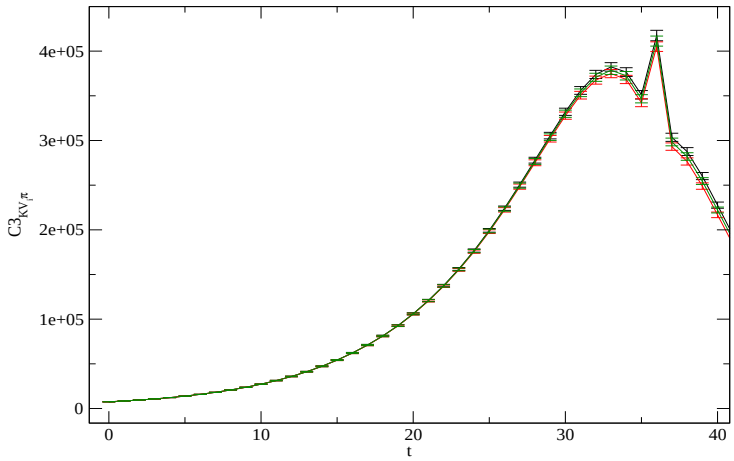

Figure 6.50: three-point function of $n = 1$

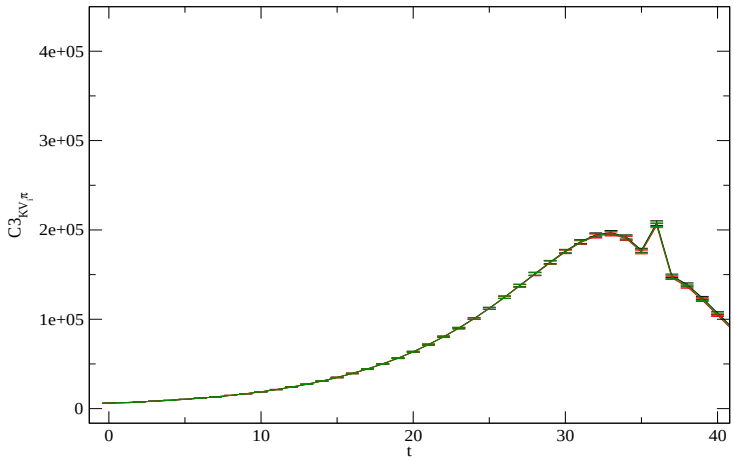

Figure 6.51: three-point function of $n = 2$

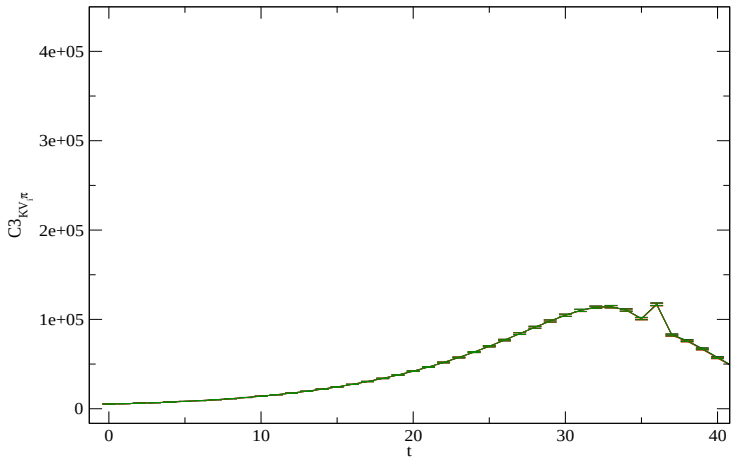

Figure 6.52: three-point function of $n = 3$

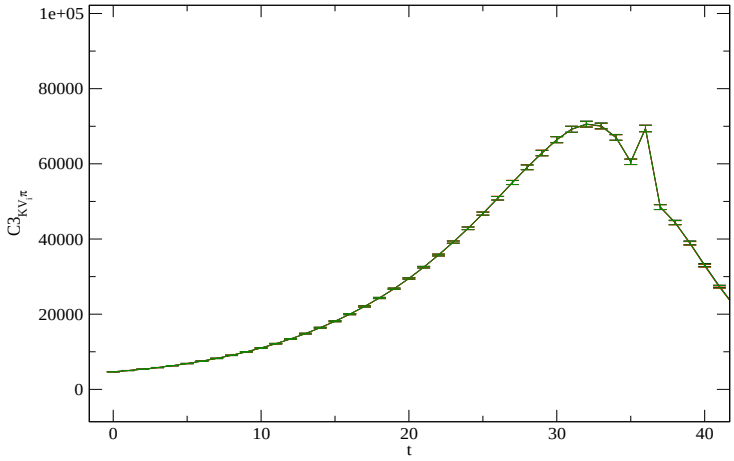

Figure 6.53: three-point function of $n = 4$

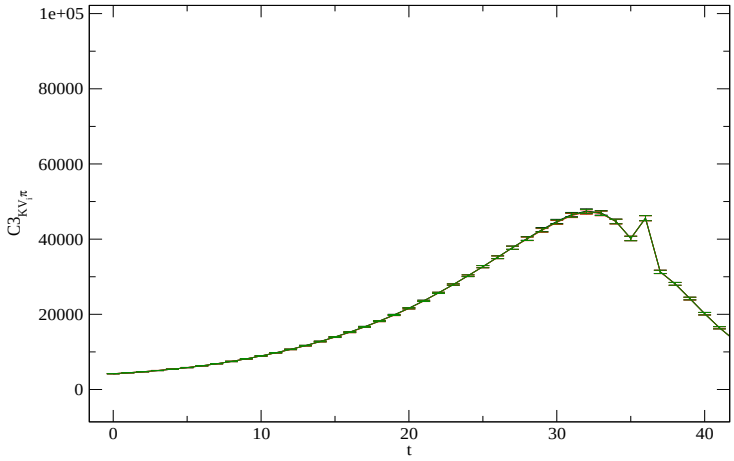

Figure 6.54: three-point function of $n = 5$

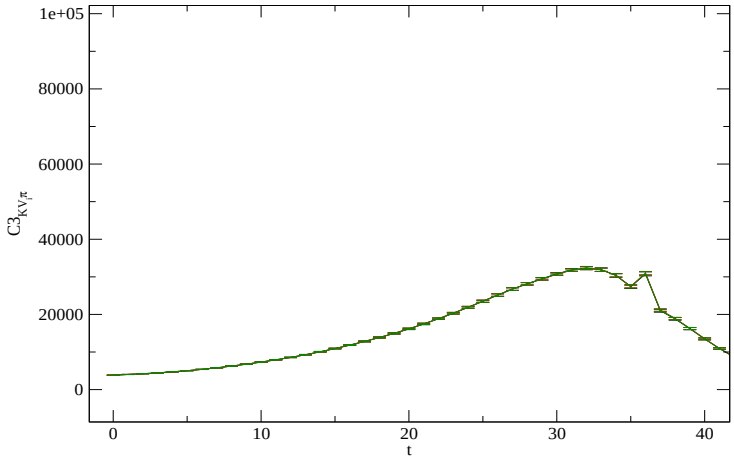

Figure 6.55: three-point function of $n = 6$

6.3 Ratios for electromagnetic form factors

After calculations of two-point functions and three-point functions with vector current of mesons, the hadronic matrix element $\langle Y|V_\mu|X\rangle$ including form factor(s) has to be extracted from ratio(s) with these functions. in this section, the results of ratios with these functions, as the current-time dependent quantities, are shown. When the current time is in the middle region of source-sink time separation ($0 = t_i \ll t \ll t_f$), the ratio for electromagnetic form factors $R_X(q,t)$ with the vector current of temporal component (V_4) is given as

$$R_X(q,t) = \frac{2m_X Z_V C_4^{XX}(\vec{p},t)}{(m_X + E_X(\vec{p}))Z_X(\vec{0})Z_X(\vec{p})} e^{E_X(\vec{p})(t-t_i)} \to f_X(q^2)\ (X = \pi,\ K), \tag{6.3.1}$$

where m_X is X meson mass, Z_X is defined by $Z_X(\vec{p}) = \langle 0|O_\pi|X(\vec{p})\rangle$, Z_V is the current renormalization factors. The m_X and Z_X are estimated by fitting two-point functions.

When pion mass is heavy, for example Ref. [14], the form factor is extracted as plateau of the quantity R_X on the middle region in source-sink time separation. However when pion mass is light and the temporal periodicity is not large enough, R_X in the middle region has current-time dependence due to the wrapping around effect [36].

Thus extraction including the effect should be done by the following form

$$f_0 + f_1 \times \frac{e^{-E_{2X}\times t} e^{-E_\pi \times (T-t_f)} - e^{-E_{2X}\times (t_f - t)} e^{-m_\pi \times (T-t_f)}}{e^{-E_X \times t} e^{-m_\pi \times (t_f - t)}}, \tag{6.3.2}$$

where the source time slice is fixed $t_i = 0$, E_{2X} is the energy of propagating two X mesons. After the fit form is employed, the f_0 in the form is obtained as form factor.

The ratio could be constructed by the vector current of spatial components (V_i ($i = 1,2,3$)). However the data of V_i are noisier than data of V_4, hence the data of V_i are rejected.

6.3.1 Ratio for pion electromagnetic form factors $R_\pi(q,t)$

The figures show the current-time dependence of $R_\pi(q,t)$ in source-sink time separation $|t_f - t_i| = 36 \approx 3.0$ fm. The region between vertical dashed lines represents the fit range $t = 15-21$ for extracting form factor. the figures show that the wrapping around effect in P+AP might be suppressed from the results in other conditions.

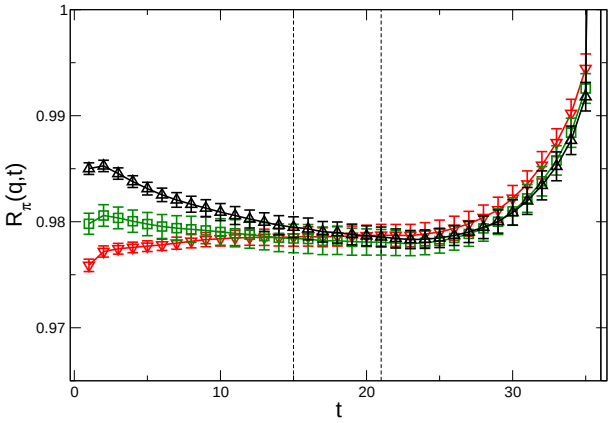

Figure 6.56: $R_\pi(q,t)$ of $n = 1$

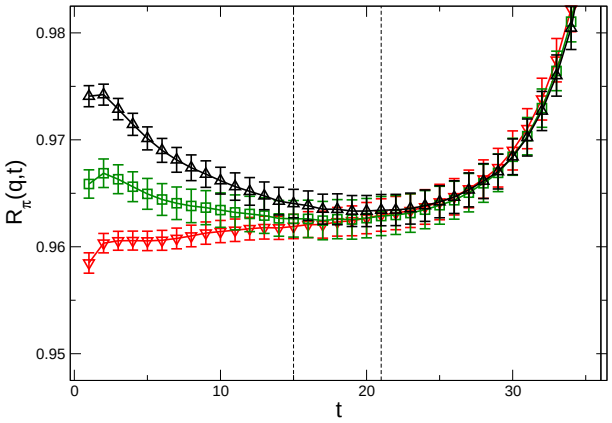

Figure 6.57: $R_\pi(q,t)$ of $n = 2$

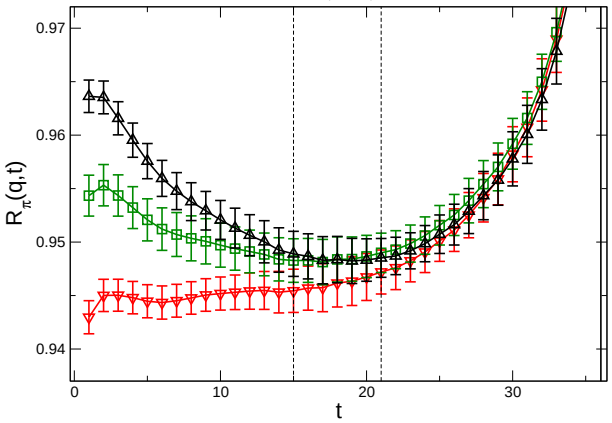

Figure 6.58: $R_\pi(q,t)$ of $n = 3$

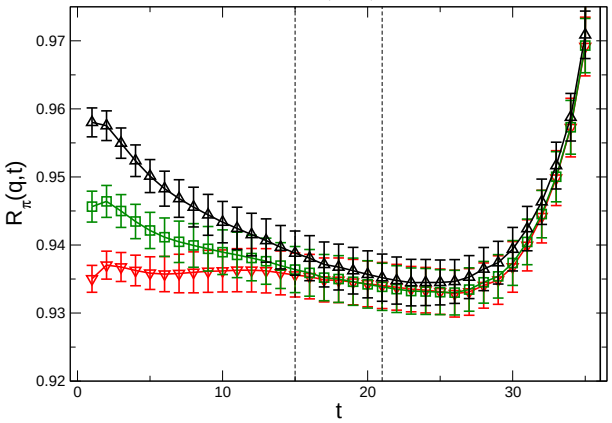

Figure 6.59: $R_\pi(q,t)$ of $n = 4$

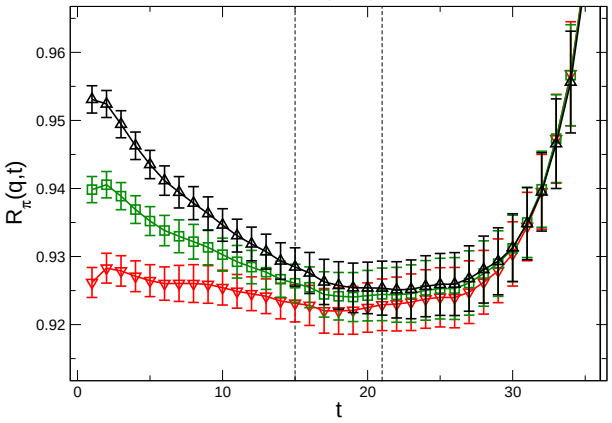

Figure 6.60: $R_\pi(q,t)$ of $n = 5$

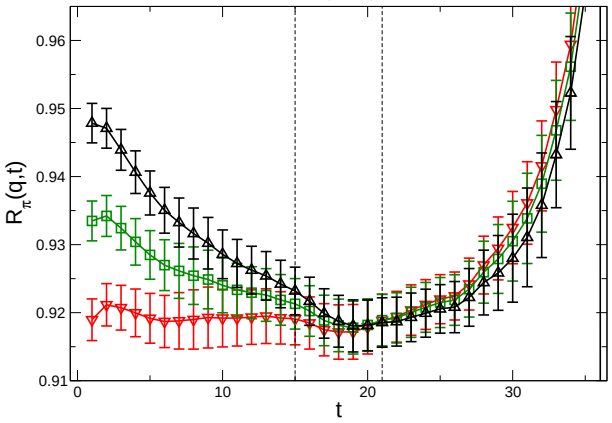

Figure 6.61: $R_\pi(q,t)$ of $n = 6$

6.3.2 Ratio for kaon electromagnetic form factors $R_K(q,t)$

The figures show the current-time dependence of $R_K(q,t)$ in source-sink time separation $|t_f - t_i| = 36 \approx 3.0$ fm The region between vertical dashed lines represents the fit range $t = 15-21$ for extracting form factor. The figures show that the wrapping around effect in all conditions might be suppressed. This is because kaon mass is heavier than pion mass and then the propagation of kaon is damped by $\exp(-m_K t)$.

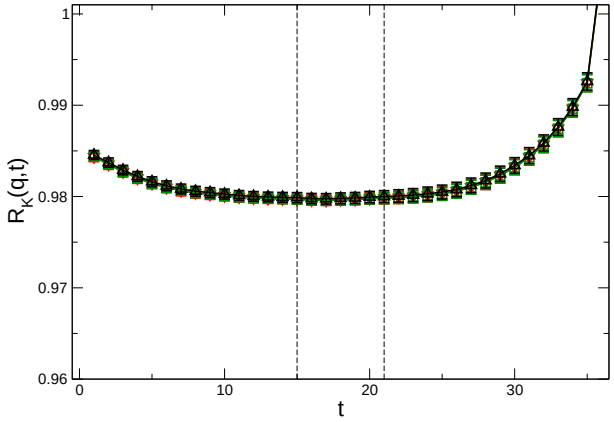

Figure 6.62: $R_K(q,t)$ of $n = 1$

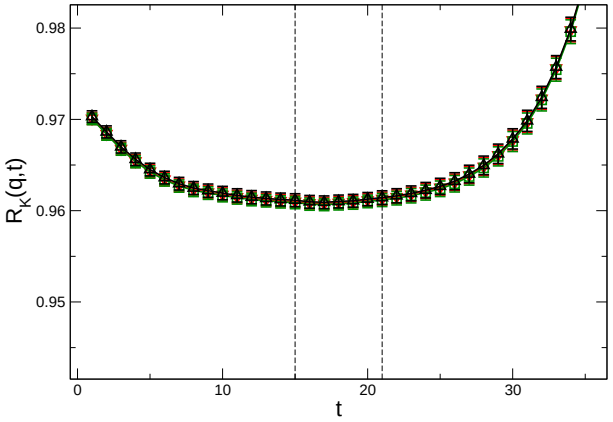

Figure 6.63: $R_K(q,t)$ of $n = 2$

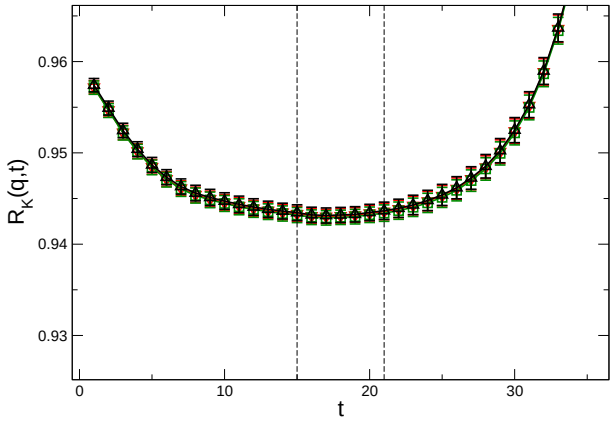

Figure 6.64: $R_K(q,t)$ of $n = 3$

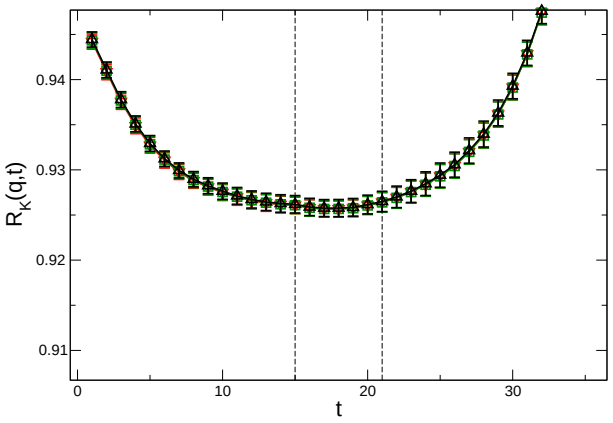

Figure 6.65: $R_K(q,t)$ of $n = 4$

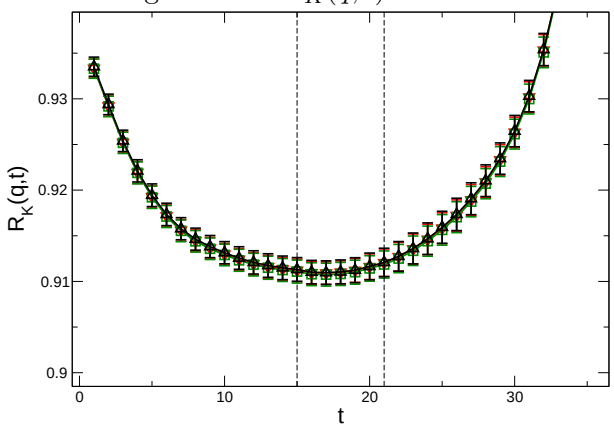

Figure 6.66: $R_K(q,t)$ of $n = 5$

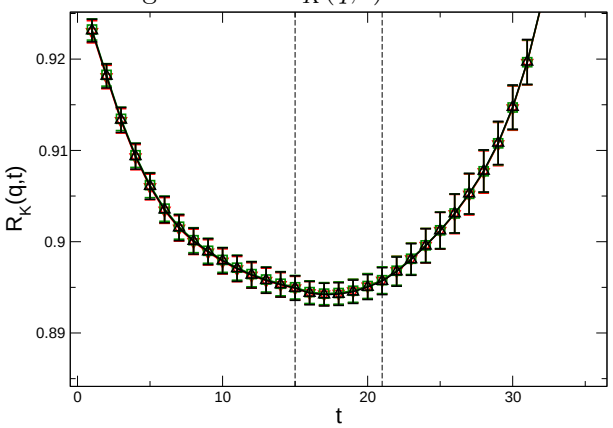

Figure 6.67: $R_K(q,t)$ of $n = 6$

6.4 Electromagnetic form factors of pion and kaon

In this section, we discuss about electromagnetic form factors of charged pion and kaon. The form factors have the information of hadronic structure and L_9 which is one of the LEC of $SU(3)$ ChPT. The informations are convenient to check the consistency with experiment and semleptonic vector form factor $f_+(q^2)$, respectively.

The electromagnetic form factors $f_X(q^2)$ of X meson could be expanded by chiral order

$$f_X(q^2) = f_X^{(2)}(q^2) + f_X^{(4)}(q^2) + \cdots . \tag{6.4.1}$$

The leading order $f_X^{(2)}(q^2)$ is given as

$$f_X^{(2)}(q^2) = 1, \tag{6.4.2}$$

due to the current conservation, and the next-to-leading order $f_X^{(4)}(q^2)$ are given as

$$f_\pi^{(4),\mathrm{SU(3)}}(q^2) = \frac{1}{f_0^2}\left[-2L_9(\mu)q^2 + 2H(m_\pi^2, q^2, \mu) + H(m_K^2, q^2, \mu)\right], \tag{6.4.3}$$

$$f_K^{(4),\mathrm{SU(3)}}(q^2) = \frac{1}{f_0^2}\left[-2L_9(\mu)q^2 + H(m_\pi^2, q^2, \mu) + 2H(m_K^2, q^2, \mu)\right]. \tag{6.4.4}$$

where

$$H(m_1^2, q^2, \mu) = \frac{1}{2}\bar{A}(m_1^2, \mu) - \bar{B}_{22}(m_1^2, m_1^2, q^2, \mu),$$

with the finite part of one-loop integral of ChPT in Appendix A, and the mean square of charge radius, as the first coefficient of form factor are given by

$$\begin{aligned}
\langle r^2\rangle_\pi &= -6\frac{df_\pi(q^2)}{dq^2}\bigg|_{q^2=0}, \\
&= \frac{12L_9(\mu)}{f_0^2} - \frac{1}{16\pi^2 f_0^2}\left(\log\left(\frac{m_\pi^2}{\mu^2}\right) + 1\right) - \frac{1}{32\pi^2 f_0^2}\left(\log\left(\frac{m_K^2}{\mu^2}\right) + 1\right), \qquad (6.4.5) \\
\langle r^2\rangle_K &= -6\frac{df_K(q^2)}{dq^2}\bigg|_{q^2=0}, \\
&= \frac{12L_9(\mu)}{f_0^2} - \frac{1}{32\pi^2 f_0^2}\left(\log\left(\frac{m_\pi^2}{\mu^2}\right) + 1\right) - \frac{1}{16\pi^2 f_0^2}\left(\log\left(\frac{m_K^2}{\mu^2}\right) + 1\right). \qquad (6.4.6)
\end{aligned}$$

The summary of the difference of parameters between 96^4 simulations and this work is as follows.

- $(\kappa_{ud}, \kappa_s) = (0.126117, 0.124790) \to (m_\pi, m_K) \approx (145, 525)$ GeV.
- spatial extent of physical unit : 8.1fm.
- 3200 measurements (100 configuration $\times$ 4 source times $\times$ 2 random source $\times$ 4 temporal axes).
- bin size : every 100 trajectories.
- 3 integer vectors each momentum of $n \leq 6$.
- Within strange mass reweighting factor for κ_s =0.124812, 0.124768.

The results of pion electromagnetic form factors with PBC in 96^4 simulations and 128^4 simulations are given as follows.

	$q^2(GeV^2)$	f_π (with 2π)	f_π (w.o. 2π)
$n=1$	0.01908(2)	0.9662(11)	0.9716(6)
$n=2$	0.03353(6)	0.9412(34)	0.9506(21)
$n=3$	0.04566(10)	0.9196(44)	0.9318(32)
$n=4$	0.05631(14)	0.9051(65)	0.9204(34)
$n=5$	0.06593(17)	0.8936(92)	0.9093(58)
$n=6$	0.07476(20)	0.8774(141)	0.9042(91)

Table 6.4: Comparison the results pion electromagnetic form factors in PBC with 2pion fit and without 2pion fit in 96^4 simulation

	$q^2(GeV^2)$	f_π (with 2π)	f_π (w.o. 2π)
$n=1$	0.01136(2)	0.9781(10)	0.9789(10)
$n=2$	0.02053(4)	0.9627(17)	0.9635(14)
$n=3$	0.02842(8)	0.9478(23)	0.9484(20)
$n=4$	0.03546(11)	0.9318(45)	0.9367(33)
$n=5$	0.04187(14)	0.9217(56)	0.9262(34)
$n=6$	0.04779(16)	0.9124(54)	0.9196(36)

Table 6.5: Comparison the results pion electromagnetic form factors in PBC with 2pion fit and without 2pion fit in 128^4 simulation

The results of pion electromagnetic form factors with P+AP simulations and 128^4 simulations are given as follows.

	$q^2(GeV^2)$	f_π (with 2π)	f_π (w.o. 2π)
$n=1$	0.01136(2)	0.9779(12)	0.9782(12)
$n=2$	0.02053(4)	0.9628(21)	0.9626(18)
$n=3$	0.02842(7)	0.9493(23)	0.9484(20)
$n=4$	0.03546(9)	0.9315(45)	0.9349(34)
$n=5$	0.04187(13)	0.9222(55)	0.9246(33)
$n=6$	0.04780(15)	0.9150(54)	0.9190(37)

Table 6.6: Comparison the results of pion electromagnetic form factors in P+AP with 2pion fit and without 2pion fit in 128^4 simulation

Comparing the results in the table 6.4 and the table 6.5, in spite of that the calculations in the same PBC are done, the deviations of the results between two fit forms of 128^4 simulations are tend to be smaller than 96^4 ones. Comparing the results in the table 6.5 and the table 6.6, the deviations of the results in P+AP between two fit forms simulations are tend to be smaller than ones in PBC. Thus, we consider that pion wrapping around effect could be suppressed by P+AP calculations, accordingly wrapping around effects of other mesons might be more suppressed. In the following of electromagnetic form factor analysis, the ones of P+AP calculations with two-meson fit are adopted in 128^4 simulations.

6.4.1 Pion charge radius and L_9

The momentum transfer dependence of the form factors and the curves by Eq. (6.4.4) present in Fig.6.68.

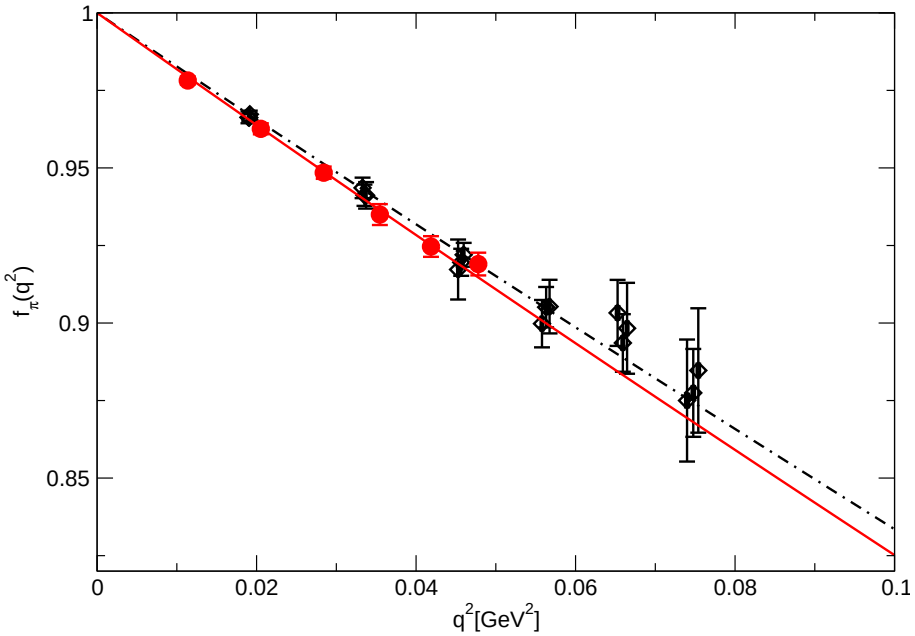

Figure 6.68: momentum dependance of pion electromagnetic form factors. Red filled symbols represent the pion electromagnetic form factors in 128^4 simulations. Black diamond symbols represent the form factors in 96^4 simulations including strange mass reweighted ones. Red solid line represents the NLO SU(3) correlated fit with Eq. (6.4.4) of 128^4 form factors whose fit range is $n = 1 - 6$. Black dashed line represents the NLO SU(3) correlated fit with Eq. (6.4.4) of 96^4 form factors including strange mass reweighted ones whose fit range is $n = 1 - 3$.

In this fit, $f_0 = 0.074$ GeV is the decay constant of $SU(3)$ chiral limit which is estimated by the combination the decay constant of $SU(2)$ chiral limit f [26, 36] and the ratio $f/f_0 = 1.23$ [2, 14], and normalized by $\sqrt{2}$. In this analysis, we obtain

$$1000L_9(\mu) = 3.801(185), \tag{6.4.7}$$

and by using Eq. (6.4.6) and this value, pion mean square charge radius is given as

$$\langle r^2 \rangle_\pi = 0.426(15)(\text{fm}^2), \tag{6.4.8}$$

whose correlated $\chi^2/d.o.f$=0.91(0.80). In 96^4 simulations, the results with SU(3) whose fit range is $n = 1-3$ (this result of the range has the smallest $\chi^2/d.o.f$ in this simulation) with only statistical error are given by $1000L_9(\mu) = 3.659(127)$ and $\langle r^2 \rangle_\pi = 0.407(11)(\text{fm}^2)$ whose correlated $\chi^2/d.o.f$=0.75(0.51). And the experimental charge radius of pion is $\langle r^2 \rangle_\pi = 0.452(11)(\text{fm}^2)$. Results in 128^4 simulation are consistent with 96^4 simulations and experiment and statistical errors of the results are lesser than 96^4 results.

In correlated NLO $SU(2)$ ChPT fit analysis (fit form is from the Appendix D) 128^4 simulation,

we also obtain

$$100l_6(\mu) = -1.267(55), \tag{6.4.9}$$

and by using NLO $SU(2)$ ChPT fit and this value, pion mean square charge radius is also given as

$$\left\langle r^2 \right\rangle_\pi = 0.426(16)(\mathrm{fm}^2). \tag{6.4.10}$$

The radius in NLO $SU(3)$ ChPT is consistent with one in NLO $SU(2)$ ChPT.

6.4.2 Kaon charge radius and L_9

Similar to the analysis of pion form factor, the momentum transfer dependence of the kaon electromagnetic form factors and the curves by Eq. (6.4.4) present in Fig.6.69 (There is no data of kaon in 96^4 calculations).

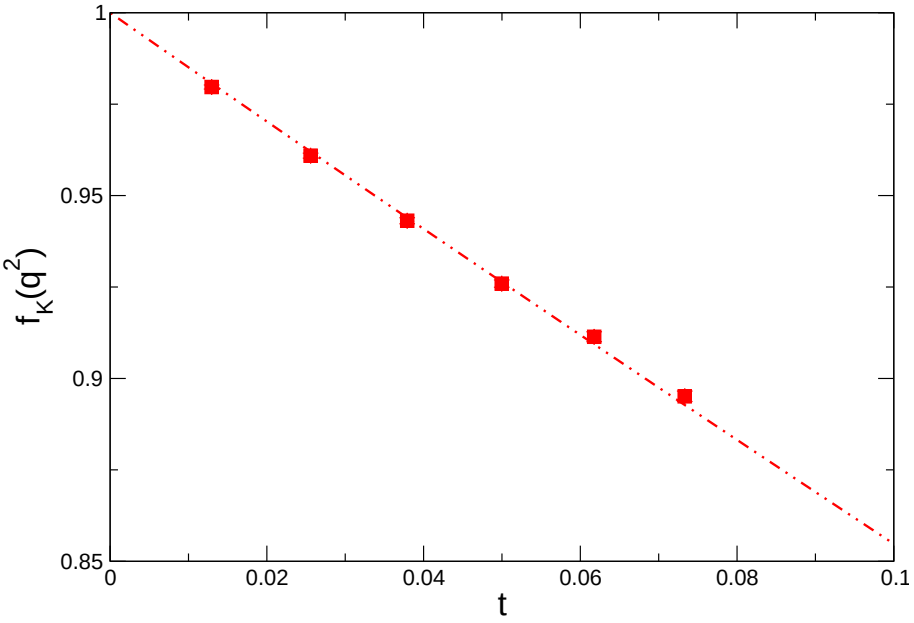

Figure 6.69: momentum dependance of pion electromagnetic form factors. Red filled symbols represent the pion electromagnetic form factors in 128^4 simulations. Red solid line represents the NLO SU(3) correlated fit with Eq. (6.4.4)of 128^4 form factors whose fit range is $n = 1 - 6$.

In this analysis, we obtain

$$1000L_9(\mu) = 3.545(38), \tag{6.4.11}$$

and by using 6.4.6 and this value, kaon mean square charge radius is given as

$$\langle r^2 \rangle_K = 0.348(3)(\mathrm{fm}^2), \tag{6.4.12}$$

whose correlated $\chi^2/d.o.f$=1.86(1.22). And the experimental charge radius of pion is $\langle r^2 \rangle_K = 0.314(34)(\mathrm{fm}^2)$. Our result are consistent with experiment.

6.5 Ratio for semileptonic form factors $d_{1,2,3}(q,t)$

When the current time is in the middle region of source-sink time separation ($0 = t_i \ll t \ll t_f$), the ratios for semileptonic form factors $d_{1,2,3}(q,t)$ with the vector current are defined by the combination of the meson two-point functions and the three-point functions. The ratio d_1 is needed to extract the scalar form factor at $n = 0$ ($q^2_{max} = -(m_K - m_\pi)^2$) and constructed by three-point functions of temporal component of the vector current V_4 with zero momentum.

$$d_1 = \frac{C_4^{\pi K}(\vec{0},t)C_4^{K\pi}(\vec{0},t)}{C_4^{KK}(\vec{0},t)C_4^{\pi\pi}(\vec{0},t)} \to \frac{(m_K+m_\pi)^2}{4m_K m_\pi}(f_0(q^2_{max}))^2 \tag{6.5.1}$$

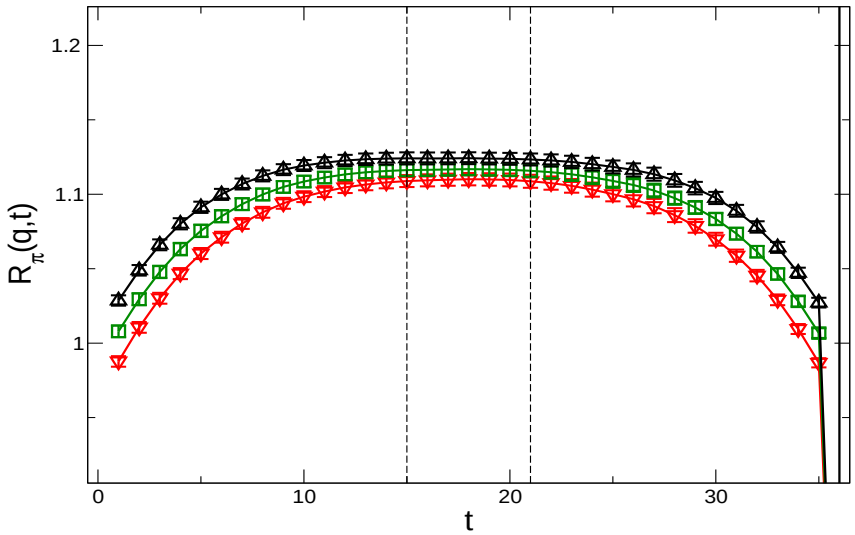

Figure 6.70: $d_1(q,t)$ of $n = 0$

The Fig.**??** shows that the plateau appears on the middle region of source-sink separation ($0 = t_i \ll t \ll t_f$) in all boundary conditions. And the current-time independent quantities is extracted by constant fit whose range is $t = 15-21$, in this work, the extraction are done about the other ratios. The ratio d_2 is related to $f_+(q^2)$ and the ratio of components of vector form factors $\xi(q^2) = f_-(q^2)/f_+(q^2)$ and constructed by two-point functions corresponding to moving meson and three-point functions of two alternating meson interpolators with temporal component of the vector current V_4.

$$d_2(q,t) = \frac{C_4^{XY}(\vec{p},t)C^X(\vec{p},t,t_i)}{C_4^{XY}(\vec{0},t)C^X(\vec{p},t,t_i)} \to \left(\frac{E_X(\vec{p})+m_Y}{m_X+m_Y} + \frac{E_X(\vec{p})-m_Y}{m_X+m_Y}\xi(q^2)\right)\frac{f_+(q^2)}{f_0(q^2_{max})}, \tag{6.5.2}$$

The ratio d_3 for extraction $\xi(q^2)$ is constructed by kaon three-point functions and three-point functions of two alternating meson interpolators with spatial component of the vector current V_i.

$$d_3(q,t) = \frac{C_i^{XY}(\vec{p},t)C_4^{YY}(\vec{p},t)}{C_i^{YY}(\vec{p},t)C_4^{XY}(\vec{p},t)} \to \frac{(E_Y(\vec{p})+m_Y)(1-\xi(q^2))}{E_X(p)+m_Y+(m_Y-E_X(p))\xi(q^2)}, \tag{6.5.3}$$

In this work, there are two construction patterns of $d_{2,3}$ by the choice of source meson. One is the "moving pion", which is the result of source pion with non zero momentum and sink kaon with zero momentum, in other words, the two or three-point functions' labels of meson in the ratios are fixed by $X = \pi$, $Y = K$. The other is the "moving kaon", which is the result of switching the source and

sink mesons (the labels are fixed by $X = \pi$, $Y = K$).

6.5.1 Ratios of moving pion

$d_2(q,t)$ of moving pion

When $q^2 = -(m_K^2 + m_\pi^2 - 2E_\pi(p)m_K)$, d_2 is given as

$$d_2 = \frac{C_4^{\pi K}(\vec{p},t)C^{\pi}(\vec{0},t)}{C_4^{\pi K}(\vec{0},t)C^{\pi}(\vec{p},t)} \to \left(\frac{E_\pi(\vec{p}) + m_K}{m_\pi + m_K} + \frac{E_\pi(\vec{p}) - m_K}{m_\pi + m_K}\xi(q^2)\right)\frac{f_+(q^2)}{f_0(q^2_{max})}. \tag{6.5.4}$$

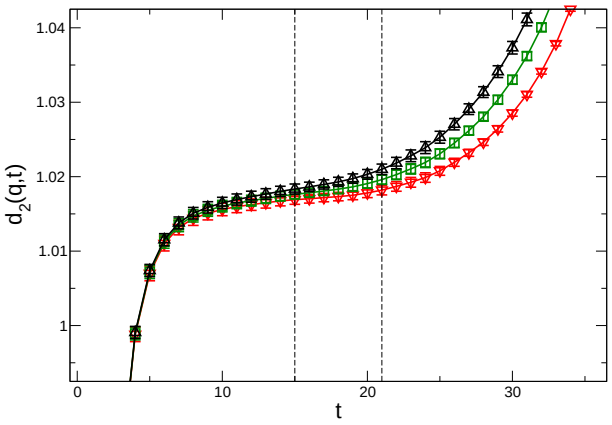

Figure 6.71: $d_2(q,t)$ of $n = 1$

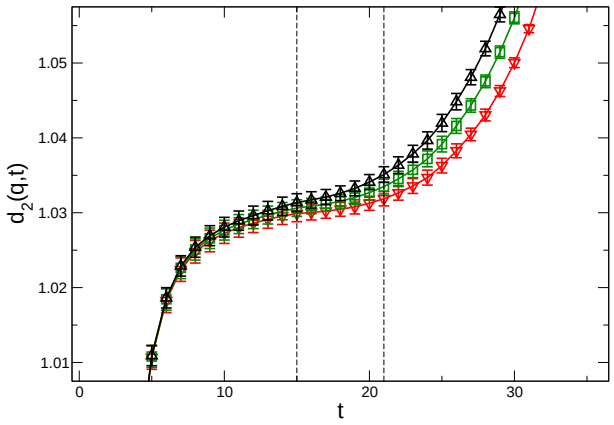

Figure 6.72: $d_2(q,t)$ of $n = 2$

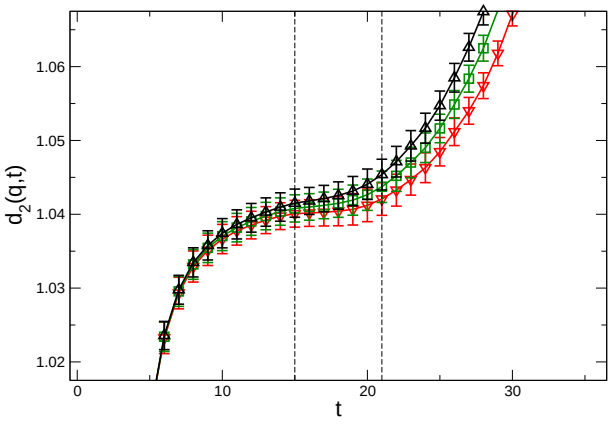

Figure 6.73: $d_2(q,t)$ of $n = 3$

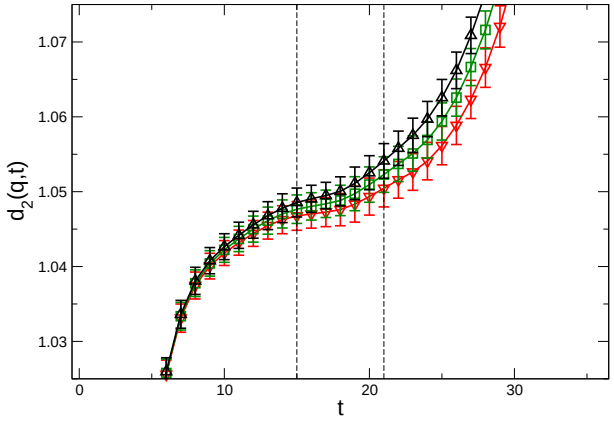

Figure 6.74: $d_2(q,t)$ of $n = 4$

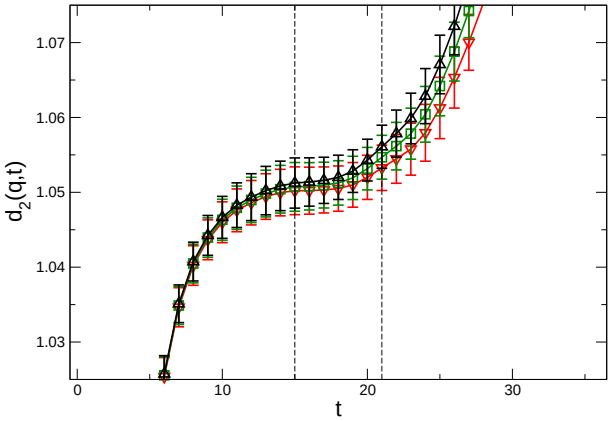

Figure 6.75: $d_2(q,t)$ of $n = 5$

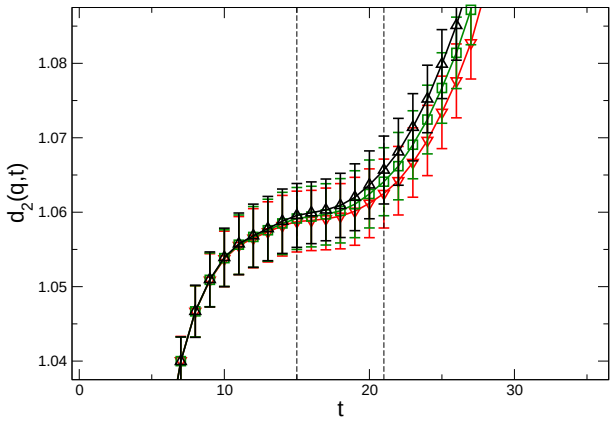

Figure 6.76: $d_2(q,t)$ of $n = 6$

$d_3(q,t)$ of moving pion

When $q^2 = -(m_K^2 + m_\pi^2 - 2E_\pi(p)m_K)$, d_3 is given as

$$d_3 = \frac{C_i^{\pi K}(\vec{p},t)C_4^{KK}(\vec{p},t)}{C_i^{KK}(\vec{p},t)C_4^{\pi K}(\vec{p},t)} \to \left(\frac{E_\pi(\vec{p}) + m_K}{p_i}\frac{p_i + p_i\xi(q^2)}{E_\pi(p) + m_K + (m_K - E_\pi(p))\xi(q^2)}\right). \tag{6.5.5}$$

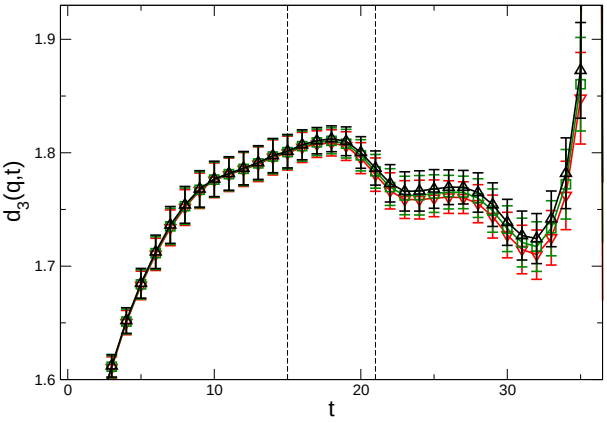

Figure 6.77: $d_3(q,t)$ of $n = 1$

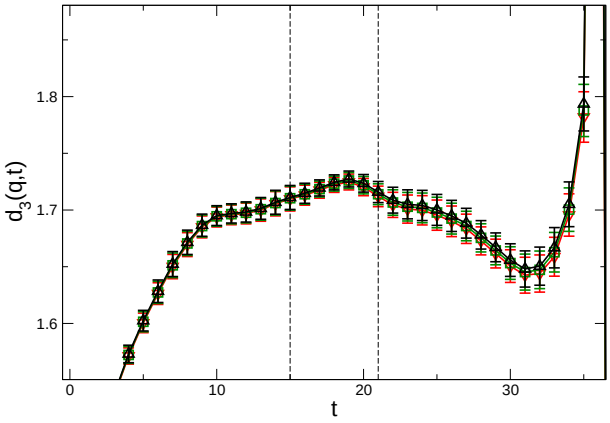

Figure 6.78: $d_3(q,t)$ of $n = 2$

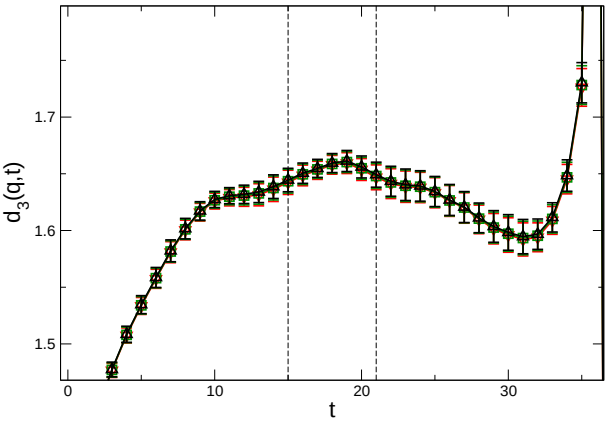

Figure 6.79: $d_3(q,t)$ of $n = 3$

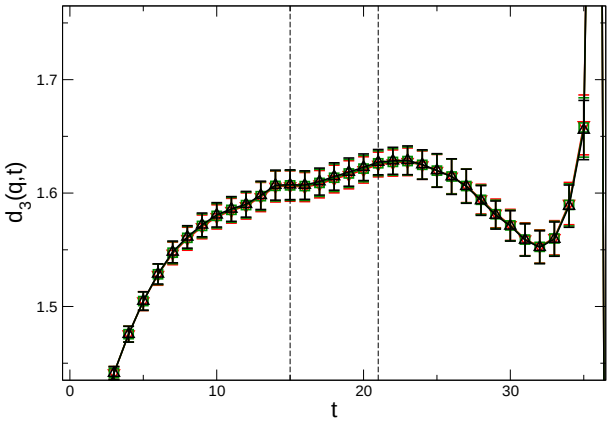

Figure 6.80: $d_3(q,t)$ of $n = 4$

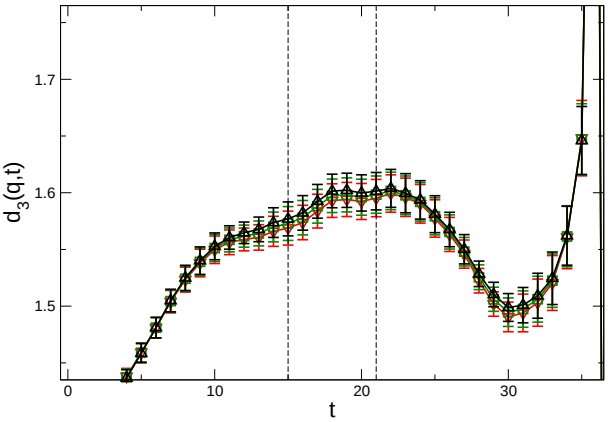

Figure 6.81: $d_3(q,t)$ of $n = 5$

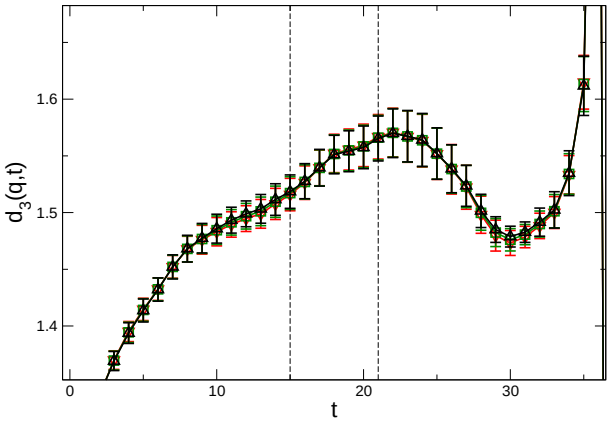

Figure 6.82: $d_3(q,t)$ of $n = 6$

6.5.2 Ratios of moving kaon

$d_2(q,t)$ of moving kaon

When $q^2 = -(m_K^2 + m_\pi^2 - 2E_K(p)m_\pi)$, d_2 is given as

$$d_2 = \frac{C_4^{K\pi}(\vec{p},t)C^K(\vec{0},t)}{C_4^{K\pi}(\vec{0},t)C^K(\vec{p},t)} \to \left(\frac{E_K(\vec{p})+m_\pi}{m_\pi+m_K} + \frac{m_\pi - E_K(\vec{p})}{m_\pi+m_K}\xi(q^2)\right)\frac{f_+(q^2)}{f_0(q^2_{max})}. \tag{6.5.6}$$

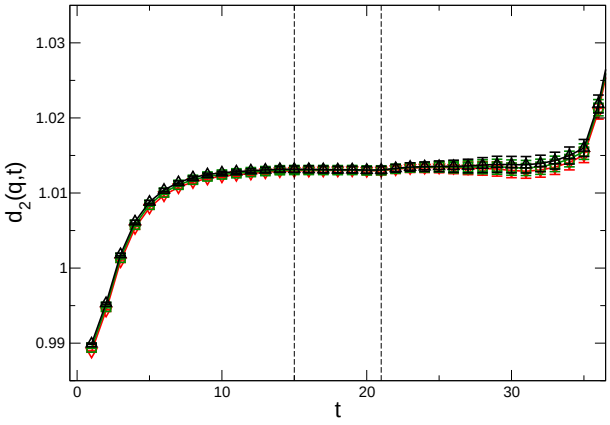

Figure 6.83: $d_2(q,t)$ of $n = 1$

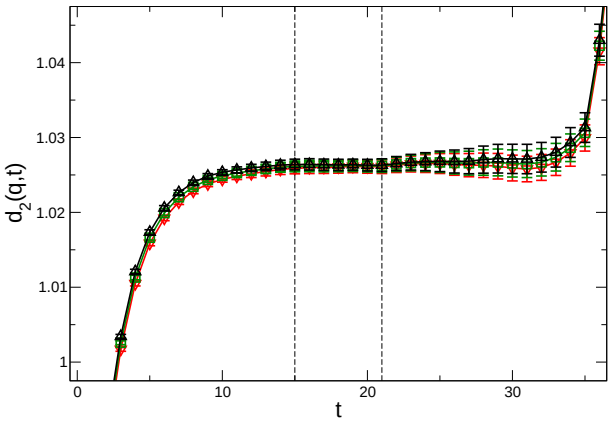

Figure 6.84: $d_2(q,t)$ of $n = 2$

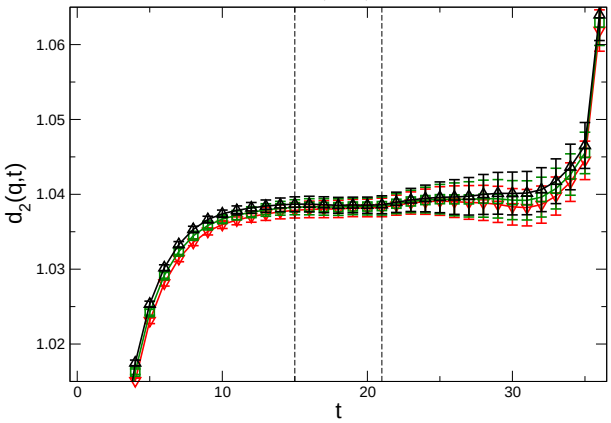

Figure 6.85: $d_2(q,t)$ of $n = 3$

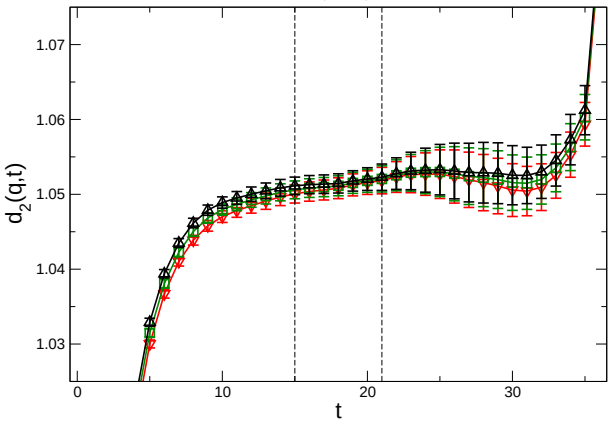

Figure 6.86: $d_2(q,t)$ of $n = 4$

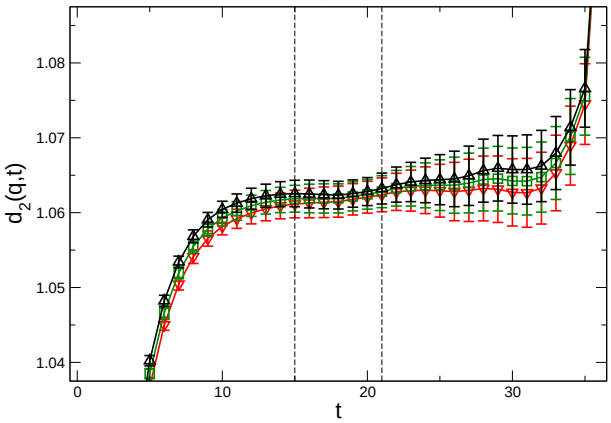

Figure 6.87: $d_2(q,t)$ of $n = 5$

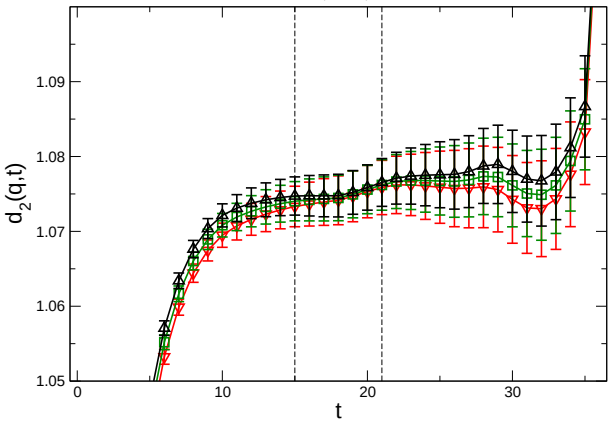

Figure 6.88: $d_2(q,t)$ of $n = 6$

$d_3(q,t)$ of moving kaon

When $q^2 = -(m_K^2 + m_\pi^2 - 2E_K(p)m_\pi)$, d_3 is given as

$$d_3 = \frac{C_i^{K\pi}(\vec{p},t)C_4^{KK}(\vec{p},t)}{C_i^{KK}(\vec{p},t)C_4^{K\pi}(\vec{p},t)} \to \left(\frac{E_K(\vec{p})+m_K}{p_i}\frac{p_i + p_i\xi(q^2)}{E_K(p)+m_\pi+(m_\pi - E_K(p))\xi(q^2)}\right). \tag{6.5.7}$$

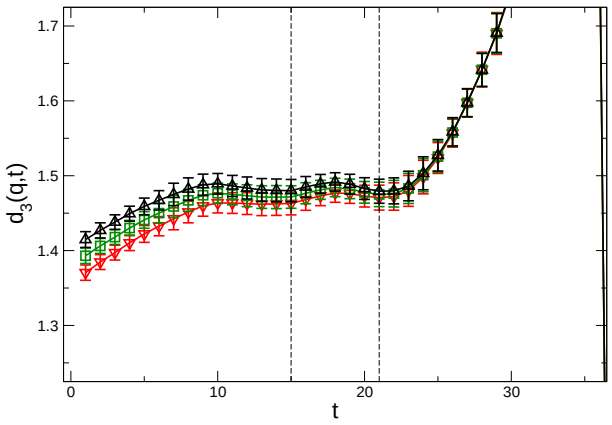

Figure 6.89: $d_3(q,t)$ of $n = 1$

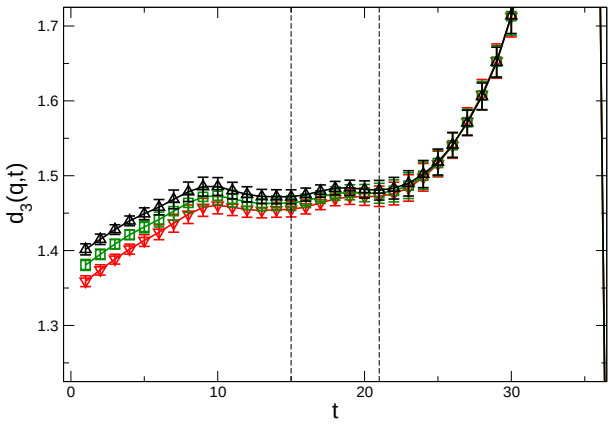

Figure 6.90: $d_3(q,t)$ of $n = 2$

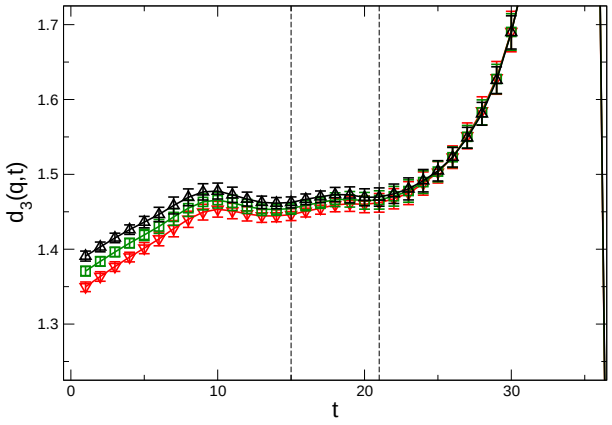

Figure 6.91: $d_3(q,t)$ of $n = 3$

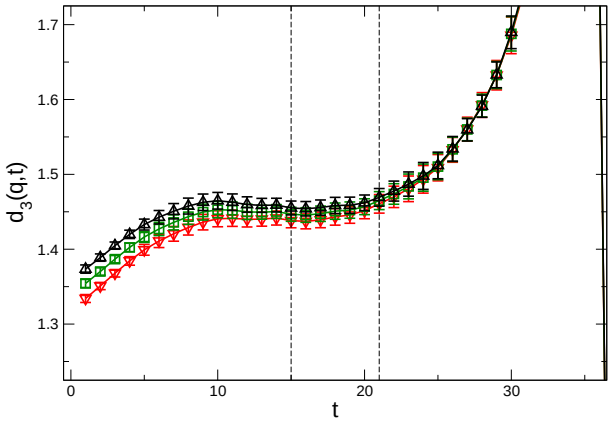

Figure 6.92: $d_3(q,t)$ of $n = 4$

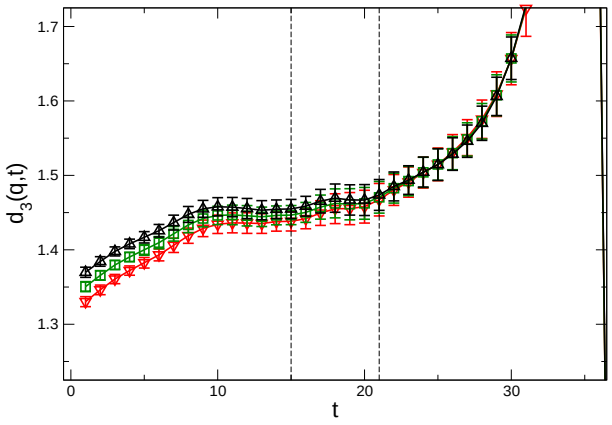

Figure 6.93: $d_3(q,t)$ of $n = 5$

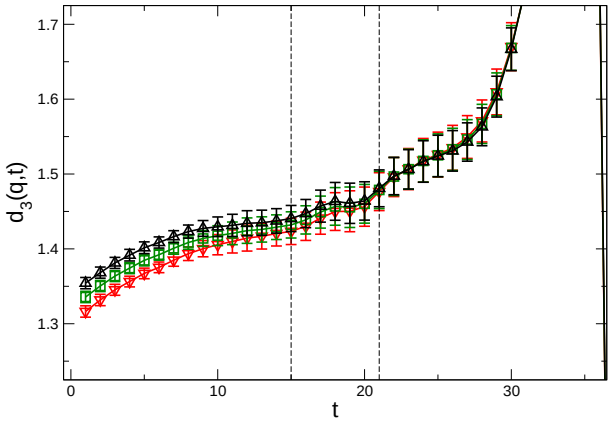

Figure 6.94: $d_3(q,t)$ of $n = 6$

From the current-time dependent quantities, the current-time independent quantities are extracted and combined, and then the form factor as functions of momentum transfer is obtained.

6.6 Semileptonic form factors

After the extraction of current-time independent quantities from the ratios $d_{1,2,3}(q,t)$, the semileptonic form factors $f_{+,0}$ are constructed from the quantities. In this section, momentum dependence of semileptonic form factors in various periodic boundary conditions are shown.

6.6.1 Momentum dependence of semileptonic form factors

Momentum dependence of semileptonic form factors in PBC

	$q^2(GeV^2)$	f_0	f_+
$n=0$	-0.1328(6)	1.0601(19)	
$n=1$	-0.0910(3)	1.0261(17)	1.0821(26)
$n=2$	-0.0573(3)	1.0004(19)	1.0337(23)
$n=3$	-0.0282(2)	0.9786(26)	0.9940(28)
$n=4$	-0.0023(2)	0.9617(24)	0.9630(25)
$n=5$	0.0213(2)	0.9459(37)	0.9339(33)
$n=6$	0.0431(1)	0.9315(50)	0.9094(41)

Table 6.7: The results of f_0, f_+ with source pion which moves only ($\vec{p}_\pi = \frac{2\pi}{L}\vec{n}$ and $\vec{p}_K = \vec{0}$)

	$q^2(GeV^2)$	f_0	f_+
$n=0$	-0.1328(6)	1.0601(19)	
$n=1$	-0.1293(6)	1.0555(22)	1.1230(121)
$n=2$	-0.1259(6)	1.0516(24)	1.1153(88)
$n=3$	-0.1225(6)	1.0475(27)	1.1113(84)
$n=4$	-0.1192(6)	1.0448(30)	1.1083(97)
$n=5$	-0.1160(7)	1.0382(44)	1.0895(173)
$n=6$	-0.1129(7)	1.0354(66)	1.0848(239)

Table 6.8: The results of f_0, f_+ with source kaon which moves only ($\vec{p}_K = \frac{2\pi}{L}\vec{n}$ and $\vec{p}_\pi = \vec{0}$)

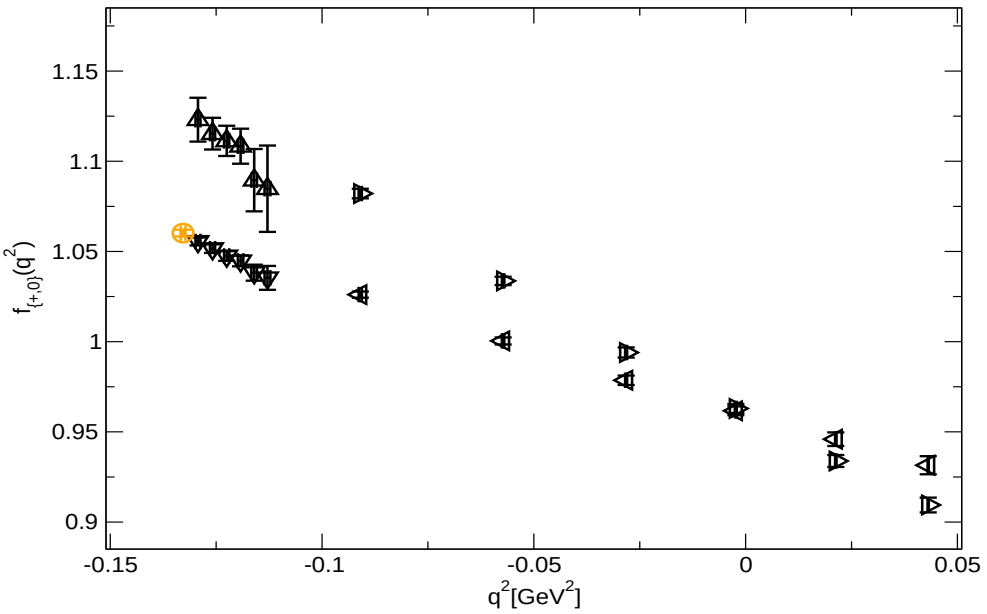

Figure 6.95: momentum dependance of semileptonic form factors in PBC. Right triangle symbols represent the result of f_0 of moving source pion and left triangle symbols represent the result of f_+ of moving source pion (in table 6.7). Up triangle symbols represent the result of f_0 of moving source kaon and down triangle symbols represent the result of f_+ of moving source kaon (in table 6.8). The far left orange circle symbol represents $f_0(q^2_{max})$ from d_1.

	$q^2(GeV^2)$	f_0	f_+
$n=0$	-0.1327(6)	1.0533(19)	
$n=1$	-0.0909(4)	1.0173(18)	1.0722(24)
$n=2$	-0.0572(3)	0.9916(20)	1.0243(22)
$n=3$	-0.0282(2)	0.9701(27)	0.9853(28)
$n=4$	-0.0023(2)	0.9530(27)	0.9542(25)
$n=5$	0.0213(2)	0.9368(38)	0.9252(34)
$n=6$	0.0431(1)	0.9240(52)	0.9021(43)

Table 6.9: The results of f_0, f_+ with source pion which moves only ($\vec{p}_\pi = \frac{2\pi}{L}\vec{n}$ and $\vec{p}_K = \vec{0}$)

	$q^2(GeV^2)$	f_0	f_+
$n=0$	-0.1327(6)	1.0533(19)	
$n=1$	-0.1292(6)	1.0491(24)	1.1283(128)
$n=2$	-0.1258(6)	1.0454(27)	1.1207(98)
$n=3$	-0.1224(6)	1.0417(30)	1.1168(93)
$n=4$	-0.1191(6)	1.0395(34)	1.1148(108)
$n=5$	-0.1159(7)	1.0333(49)	1.0964(184)
$n=6$	-0.1128(7)	1.0309(71)	1.0914(244)

Table 6.10: The results of f_0, f_+ with source kaon which moves only ($\vec{p}_K = \frac{2\pi}{L}\vec{n}$ and $\vec{p}_\pi = \vec{0}$)

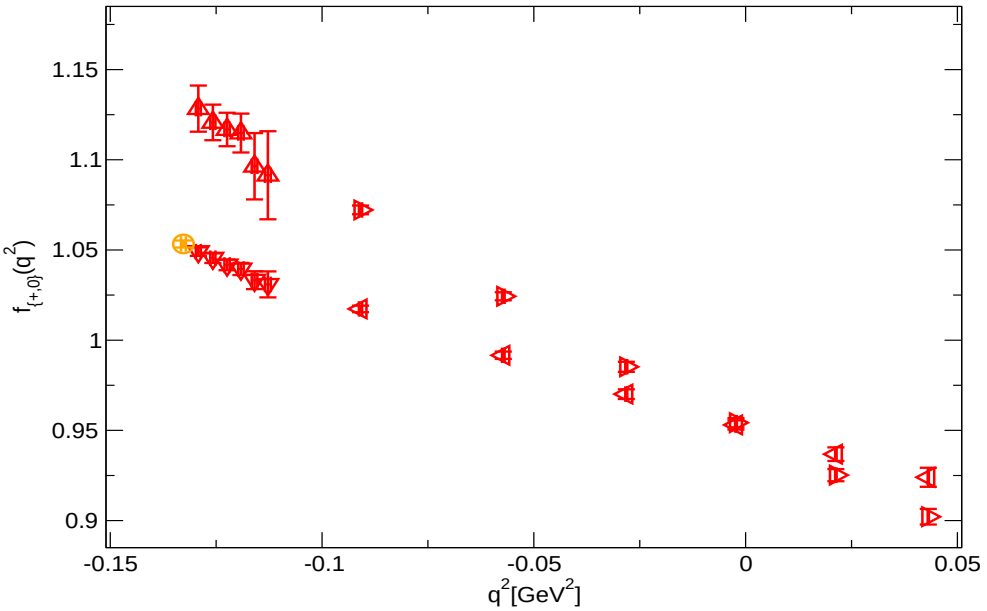

Figure 6.96: momentum dependance of semileptonic form factors in APBC. Right triangle symbols represent the result of f_0 of moving source pion and left triangle symbols represent the result of f_+ of moving source pion (in table 6.9). Up triangle symbols represent the result of f_0 of moving source kaon and down triangle symbols represent the result of f_+ of moving source kaon (in table 6.10). The far left orange circle symbol represents $f_0(q^2_{max})$ from d_1.

	$q^2(GeV^2)$	f_0	f_+
$n=0$	-0.1328(6)	1.0566(20)	
$n=1$	-0.0910(3)	1.0216(18)	1.0722(24)
$n=2$	-0.0573(3)	0.9959(20)	1.0289(22)
$n=3$	-0.0283(2)	0.9742(26)	0.9894(27)
$n=4$	-0.0024(2)	0.9571(25)	0.9585(25)
$n=5$	0.0212(2)	0.9412(36)	0.9294(31)
$n=6$	0.0431(1)	0.9276(50)	0.9056(41)

Table 6.11: The results of f_0, f_+ with source pion which moves only ($\vec{p}_\pi = \frac{2\pi}{L}\vec{n}$ and $\vec{p}_K = \vec{0}$)

	$q^2(GeV^2)$	f_0	f_+
$n=0$	-0.1328(6)	1.0566(20)	
$n=1$	-0.1293(6)	1.0522(23)	1.1230(124)
$n=2$	-0.1259(6)	1.0484(25)	1.1181(93)
$n=3$	-0.1226(6)	1.0445(28)	1.1141(88)
$n=4$	-0.1193(6)	1.0420(32)	1.1116(102)
$n=5$	-0.1161(6)	1.0357(47)	1.0930(178)
$n=6$	-0.1129(7)	1.0331(69)	1.0881(241)

Table 6.12: The results of f_0, f_+ with source kaon which moves only ($\vec{p}_K = \frac{2\pi}{L}\vec{n}$ and $\vec{p}_\pi = \vec{0}$)

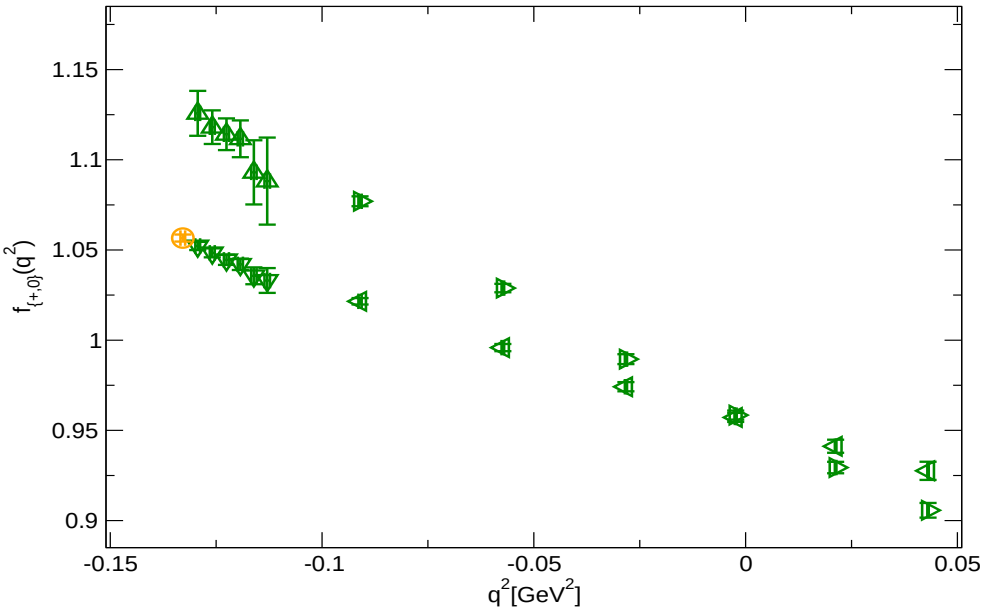

Figure 6.97: momentum dependance of semileptonic form factors in P+AP. Right triangle symbols represent the result of f_0 of moving source pion and left triangle symbols represent the result of f_+ of moving source pion (in table 6.11). Up triangle symbols represent the result of f_0 of moving source kaon and down triangle symbols represent the result of f_+ of moving source kaon (in table 6.12). The far left orange circle symbol represents $f_0(q^2_{max})$ from d_1.

The wrapping around effect might be suppressed as above results, and therefore the results of the form factors in P+AP are applied from the next analyses. And the data of moving kaon are not utilized. This is because the data are noisier than moving pion's one and too far to extrapolate to the target momentum transfer $q^2 = 0$ in all boundary conditions.

6.6.2 Monopole fit

We first employ the monopole ansatz which is based on vector meson dominance hypothesis as interpolation form given by

$$f_+(q^2) = \frac{F}{1 + q^2/M_V^2} \quad \text{and} \quad f_0(q^2) = \frac{F}{1 + q^2/M_S^2}, \tag{6.6.1}$$

where the fit parameters are F, M_V, and M_S, and $F = f_+(0) = f_0(0)$.

Using the fit forms we perform the uncorrelated simultaneous fit with the data for $f_+(q^2)$ and $f_0(q^2)$.

The left panel of Fig. 6.98 shows the simultaneous fit result of $f_+(q^2)$ and $f_0(q^2)$ using the monopole forms in equation (6.6.1). The $f_0(q^2_{max})$ is not included in the fit. The value of χ^2/d.o.f. $= 0.03(0.08)$ in the uncorrelated fit. The right panel of Fig. 6.98 shows the fit result of the form factor at $q^2 = 0$. The monopole ansatz gives a similar result, whose uncorrelated χ^2/d.o.f. ≈ 0.03.

From the two interpolations we obtain the results of the semileptonic from factor at $q^2 = 0$ given by

$$f_+(0) = f_0(0) = 0.9552(36) \quad \text{(monopole)} \tag{6.6.2}$$

The systematic error of the fit form dependence is much smaller than the statistical error as expected. And the result by not using the constraint $f_+(0) = f_0(0)$ are similar to one by using the constraint.

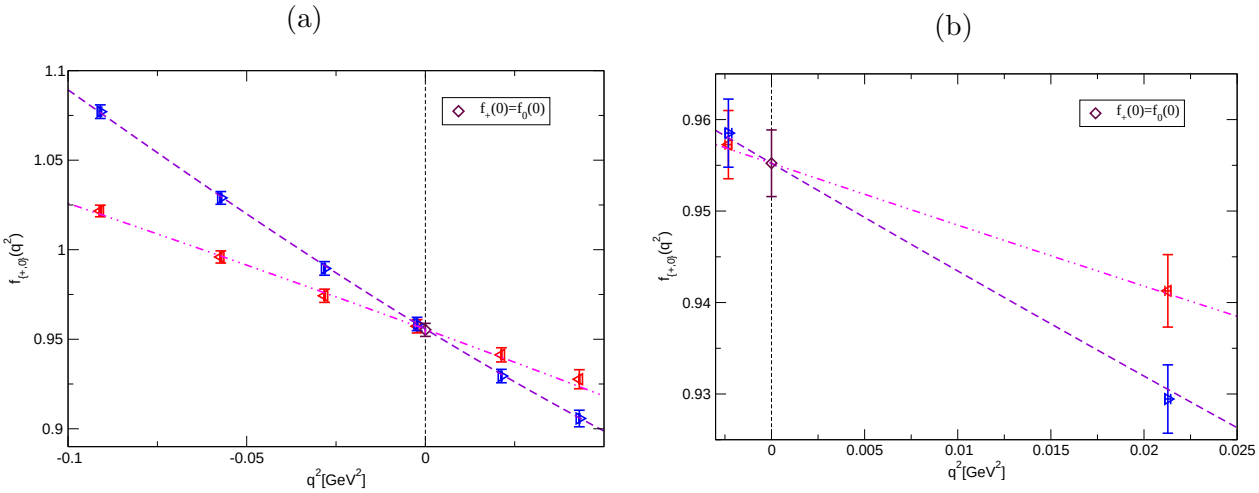

Figure 6.98: (a) momentum transfer dependence of semileptonic form factors. The blue right triangle and red left triangle symbols denote $f_+(q^2)$ and $f_0(q^2)$, respectively. The violet dashed and magenta two-dot-dashed curves represent the simultaneous fit result of $f_+(q^2)$ and $f_0(q^2)$, respectively. The diamond symbol denotes the fit result of $f_+(0) = f_0(0)$. (b) The same figure as (a), but near $q^2 = 0$ region between the momentum $n = 4$ and $n = 5$.

6.6.3 NLO ChPT + NNLO analytic

The momentum transfer dependencde of semileptonic form factors could be sprit by chiral order [43].

$$f_{+,0}(q^2) = f_{+,0}^{(2)}(q^2) + f_{+,0}^{(4)}(q^2) + f_{+,0}^{(6)}(q^2), \tag{6.6.3}$$

where $f_{+,0}^{(2)}(q^2), f_{+,0}^{(4)}(q^2)$ and $f_{+,0}^{(6)}(q^2)$, represent LO, NLO, NNLO part, respectively. The current conservation determines the normalization of vector form factor and scalar form factor in the chiral limit, This is

$$f_{+,0}^{(2)}(q^2) = 1. \tag{6.6.4}$$

The formulae of semileptonic form factors of NLO (chiral order of $O(p^4)$) was first calculated within the SU(3) ChPT framework by Gasser and Leutwyler in this work [11]

$$\begin{aligned} f_+(q^2) &= f_+^{(2)}(q^2) + f_+^{(4)}(q^2) \\ &= 1 - 2\frac{q^2}{f_0^2}L_9(\mu) + \frac{3}{8f_0^2}(\bar{A}(m_\eta^2,\mu) + \bar{A}(m_\pi^2,\mu) + 2\bar{A}(m_K^2,\mu)) \\ &+ \frac{3}{2f_0^2}(\bar{B}_{22}(m_\pi^2, m_K^2, q^2, \mu) + \bar{B}_{22}(m_K^2, m_\eta^2, q^2, \mu)), \end{aligned} \tag{6.6.5}$$

and

$$\begin{aligned} f_0(q^2) &= f_0^{(2)}(q^2) + f_0^{(4)}(q^2) \\ &= 1 - 4\frac{q^2}{f_0^2}L_5(\mu) + \frac{3}{8f_0^2}(\bar{A}(m_\eta^2,\mu) + \bar{A}(m_\pi^2,\mu) + 2\bar{A}(m_K^2,\mu)) \\ &+ \frac{3}{2f_0^2}(\bar{B}_{22}(m_\pi^2, m_K^2, q^2, \mu) + \bar{B}_{22}(m_K^2, m_\eta^2, q^2, \mu)) \\ &+ \frac{1}{f_0^2}(1/2\bar{A}(m_\eta^2,\mu) - 5/12\bar{A}(m_\pi^2,\mu) + 7/12\bar{A}(m_K^2,\mu) \\ &+ \bar{B}(m_\pi^2, m_K^2, q^2, \mu)(-m_\pi^2/12 - 5m_K^2/12 - 5q^2/12) \\ &+ \bar{B}(m_K^2, m_\eta^2, q^2, \mu)(m_\pi^2/12 - 7m_K^2/12 - q^2/4) \\ &+ \bar{B}_1(m_\pi^2, m_K^2, q^2, \mu)(-7m_\pi^2/12 - 19m_K^2/12 - 5q^2/12) \\ &+ \bar{B}_1(m_K^2, m_\eta^2, q^2, \mu)(-1m_\pi^2/12 + 23m_K^2/12 + q^2/4) \\ &+ \bar{B}_{21}(m_\pi^2, m_K^2, q^2, \mu)(3m_\pi^2/2 - 3m_K^2/2 + 5q^2/6) \\ &+ \bar{B}_{21}(m_K^2, m_\eta^2, q^2, \mu)(3m_\pi^2/2 - 3m_K^2/2 + q^2/2) \\ &+ \bar{B}_{22}(m_\pi^2, m_K^2, q^2, \mu)(-5/6) \\ &+ \bar{B}_{22}(m_K^2, m_\eta^2, q^2, \mu)(-1/2)). \end{aligned} \tag{6.6.6}$$

where $\bar{A}$ and $\bar{B}_{ij}$ represent one-loop integrals and m_η is obtained by using Gell-Mann-Okubo relation $3m_\eta^2 = 4m_K^2 - m_\pi^2$. Definitions of the integrals are in Appendix A. $\mu = 0.77$ GeV is the renormalization scale and $f_0 = 0.074$ GeV is the decay constant of $SU(3)$ chiral limit which is estimated by the combination the decay constant of $SU(2)$ chiral limit f [26,36] and the ratio $f/f_0 = 1.23$ [2,14], and normalized by $\sqrt{2}$.

In addition, the analytic terms are introduced as the formulae of NNLO for obtaining nontrivial

value $f_{+,0}(0)$

$$f^{(6)}_{+,0}(q^2) = c_0^{+,0} + c_2^{+,0}(-q^2)^2. \tag{6.6.7}$$

In specific, including the chiral symmetry breaking effect, the parameter c_0 could be rewritten,

$$c_0^{+,0} = \frac{-8}{f_0^4}(m_\pi^2 - m_K^2)^2 C_0^{+,0}, \tag{6.6.8}$$

In this work, Using the constraint $f_+(0) = f_0(0)$, the one parameter c_0^+ is reduced and the simultaneous fit is done.

The Fig. 6.99 shows the result of the interpolation to zero momentum transfer with NLO ChPT with NNLO analytic term by uncorrelated fit and the table 6.13 show the result of LEC in NLO ChPT as fit parameters. The ChPT form gives the result, whose uncorrelated χ^2/d.o.f. $= 0.03(0.06)$ and the result by not using the constraint $f_+(0) = f_0(0)$ are similar to one by using the constraint.

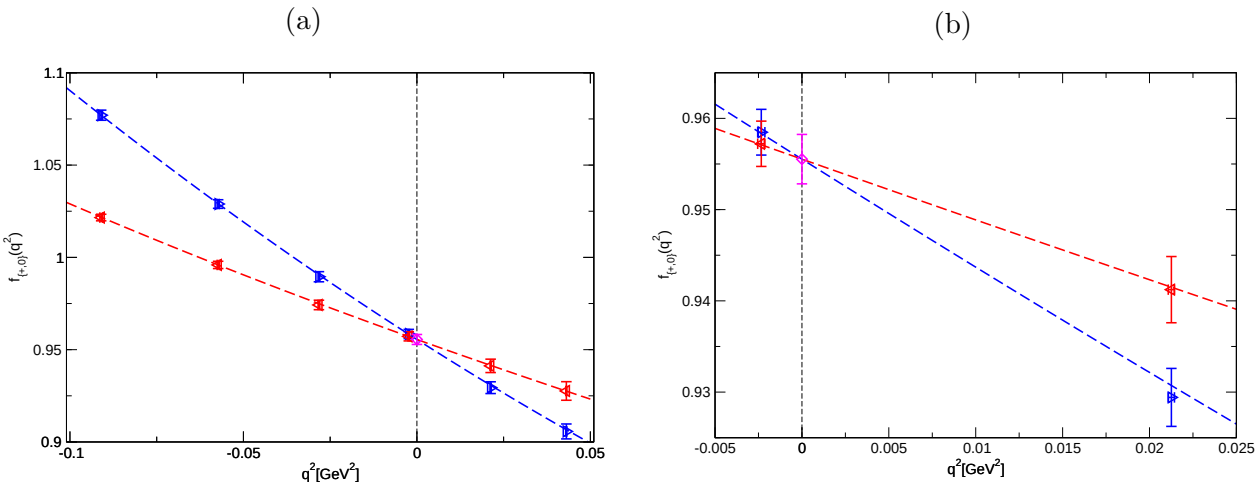

Figure 6.99: (a) momentum transfer dependence of semileptonic form factors. The blue right triangle and red left triangle symbols denote $f_+(q^2)$ and $f_0(q^2)$, respectively. The blue dashed and red dashed curves represent the simultaneous fit result of $f_+(q^2)$ and $f_0(q^2)$, respectively. The magenta diamond symbol denotes the fit result of $f_+(0) = f_0(0)$. (b) The same figure as (a), but near $q^2 = 0$ region between the momentum $n = 4$ and $n = 5$.

	$1000L_9$
K_{l3} (this work)	3.190(110)(2)(144)
pion EM (this work)	3.801(185)(2)(171)
kaon EM (this work)	3.545(38)(2)(160)
96^4 pion ff	3.659(127)(9)(165)
JLQCD(15A) [45]	$4.6(1.1)(^{+0.1}_{-0.5})(0.4)$
JLQCD(14) [46]	2.4(0.8)(1.0)
RBC/UKQCD(08A) [14]	3.08(23)(51)
Gasser [10]	6.9(7)

	$1000L_5$
K_{l3} (this work)	0.566(55)(0)(25)
$f_K/f\pi$ [32]	0.547(10)
N_f=2+1+1 [2]	1.19(25)
N_f=2+1 [2]	$0.98(16)(^{+28}_{-41})$
Gasser [10]	1.4(5)

Table 6.13: Comparison the results of this work and other previous studies of LECs in NLO ChPT L_5, L_9 at $\mu = 0.77$ GeV. Reweighted 96^4 pion electromagnetic form factor is in Ref. [42] and the assignment of errors is the same as in this work ($O(e^{-m_\pi L}) \approx 0.2\%$ in 96^4 simulation). The L_5 from decay constant ratio is the result of estimation from the decay constant ratio $f_K/f_\pi = 1.1914(16)$ in Ref. [32] and the relation within NLO ChPT in Ref. [10].

The second error of the LECs with ChPT fit in the table 6.13 is estimated by the finite size effect of $O(e^{-m_\pi L}) \approx 0.06\%$ in 128^4 simulation. and the third error is assigned discretization error by $O((a\Lambda_{QCD})^2) \approx 4.5\%$ with $\Lambda_{QCD} = 0.5$ GeV.

From the two interpolations to $q^2 = 0$, we obtain the results of the semileptonic from factor at $q^2 = 0$ with statistical error given by

$$f_+(0) = f_0(0) = 0.9555(27)(\text{uncorrelated NLO ChPT} + \text{NNLO analytic}) \tag{6.6.9}$$

and the table 6.13 shows that the fit in this work is consistent with previous studies of lattice QCD and phenomenological approach. The result is similar to the result by not using the constraint $f_+(0) = f_0(0)$

$$f_+(0) = 0.9555(26),\ f_0(0) = 0.9554(27). \tag{6.6.10}$$

The figure 6.100 shows the result of the interpolation to zero momentum transfer with NLO ChPT with NNLO analytic term by correlated fit with 6×6 (number of full accessible momenta) covariance matrices for each form factor and not using the constraint $f_+(0) = f_0(0)$. The figure 6.101 shows the result of the interpolation to zero momentum transfer with NLO ChPT with NNLO analytic term by correlated simultaneous fit with 12×12 covariance matrix for all form factors and using the constraint $f_+(0) = f_0(0)$.

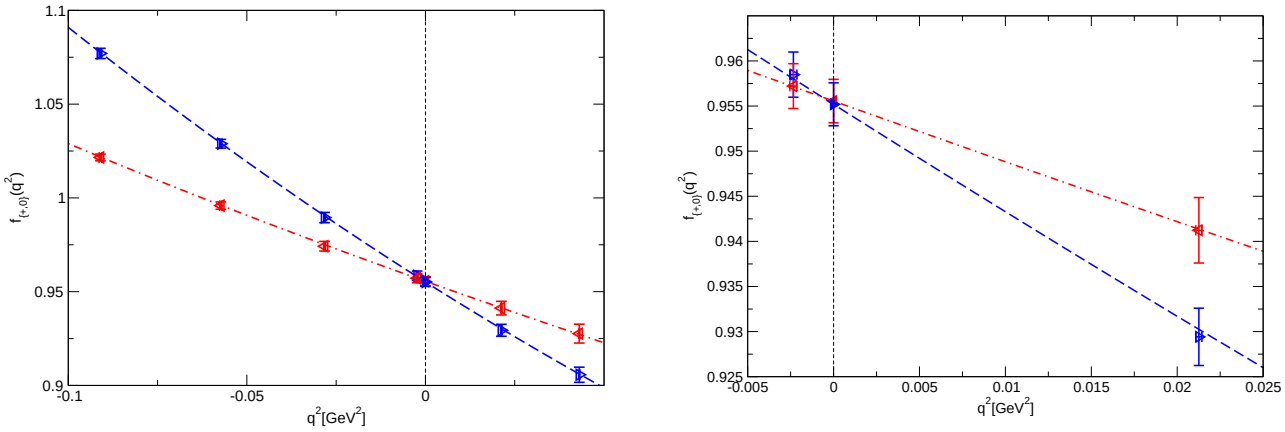

Figure 6.100: momentum transfer dependence of semileptonic form factors with correlated fit by NOT using constraint $f_+(0) = f_0(0)$. The blue filled right triangle and red filled left triangle symbols denote $f_+(q^2)$ and $f_0(q^2)$ at $q^2 = 0$, respectively. The other symbols and lines represent the same in the figure 6.99.

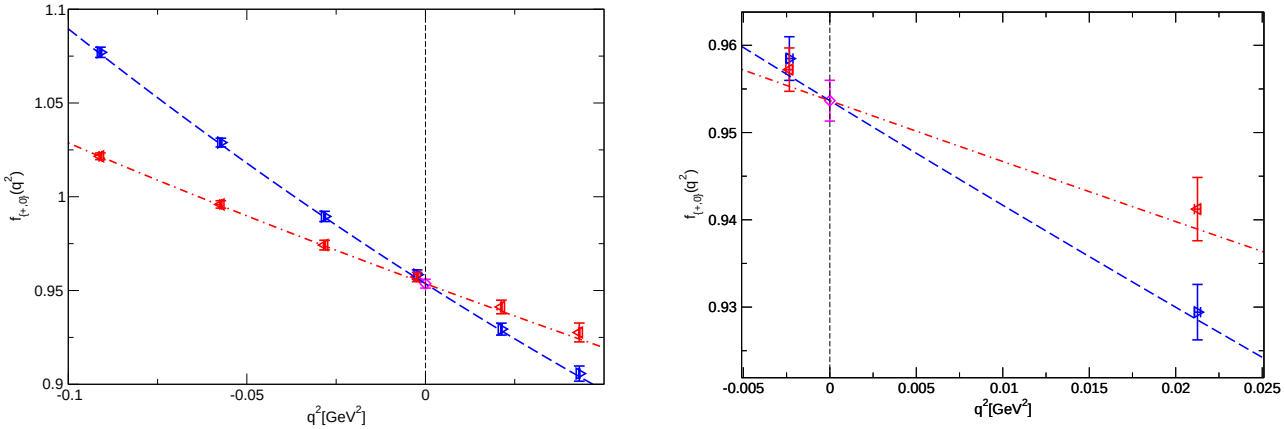

Figure 6.101: momentum transfer dependence of semileptonic form factors. The magenta diamond symbol denote $f_+(0) = f_0(0)$. The other symbols and lines represent the same in the figure 6.99.

After the analysis, we obtain the LECs

$$1000L_9(\mu) = 3.230(63)(2)(145),\ \ 1000L_5(\mu) = 0.607(39)(0)(26) \tag{6.6.11}$$

The assignments of the errors is the same as the uncorrelated analyses.

From the two interpolations to $q^2 = 0$, we obtain the results of the semileptonic from factor at $q^2 = 0$ with statistical error given by

$$f_+(0) = 0.9551(24),\ \ f_0(0) = 0.9555(24). \tag{6.6.12}$$

The ChPT forms give the result without the constraint, whose correlated χ^2/d.o.f. ≈ 0.3. However the result of correlated simultaneous fit with 12×12 covariance matrix for all form factor is obtained as

$$f_+(0) = f_0(0) = 0.9536(23)(\text{correlated NLO ChPT} + \text{NNLO analytic}) \tag{6.6.13}$$

whose correlated χ^2/d.o.f. $= 2.03(1.03)$.

The result of the correlated simultaneous fit in Eq.(6.5.12) is smaller than the ones without the constraint in Eq.(6.5.11). Furthermore, χ^2/d.o.f. of correlated simultaneous fit is considerably higher than the one without the constraint. These tendencies do not exist in the uncorrelated analyses. We consider that it is caused by inadequate measurements or configurations for the fit to obtain the 12×12 covariance matrix. Thus, the results of the uncorrelated fit are adopted in the following analysis.

After the interpolation to the zero momentum transfer, $f_+(0) = f_0(0)$ is obtained, and the contributions of chiral order are explicitly given as

$$\begin{aligned} f_{+,0}(0) &= f_{+,0}^{(2)}(0) + f_{+,0}^{(4)}(0) + f_{+,0}^{(6)}(0) \\ &= 1 + (\textit{Loop contribution term of NLO}) + \frac{-8}{f_0^4}(m_\pi^2 - m_K^2)^2 C_0^{+,0}. \end{aligned} \tag{6.6.14}$$

where $C_0^{+,0}$ is in the NNLO analytic term and it is obtained by uncorrelated analyses.

$$C_0^{+,0} = 5.376(1.914)(0.003)(0.242) \times 10^{-7}. \tag{6.6.15}$$

The assignments of the errors is the same as LEC in NLO ChPT (see in the table 6.13), and then $f(0)$ of uncorrelated fit with systematic errors is given as

$$f_{+,0}(0) = f_+(0) = f_0(0) = 0.955523(2727)(10)(424). \tag{6.6.16}$$

The error from finite size effect is quite small, and therefore the error from finite size effect could be ignored

$$f_{+,0}(0) = f_+(0) = f_0(0) = 0.9555(27)(4), \tag{6.6.17}$$

and then the value is utilized in the next analyses.

6.7 $|V_{us}|$

From 2.2.1 in Chapter 2,the result of combination of semileptonic decay measurements with isospin correlation is $|V_{us}|f_+(q^2 = 0) = 0.2165(4)$ [3] the result of $|V_{us}|$ from the ChPT analyses lead to

$$|V_{us}| = 0.22658(65)(41)(10). \tag{6.7.1}$$

The first error is statistical, the second one is estimated by the error propagation from experiment values and the third one is derived from discretization effect.

The result of $|V_{us}|$ from the monopole ansatz lead to

$$|V_{us}| = 0.22664(86)(41). \tag{6.7.2}$$

The first error is statistical, the second one is estimated by the error propagation from experiment values excluding the error from discretization effect due to the overestimation.

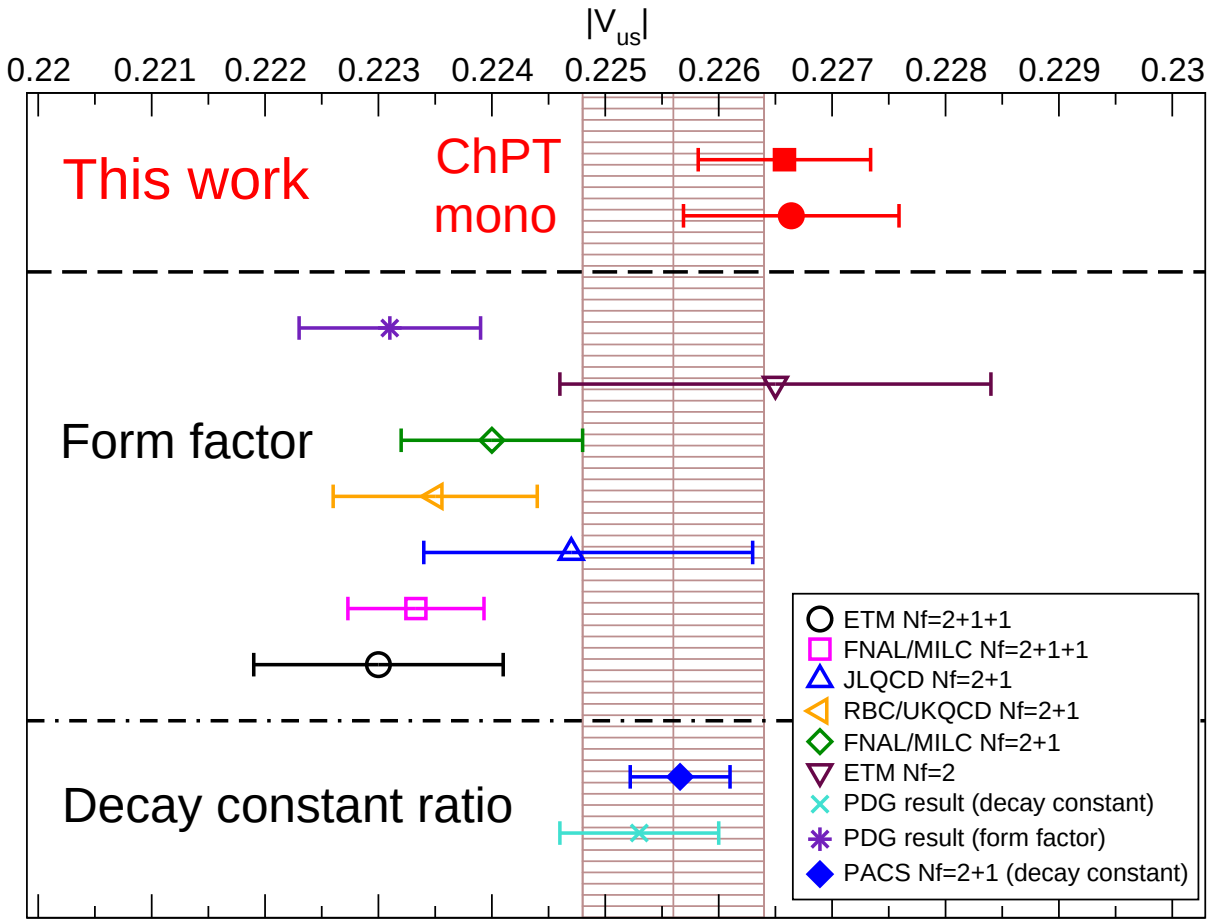

Figure 6.102: Comparison with our results and other previous form factor studies. The red filled circle and red filled square symbols represent the result in this work by monopole ansatz with total error and one by ChPT analyses with total error, respectively. The brown band represents the estimation by combination unitary condition of CKM matrix $|V_{ub}|^2 + |V_{us}|^2 + |V_{ub}|^2 = 1$ and $|V_{ud}| = 0.97420(21)$ [30] ignoring $|V_{ub}|$ due to the small values. The symbols between horizontal dashed line and horizontal dot-dashed line in the figure are the results of form factor calculations by lattice QCD [31, 37–41]. The symbols below horizontal dot-dashed line in the figure are the results from the combination the experiment the decay constant ratio calculations by lattice QCD. PDG results are quoted from Ref. [3].

The result from decay constant ratio of PACS (the filled diamond symbol in the Fig. 6.102) is estimated by the combination $f_K/f_\pi = 1.1914(16)$ [32] and $\frac{|V_{us}|}{|V_{ud}|}\frac{f_K}{f_\pi} = 0.2760(4)$ [3].

The Fig.6.102 shows that the results in this work is consistent with the result from unitary condition and the ones from decay constant ratio and higher than the PDG's result of form factor and most of lattice calculations. In other words, the results in this work are unfavorable signature beyond the SM and the unitarity may have sensitivity to new physics at the TeV scale [47].

6.8 Slope of form factor

The test of slope of form factor is useful for consistency check with experiment [49]. The slope of form factors is defined by

$$\lambda'_{(+,0)} = -\frac{m^2_{\pi_\pm}}{f_{(+,0)}(0)}\frac{f_{(+,0)}(q^2)}{dq^2}\bigg|_{q^2=0}. \tag{6.8.1}$$

The results of JLQCD are quote from [31], and these are

$$\lambda'_{(+)} = 3.08(14)(^{+12}_{-4})(25) \times 10^{-2}, \lambda'_{(0)} = 1.98(15)(^{+12}_{-4})(16) \times 10^{-2}. \tag{6.8.2}$$

The first error is statistical, the second one is from the chiral extrapolation and the third one is derived from discretization effect.

The results of ChPT analyses in this work is obtained

$$\lambda'_{(+)} = 2.44(8)(11) \times 10^{-2}, \lambda'_{(0)} = 1.37(8)(6) \times 10^{-2}, \tag{6.8.3}$$

and the results of monopole ansatz with statistical error and discretization effect in this work is obtained

$$\lambda'_{(+)} = 2.54(6)(12) \times 10^{-2}, \lambda'_{(0)} = 1.46(5)(7) \times 10^{-2}. \tag{6.8.4}$$

These slope of form factors of this work show that the our calculations of form factor are consistent with results of JLQCD and experimental results.

Chapter 7

Conclusion

We present results of the semileptonic form factors $f_+(q^2)$ and $f_0(q^2)$ in $N_f = 2+1$ Wilson fermion and Iwasaki gauge action with stout smeared link Wilson clover action at the physical point ($m_\pi = 0.135$ GeV) on a large volume, whose physical spatial extent is 10.8 fm. Thanks to the physical point calculation, the uncertainty from chiral extrapolation could be suppressed. Thanks to the large extent of the lattice, the order of finite size effect is $O(e^{-m_\pi L}) \approx 0.06\%$. This is quite small value. The two meson wrapping around effect could be suppressed enough by the large extent of the lattice with the combination of calculation in periodic boundary condition and anti periodic boundary condition. And this work is truly unquenched simulation hence the difference between valence quark masses with quark propagator and sea quark masses with quark determinant does not have to be considered.

The accessible momentum has high resolution because of the spatial extent, therefore the interpolations to zero momentum transfer of semileptonic form factors are carried out stably by using the NLO SU(3) ChPT with NNLO analytic terms and monopole forms. NLO SU(3) ChPT with NNLO analytic terms yields

$$f_+(0) = f_+(0) = 0.9555(27)(4). \tag{7.0.1}$$

The first error is statistical, the second one is derived from discretization effect.

The results of $f_{+,0}(0)$ could be determined by the sub-percent (0.3%) accuracy for these forms. Using the result of the form factors at the zero momentum transfer and the experimental value $|V_{us}|f_{+,0}(0) = 0.2165(4)$, $|V_{us}|$ is given by

$$|V_{us}| = 0.22658(65)(41)(10). \tag{7.0.2}$$

The first error is statistical, the second one is estimated by the error propagation from experiment values and the third one is derived from discretization effect.

Our value is relatively higher than the PDG's value and other lattice calculations, while it agrees with the values estimated from the decay constants and the one from the unitarity condition $\Delta_u = 0$. In other words, the signal in this work is unfavorable signal of beyond the SM. From the interpolations we evaluate the slope of the form factors, and find that our results are consistent with the experimental values.

However the systematics estimation of this work might not be fully done. At first, the discretization effect is considered. In this works the error from this effect is estimated by using the product of lattice spacing and 0.5 GeV as QCD scale. This is because the calculation is done in single lattice spacing

thus the continuum limit $a \to 0$ could not be taken by some functions of lattice spacing. Probably, the uncertainty from correct estimation might be smaller than one from the rough estimation in this work thanks to the $O(a)$ improvement in our configurations. Thus the other lattice spacing calculations are need to be done (if possible, the lattice spacing is finer than one in this work). The second systematic error to be considered is the effect of isospin breaking and electromagnetic correction. The uncertainties are typically $0.1 - 0.2\%$, and as the accuracy of form factor calculation becomes this level. The some excellent control of these effect will be progressively important. In this work, The "continuum" ChPT form is used. However the deviation between "continuum" ChPT and "discrete" ChPT might exist as the the origin of systematic errors. In recent study [41], the NLO form of ChPT for partially quenched staggered quarks was used. There are some studies of the Wilson fermion type ChPT [51, 52]. However the form factor analysis with the Wilson fermion type ChPT still has not been carried out. The analysis probably should be done.

Acknowlegdement

I would like to thank Prof. T. Yamazaki for his guidances and discussions and members of PACS collaboration for their suggestions. I also appreciate all staffs and students of Particle Theory Group of the University of Tsukuba, especially to my colleague A. Suzuki, for their supports. The 128^4 measurements in this work are supported by the Oakforest-PACS at Joint Center for Advanced High Performance Computing. The 96^4 measurements in this work are supported by the PRIMRGY cx400 (tatara), Research Institute for Information Technology, Kyusyu University and HA-PACS, Center for Computational Sciences, University of Tsukuba.

Bibliography

[1] A. S. Kronfeld, 100 Years of Subatomic Physics, pp. 493-518 (2013), [arXiv:physics.hist-ph/1209.3468].

[2] FLAG working group (S. Aoki *et al*), Eur Phys J C Part Fields. 2017;77(2):112, [arXiv:hep-lat/1607.00299v1].

[3] Particle Data Group (M. Tanabashi *et al*), Phys. Rev. D **98**, 030001 (2018).

[4] M. Kobayashi and T. Maskawa, Prog. of Theoretical Physics. **49**, (2):652-657.

[5] H. Lewtwyler, M.Roos, Z. Phys. C **25** (1984) 91.

[6] N. Cabibbo, Phys. Rev. Lett. **10**, 531 (1963).

[7] L.L Chau, W.Y Keung, Phys. Rev. Lett. **53**, 1802 (1984).

[8] S. Weinberg, Physica **A96** (1979) 327.

[9] J.Gasser, H. Lewtwyler, Ann. Phys. **158**, 142 (1984).

[10] J.Gasser, H. Lewtwyler, Nucl. Phys. B **250**, 465 (1985).

[11] J.Gasser, H. Lewtwyler, Nucl. Phys. B **250**, 517 (1985).

[12] J. Bijnens, *et al.*, JHEP **9902** (1999) 020, [arXiv:hep-ph/9902437]

[13] J. Bijnens, *et al.*, Ann. Phys. **280**, (2000) 100, [arXiv:hep-ph/9907333].

[14] RBC/UKQCD collaboration (P.A. Boyle *et al.*), JHEP **0807** (2008) 112, [arXiv:hep-lat/0804.3971].

[15] K. Symanzik, Nucl. Phys. B. **226**, 187 (1983).

[16] K. Symanzik, Nucl. Phys. B. **226**, 205 (1983).

[17] M. Lüescher, P. Weisz, Commun. Math. Phys. **97**, 59 (1985).

[18] M. Lüescher, P. Weisz, Erratum, Commun. Math. Phys. **98**, 433 (1985).

[19] B. Sheikholeslami, R. Wohlert, Nucl. Phys. B **259**, 572 (1985).

[20] R. Wohlert (unpublished) DESY 87-069 (1987).

[21] M. Lüescher, P. Weisz, Nucl. Phys. B **479**, 429 (1996).

[22] G. P. Lepage, P. B. Mackenzie, Phys. Rev. D **48** 2250 (1993).

[23] Y. Taniguchi, PoS LATTICE**2012** (2012) 236, [arXiv:hep-lat/1303.0104].

[24] M. Albanese *et al.*, Phys. Lett. B **192**, 163 (1987).

[25] C. Morningstar, M. Peardon, Phys. Rev. D **69** 054501 (2004).

[26] PACS collaboration (N. Ukita *et al*), PoS LATTICE**2015** (2015) 075, [arXiv:hep-lat/1511.09222].

[27] W.J. Marciano, Phys. Rev. Lett. **93**, 231803 (2004) [arXiv:hep-ph/0402299].

[28] The FlaviaNet Kaon Working Group (M. Antonelli *et al.*), Eur. Phys. J. C **69**, 399 (2010).

[29] KLOE collaboration (F. Ambrosino *et al.*), Phys. Lett. B **632**, 76 (2006), [arXiv:hep-ex/0509045].

[30] J.C. Hardy, I.S.Towner, PoS CKM2016, 028 (2016).

[31] JLQCD collaboration (S. Aoki *et al.*), Phys. Rev. D **96**, 034501, [arXiv:hep-lat/1705.00884v1].

[32] PACS collaboration (N. Ukita *et al.*), Phys. Rev. D **99**, 014504, [arXiv:hep-lat/1807.06237v1].

[33] C. Morningstar, M. Peardon, Phys. Rev. D **69**, 054501(2004).

[34] Y. Iwasaki, arXiv:hep-lat/1111.7054v1.

[35] JLQCD collaboration (S. Aoki *et al*), Phys. Rev. D77 (2008) 094503.

[36] PACS collaboration (J. Kakazu. *et al.*), PoS LATTICE**2016** (2017) 160.

[37] RBC/UKQCD collaboration (P.A. Boyle *et al.*), JHEP **1506** (2015) 164, [arXiv:hep-lat/1504.01692].

[38] ETM collaboration (V. Lubicz *et al.*), PoS LATTICE**2010** (2010) 316, [arXiv:hep-lat/1012.3573].

[39] ETM collaboration (N. Carrasco *et al.*), PoS LATTICE**2015** (2015) 339, [arXiv:hep-lat/1511.04880v1].

[40] FNAL/MILC collaboration (A. Bazavov *et al.*), Phys. Rev. D **87** (2013) 073012, [arXiv:hep-lat/1212.4993].

[41] FNAL/MILC collaboration (A. Bazavov *et al.*), arXiv:hep-lat/1809.02827v1.

[42] PACS collaboration (J. Kakazu. *et al.*), talk in "35th International Symposium on Lattice Field Theory (Lattice 2017)" .

[43] P. Post, K. Schilcher, Eur. Phys. J.C 25, 427 (2002) [arXiv:hep-ph/0112352].

[44] J. Bijnens, P.Talavera, Nucl. Phys. B 669, 341 (2003) [arXiv:hep-ph/0303103v2].

[45] JLQCD collaboration (S. Aoki *et al*), Phys. Rev. D **93** (2016) 034504, [arXiv:hep-lat/1510.06470].

[46] JLQCD collaboration (H. Fukaya *et al*), Phys. Rev. D **90** (2014) 034506, [arXiv:hep-lat/1405.4077].

[47] M. González-Alonso, J.M. Camalich, JHEP **1612** (2016) 052.

[48] J. Bijnens, P.Talavera, JHEP **0203** (2002) 046, [arXiv:hep-ph/0203049v1].

[49] M. Moulson, PoS CKM **2016**, 033, [arXiv:hep-ex/1704.04104].

[50] M. Ademollo, R. Gatto, Phys. Rev. Lett. **13**, 264 (1964).

[51] O. Baer *et al*, Phys. Rev. D **70**, 034508 [arXiv:hep-lat/0306021].

[52] S. Aoki, Phys. Rev. D **68** 054508, [arXiv:hep-lat/0306027v2].

Appendix A

One loop integral in ChPT

This section is the review of the article [48]. Through the calculation one has to use one-loop integrals. We only have to deal with the following set of functions in the remainder we use $d = 4 - 2\epsilon$.

$$\begin{aligned}
A(m_1^2,\mu) &= \int \frac{d^dq}{(2\pi)^d}\frac{1}{q^2-m_1^2}, \\
B(m_1^2,m_2^2,p^2,\mu) &= \int \frac{d^dq}{(2\pi)^d}\frac{1}{(q^2-m_1^2)((q-p)^2-m_2^2)}, \\
B_\mu(m_1^2,m_2^2,p^2,\mu) &= \int \frac{d^dq}{(2\pi)^d}\frac{q_\mu}{(q^2-m_1^2)((q-p)^2-m_2^2)} \\
&= p_\mu B_1(m_1^2,m_2^2,p^2,\mu), \\
B_{\mu\nu}(m_1^2,m_2^2,p^2,\mu) &= \int \frac{d^dq}{(2\pi)^d}\frac{q_\mu q_\nu}{(q^2-m_1^2)((q-p)^2-m_2^2)} \\
&= p_\mu p_\nu B_{21}(m_1^2,m_2^2,p^2,\mu) + g_{\mu\nu}B_{22}(m_1^2,m_2^2,p^2,\mu). \qquad \text{(A.0.1)}
\end{aligned}$$

The functions could be expanded by the series of ϵ as follows

$$\begin{aligned}
A(m_1^2,\mu) &= \frac{m_1^2}{16\pi^2}\lambda_0 + \bar{A}(m_1^2,\mu) + \epsilon\bar{A}^\epsilon(m_1^2,\mu) + \ldots, \\
B_{ij}(m_1^2,m_2^2,p^2,\mu) &= \frac{1}{16\pi^2}pole(B_{ij}) + \bar{B}_{ij}(m_1^2,m_2^2,p^2,\mu) + \epsilon\bar{B}^\epsilon(m_1^2,m_2^2,p^2,\mu) + \ldots, \qquad \text{(A.0.2)}
\end{aligned}$$

with $\bar{A}, \bar{B}_{ij}$ defining finite quantities. The terms of "$\lambda_0 = \frac{1}{\epsilon} + ln(4\pi) + 1 - \gamma$" and "$pole(B_{ij})$" represent the divergent part of B_{ij} where γ is Eular-Mascheroni constant.

The "$pole(B_{ij})$" are given as

$$\begin{aligned}
pole(B) = \lambda_0,\ pole(B_1) = \frac{\lambda_0}{2},\ pole(B_{21}) = \frac{\lambda_0}{3}, \\
pole(B_{22}) = \frac{\lambda_0}{4}(m_1^2 + m_2^2 - \frac{p^2}{3}). \qquad \text{(A.0.3)}
\end{aligned}$$

After some calculation, the functions defined in equation (A.0.1) could be rewritten by the

identities of the $\bar{A}(m_1^2)$ and $\bar{B}(m_1^2, m_2^2, p^2)$ and integrals B_{ij},

$$\begin{aligned}
\bar{A}(m_1^2,\mu) &= -\frac{m_1^2}{16\pi^2}\ln(\frac{m_1^2}{\mu^2}),\\
\bar{B}(m_1^2,m_2^2,p^2,\mu) &= \frac{\bar{A}(m_1^2,\mu)-\bar{A}(m_2^2,\mu)}{\Delta}\\
&+ \frac{1}{32\pi^2}\left\{2+\left(-\frac{\Delta}{p^2}+\frac{\Sigma}{\Delta}\right)\ln\left(\frac{m_1^2}{m_2^2}\right)-\frac{\nu}{p^2}\ln\left(\frac{(p^2+\nu)^2-\Delta^2}{(p^2-\nu)^2-\Delta^2}\right)\right\},\\
B_1(m_1^2,m_2^2,p^2,\mu) &= \frac{1}{2p^2}\left(A(m_2^2,\mu)-A(m_1^2,\mu)+(\Delta+p^2)B(m_1^2,m_2^2,p^2,\mu)\right),\\
B_{22}(m_1^2,m_2^2,p^2,\mu) &= \frac{1}{2(d-1)}\left(A(m_2^2)+2m_1^2B(m_1^2,m_2^2,p^2,\mu)-(\Delta+p^2)B_1(m_1^2,m_2^2,p^2,\mu)\right),\\
B_{21}(m_1^2,m_2^2,p^2,\mu) &= \frac{1}{p^2}\left(A(m_1^2,\mu)+m_1^2B(m_1^2,m_2^2,p^2,\mu)-dB_{22}(m_1^2,m_2^2,p^2,\mu)\right), \qquad \text{(A.0.4)}
\end{aligned}$$

where $\Sigma=(m_1^2+m_2^2)$, $\Delta=(m_1^2-m_2^2)$ and $\nu=\sqrt{(p^2-(m_1-m_2)^2)(p^2-(m_1+m_2)^2)}$.

The calculation for $\bar{B}_{22}$ takes note of the cancelation of divergent part, $\bar{B}_{22}$ could be given as

$$\begin{aligned}
\bar{B}_{22}(m_1^2,m_2^2,p^2,\mu) &= \frac{1}{6}\left(\bar{A}(m_2^2,\mu)+2m_1^2\bar{B}(m_1^2,m_2^2,p^2,\mu)-(\Delta+p^2)\bar{B}_1(m_1^2,m_2^2,p^2,\mu)\right)\\
&+ \frac{1}{9}\left(\frac{3\Sigma-p^2}{32\pi^2}\right). \qquad \text{(A.0.5)}
\end{aligned}$$

For convenience in calculation for $\bar{B}_{21}$ at $p^2=0$, the $\bar{B}(p^2)/p^2$ at $p^2=0$ could be given as [10]

$$\begin{aligned}
\frac{\bar{B}(m_1^2,m_2^2,p^2,\mu)}{p^2} &\xrightarrow{p^2\to 0} \lim_{p^2\to 0}\frac{B(m_1^2,m_2^2,p^2,\mu)-B(m_1^2,m_2^2,0,\mu)}{p^2}\\
&= \frac{m_1^2}{32\pi^2}\left(\frac{\Sigma}{\Delta^2}-2\frac{m_1^2m_2^2}{\Delta^3}\ln\left(\frac{m_1^2}{m_2^2}\right)\right). \qquad \text{(A.0.6)}
\end{aligned}$$

Appendix B

Ademollo-Gatto Theorem

In this chapter we present that the semileptonic form factors could be expand by the deviation between strange quark mass and light (up or down) quarks' mass around the symmetry limit ($m_u = m_d = m_s \neq 0$) and the linear term of the deviation vanishes [11, 50].

On the assumption that the vector currents and electromagnetic currents are components of the same unitary octet and that the breaking of the unitary symmetry behaves as the eighth component of an octet, an important theorem on the non-renormalization of the strangeness violating vector currents was proved by M. Ademollo and R. Gatto [50]. In the AG formalizm, the a-th component of the current J_a to first-order in symmetry breaking term could be expanded by using the parameter ϵ, which is reminder of the symmetry breaking as

$$\begin{aligned} J_a &+ \epsilon\delta J_a = a_0 tr(\bar{B}B\lambda_a) + b_0 tr(\bar{B}\lambda_a B) \\ &+ \epsilon a\left[tr(\bar{B}B\{\lambda_a,\lambda_8\}) - \frac{\delta_{a8}}{8}tr(\bar{B}B\{\lambda_b,\lambda_b\})\right] \\ &+ \epsilon b\left[tr(\bar{B}\{\lambda_a,\lambda_8\}B) - \frac{\delta_{a8}}{8}tr(\bar{B}\{\lambda_b,\lambda_b\}B)\right] \\ &+ \epsilon c\left[tr(\bar{B}\lambda_a B\lambda_8) - tr(\bar{B}\lambda_8 B\lambda_a)\right] + \epsilon g tr(\bar{B}B)tr(\lambda_8\lambda_a) \\ &+ \epsilon h\left[tr(\bar{B}\lambda_a B\lambda_8) + tr(\bar{B}\lambda_8 B\lambda_a) - \frac{\delta_{a8}}{8}tr(\bar{B}\lambda_b B\lambda_b) - \frac{6}{5}f_{a8b}f_{cde}tr(\bar{B}\lambda_d B\lambda_e)\right], \end{aligned} \quad \text{(B.0.1)}$$

where $B(\bar{B})$ represents the baryon matrix. However in this work, $B(\bar{B})$ is correspond to the meson matrix (5.2.1) in Chapter 5, λ_a represent the Gell-mann matrices ($a = 1\cdots 8$) and $a_0,\ b_0\ \cdots\ h$ are coupling constants.

Considering the electromagnetic current, defined as $J_{EM} = J_3 + 1/\sqrt{3}J_8$, the expansion becomes

$$\begin{aligned} &(a_0 + \frac{2a\epsilon}{\sqrt{3}})tr(\bar{B}B\lambda_3) + (b_0 + \frac{2b\epsilon}{\sqrt{3}})tr(\bar{B}\lambda_3 B) \\ &+ \frac{1}{\sqrt{3}}(a_0 - \frac{2a\epsilon}{\sqrt{3}})tr(\bar{B}B\lambda_8) + \frac{1}{\sqrt{3}}(b_0 - \frac{2b\epsilon}{\sqrt{3}})tr(\bar{B}\lambda_8 B) \\ &+ \frac{2}{\sqrt{3}}(g + \frac{2(a+b)\epsilon}{3})tr(\bar{B}B\lambda_8) \\ &+ \epsilon c\left[tr(\bar{B}\lambda_3 B\lambda_8) - tr(\bar{B}\lambda_8 B\lambda_3)\right] \\ &+ \epsilon h\left[tr(\bar{B}\lambda_3 B\lambda_8) + tr(\bar{B}\lambda_8 B\lambda_3)\right], \end{aligned} \quad \text{(B.0.2)}$$

and the in the limit to zero momentum transfer, due to that the current is not renormalized, the

expansion becomes

$$-\frac{1}{2}(tr(\bar{B}B\lambda_3) - tr(\bar{B}\lambda_3 B)) - \frac{1}{2\sqrt{3}}(tr(\bar{B}B\lambda_8) - tr(\bar{B}\lambda_8 B)) \tag{B.0.3}$$

Thus we have the relations among the coupling constant,

$$a_0 = -\frac{1}{2},\ b_0 = \frac{1}{2}\ a = b = c = g = h = 0. \tag{B.0.4}$$

The relation present that the electromagnetic charge do not need to require any corrections to first-order of the symmetry breaking, and as the similar discussion about strangeness violating vector current, the terms of first-order of the unitary symmetry breaking vanish.

Appendix C

Other results of semileptonic form factors

In this section, the tables of results by some fit ansatz, for instance uncorrelated fit parameters, are shown. the range of momentum transfer is the same as monopole and $SU(3)$ChPT (n=1-6).

Polynominal fit

$$f_{+,0}(q^2) = f_{+,0}(0)(1 + \Sigma_{k=1}^{l} a_n (q^2)^k)$$

z expansion fit

The fit form is the function of regular function of momentum transfer by using the nature of conformal transformation.

$$\begin{aligned} t_{cut} = (m_K + m_\pi)^2, t_0 = (m_K + m_\pi)(\sqrt{m_K} - \sqrt{m_\pi})^2 \\ z(q^2) = \frac{\sqrt{t_{cut} + q^2} - \sqrt{t_{cut} - t_0}}{\sqrt{t_{cut} + q^2} + \sqrt{t_{cut} - t_0}} \\ z(q^2 = 0) = z_0 \\ f_{+,0}(q^2) = f_{+,0}(0)(1 + \Sigma_{k=1}^{l} a_n (z - z_0)^k) \end{aligned}$$

SU(2) ChPT fit

The fit form is the NLO SU(2) ChPT ansatz without eta meson mass [38].

$$\begin{aligned} f_+(q^2) = F_+ \left(1 + (C_0^+ + C_1^+ s)x + \frac{m_K^2}{(4\pi f)^2}\left(-\frac{3}{4} x \log x - x T_1^+(s) - T_2^+(s)\right)\right) \\ f_0(q^2) = F_0 \left(1 + (C_0^0 + C_1^0 s)x + \frac{m_K^2}{(4\pi f)^2}\left(-\frac{3}{4} x \log x + x T_1^0(s) - T_2^0(s)\right)\right) \\ s = -\frac{q^2}{m_K^2}, x = \frac{m_\pi^2}{m_K^2} \\ T_1^+(s) = [(1-s)\log(1-s) + s(1-s/2)]3(1+s)/4s^2 \\ T_2^+(s) = [(1-s)\log(1-s) + s(1-s/2)](1-s)^2/4s^2 \\ T_1^0(s) = [\log(1-s) + s(1+s/2)](9+7s^2)/4s^2 \\ T_2^0(s) = [(1-s)\log(1-s) + s(1-s/2)](1-s)(3+5s)/4s^2 \end{aligned}$$

Results of polynominal fit

PBC	$f_+(0)$	a_1	a_2	a_3	a_4	$\chi^2/d.o.f$
$l=1$	0.9606(26)	-7.36(18)				1.19(42)
$l=2$	0.9593(27)	-6.90(19)	45.2(8.8)			0.07(0.17)
$l=3$	0.9595(25)	-6.87(17)	36,7(25.3)	-577(1486)		0.08(0.18)
$l=4$	0.9595(25)	-6.81(27)	38.5(27.1)	-1514(4269)	$-0.51(2,04)\times 10^5$	0.16(0.39)

PBC	$f_0(0)$	a_1	a_2	a_3	a_4	$\chi^2/d.o.f$
$l=1$	0.9600(27)	-4.06(14)				0.27(22)
$l=2$	0.9597(26)	-3.81(23)	19.4(9.3)			0.04(9)
$l=3$	0.9598(25)	-3.80(22)	15.3(28.3)	-244(1314)		0.05(0.1)
$l=4$	0.9599(25)	-3.65(31)	17.1(27.6)	-2945(4534)	$-1.3(2.0)\times 10^5$	0.049(0.17)

Table C.1: uncorrelated polynominal fit in PBC without the $f_+(0) = f_0(0)$

APBC	$f_+(0)$	a_1	a_2	a_3	a_4	$\chi^2/d.o.f$
$l=1$	0.9520(28)	-7.37(18)				1.26(41)
$l=2$	0.9509(28)	-6.86(19)	46.2(8.6)			0.06(0.14)
$l=3$	0.9508(26)	-6.87(17)	44.2(23.8)	-116(1421)		0.09(0.20)
$l=4$	0.9508(26)	-6.94(30)	43.6(25.6)	556(4384)	$0.36(2.2)\times 10^5$	0.17(40)

APBC	$f_0(0)$	a_1	a_2	a_3	a_4	$\chi^2/d.o.f$
$l=1$	0.9515(28)	-4.04(15)				0.28(23)
$l=2$	0.9511(28)	-3.81(23)	21.7(9.8)			0.03(8)
$l=3$	0.9511(26)	-3.82(23)	23.0(27.5)	121.3(1342)		0.04(0.11)
$l=4$	0.9511(26)	-3.76(32)	23.0(26.7)	-88(4785)	$-0.11(2.12)\times 10^4$	0.07(0.24)

Table C.2: uncorrelated polynominal fit in APBC without the $f_+(0) = f_0(0)$

P+AP	$f_+(0)$	a_1	a_2	a_3	a_4	$\chi^2/d.o.f$
$l=1$	0.9562(27)	-7.30(18)				1.21(41)
$l=2$	0.9548(26)	-6.88(21)	46.0(8.7)			0.07(0.16)
$l=3$	0.9549(25)	-6.86(17)	41.2(25.5)	-329(1472)		0.09(0.20)
$l=4$	0.9550(25)	-6.89(32)	41.3(26.7)	-391(4268)	$-0.03(2.1)\times 10^4$	0.17(0.41)

P+AP	$f_0(0)$	a_1	a_2	a_3	a_4	$\chi^2/d.o.f$
$l=1$	0.9562(27)	-4.03(15)				0.28(23)
$l=2$	0.9552(26)	-3.81(25)	20.5(10.7)			0.03(8)
$l=3$	0.9553(25)	-3.81(23)	19.5(27.3)	-50(1318)		0.04(0.10)
$l=4$	0.9553(25)	-3.72(32)	20.3(27.7)	-1513(4688)	$-4.8(22)\times 10^4$	0.06(0.21)

Table C.3: uncorrelated polynominal fit in P+AP without the $f_+(0) = f_0(0)$

Results of z expansion fit

PBC	$f_+(0)$	a_1	a_2	a_3	a_4	$\chi^2/d.o.f$
$l=1$	0.9738(25)	0.45(1)				47.2(3.3)
$l=2$	0.9577(26)	0.44(1)	1.04(3)			3.13(0.93)
$l=3$	0.9589(26)	0.37(1)	1.06(3)	2.21(32)		0.29(0.45)
$l=4$	0.9598(25)	0.38(1)	0.80(2)	2.14(33)	5.73(4.54)	0.10(0.23)

PBC	$f_0(0)$	a_1	a_2	a_3	a_4	$\chi^2/d.o.f$
$l=1$	0.9663(26)	0.28(1)				15.7(1.5)
$l=2$	0.9584(26)	0.24(1)	0.59(5)			1.03(0.44)
$l=3$	0.9596(25)	0.20(1)	0.56(3)	1.23(24)		0.06(0.17)
$l=4$	0.9598(25)	0.20(2)	0.48(19)	1.16(28)	1.63(3.83)	0.06(0.19)

Table C.4: uncorrelated polynominal fit in PBC without the $f_+(0) = f_0(0)$

APBC	$f_+(0)$	a_1	a_2	a_3	a_4	$\chi^2/d.o.f$
$l=1$	0.9652(26)	0.40(1)				47.5(3.1)
$l=2$	0.9489(27)	0.44(1)	1.07(5)			2.96(0.91)
$l=3$	0.9502(26)	0.36(1)	1.06(3)	2.12(32)		0.30(0.45)
$l=4$	0.9511(25)	0.38(1)	0.80(2)	2.01(33)	6.09(4.35)	0.08(0.20)

APBC	$f_0(0)$	a_1	a_2	a_3	a_4	$\chi^2/d.o.f$
$l=1$	0.9577(27)	0.28(1)				14.7(1.1)
$l=2$	0.9497(27)	0.24(1)	0.60(5)			0.81(0.40)
$l=3$	0.9508(26)	0.20(1)	0.57(3)	2.12(32)		0.08(0.21)
$l=4$	0.9512(25)	0.21(2)	0.45(18)	1.02(29)	2.72(3.85)	0.04(0.16)

Table C.5: uncorrelated polynominal fit in APBC without the $f_+(0) = f_0(0)$

P+AP	$f_+(0)$	a_1	a_2	a_3	a_4	$\chi^2/d.o.f$
$l=1$	0.9692(25)	0.45(1)				45.5(3.1)
$l=2$	0.9533(26)	0.44(1)	1.05(3)			2.96(0.91)
$l=3$	0.9543(25)	0.37(1)	1.60(3)	2.14(32)		0.30(0.46)
$l=4$	0.9553(25)	0.38(1)	0.79(2)	2.07(32)	5.97(4.53)	0.09(0.22)

P+AP	$f_0(0)$	a_1	a_2	a_3	a_4	$\chi^2/d.o.f$
$l=1$	0.9618(27)	0.28(1)				15.5(1.4)
$l=2$	0.9539(25)	0.24(1)	0.59(3)			0.94(43)
$l=3$	0.9550(25)	0.20(1)	0.57(3)	1.16(25)		0.07(0.20)
$l=4$	0.9553(25)	0.21(2)	0.46(18)	1.09(28)	2.1(3.8)	0.06(0.18)

Table C.6: uncorrelated polynominal fit in P+AP without the $f_+(0) = f_0(0)$

Results of SU(2) ChPT fit

PBC	$f_0(0)$	F_0	c_0^0	c_1^0	$\chi^2/d.o.f$
f_0	0.9603(35)	-1.05(63)	-22.3(3.7)	-1.14(0.72)	0.45
PBC	$f_+(0)$	F_+	c_0^+	c_1^+	$\chi^2/d.o.f$
f_+	0.9598(37)	16.2(2.8)	-13.0(0.2)	0.35(4)	0.47
APBC	$f_0(0)$	F_0	c_0^0	c_1^0	$\chi^2/d.o.f$
f_0	0.9508(37)	-1.05(66)	-22.3(3.4)	-1.05(0.67)	0.32
APBC	$f_+(0)$	F_+	c_0^+	c_1^+	$\chi^2/d.o.f$
f_+	0.9505(37)	17.0(2.8)	-13.0(0.2)	0.33(4)	0.33
P+AP	$f_0(0)$	F_0	c_0^0	c_1^0	$\chi^2/d.o.f$
f_0	0.9556(34)	-1.05(66)	-22.1(3.5)	-1.05(0.70)	0.33
P+AP	$f_+(0)$	F_+	c_0^+	c_1^+	$\chi^2/d.o.f$
f_+	0.9553(33)	16.6(2.8)	-13.0(0.2)	0.34(4)	0.36

Table C.7: uncorrelated SU(2) ChPT fit in various PBCs without the $f_+(0) = f_0(0)$

Appendix D

SU(2) ChPT for pion form factor

The pion electromagnetic form factor of NLO SU(2) ChPT given by

$$f_{\pi\pi}^{\mathrm{SU}(2)}(q^2) = 1 + \frac{2}{f^2}\left[2l_6^r q^2 + 4\tilde{\mathcal{H}}(m_\pi^2, q^2, \mu^2)\right], \tag{D.0.1}$$

$$\left\langle r_\pi^2 \right\rangle = \frac{-24l_6^r}{f^2} - \frac{1}{4\pi^2 f^2}\left(\log\left(\frac{m_\pi^2}{\mu^2}\right) + 1\right), \tag{D.0.2}$$

$$\tag{D.0.3}$$

where,

$$\tilde{\mathcal{H}}(m_\pi^2, q^2, \mu^2) = \frac{m^2 H(x)}{32\pi^2} - \frac{q^2}{192\pi^2}\log\frac{m^2}{\mu^2}, \tag{D.0.4}$$

$$H(x) = -\frac{4}{3} + \frac{5}{18}x - \frac{x-4}{6}\sqrt{\frac{x-4}{x}}\log\left(\frac{\sqrt{\frac{x-4}{x}}+1}{\sqrt{\frac{x-4}{x}}-1}\right)(x = -\frac{q^2}{m^2}). \tag{D.0.5}$$

The pion electromagnetic form factor of NNLO SU(2) ChPT given by

$$\begin{aligned} f_{\pi\pi}^{\mathrm{SU}(2),\mathrm{NNLO}}(Q^2) = 1 &+ 2x_2\left[\frac{s-4}{6}\bar{J}(s) + s\left(-l_6^r - \frac{L}{6} - \frac{1}{18N}\right)\right] \\ &+ 4x_2^2(P_V^{(2)} + U_V^{(2)}) + O(x_2^3), \end{aligned} \tag{D.0.6}$$

where

$$x_2 = \frac{M_\pi^2}{f_\pi^2}, f_\pi = f\left[1 + 2\frac{M_\pi^2}{f^2}(l_4^r - L)\right], \tag{D.0.7}$$

and

$$
\begin{aligned}
P_V^{(2)} &= s\left[\frac{-k_1}{2}+\frac{k_2}{4}+\frac{-k_4}{12}+\frac{k_6}{2}-l_4^r\left(2l_6^r+\frac{1}{9N}\right)+\frac{23L}{36N}+\frac{5}{576N}+\frac{37}{864N^2}+r_{V1}^r\right] \\
&+ \quad s^2\left[\frac{k_1}{12}+\frac{-k_2}{24}+\frac{k_6}{24}+\frac{1}{9N}\left(l_1^r-\frac{l_2^r}{2}-\frac{l_6^r}{2}-\frac{L}{12}-\frac{1}{384}-\frac{47}{192N}\right)+r_{V2}^r\right] \qquad \text{(D.0.8)} \\
U_V^{(2)} &= \bar{J}\Big[\frac{-(s^2-4s)l_1^r}{3}+\frac{(s^2-4s)l_2^r}{6}+\frac{(s-4)l_4^r}{3}+\frac{-(s^2-4s)l_6^r}{6}+ \\
&- \quad \frac{L}{36}\left(s^2+8s-48\right)+\frac{1}{N}\left(\frac{7s^2}{108}+\frac{-97s}{108}+\frac{3}{4}\right)\Big] \\
&+ \quad \frac{K_1(s)}{9}+\frac{K_1(s)}{9}\left(\frac{s^2}{8}-s+4\right)+\frac{K_3(s)}{6}\left(s-\frac{1}{3}\right)+\frac{-5K_4(s)}{3} \qquad \text{(D.0.9)}
\end{aligned}
$$

The definitions of$\bar{J}, K_1, K_2, K_3, K_4$ is as follows

$$
\begin{bmatrix} \bar{J} \\ K_1 \\ K_2 \\ K_3 \end{bmatrix} = \begin{bmatrix} 0 & 0 & z & -4N \\ 0 & z & 0 & 0 \\ 0 & z^2 & 0 & 8 \\ Nzs^{-1} & 0 & \pi^2(Ns)^{-1} & \pi^2 \end{bmatrix} \begin{bmatrix} h^3 \\ h^2 \\ h \\ -(2N^2)^{-1} \end{bmatrix} \qquad \text{(D.0.10)}
$$

$$
K_4 = \frac{1}{sz}\left(\frac{K_1}{2}+\frac{K_3}{3}+\frac{\bar{J}}{N}+\frac{(\pi^2-6)s}{12N^2}\right) \qquad \text{(D.0.11)}
$$

$$
h = \frac{1}{N\sqrt{z}}\ln\frac{\sqrt{z}-1}{\sqrt{z}+1}, z = 1-4/s, \qquad \text{(D.0.12)}
$$

where,

$$
k_i = (4l_i^r-\gamma_i L)L, \gamma_1 = 1/3, \gamma_2 = 2/3, \gamma_4 = 2, \gamma_6 = -1/3. \qquad \text{(D.0.13)}
$$

Charge radius of pion in NNLO SU(2) ChPT is described

$$
\begin{aligned}
\left\langle r_\pi^2\right\rangle^{\mathrm{SU(2),NNLO}} &= -\frac{2}{f_\pi^2}\left(6l_6^r+\frac{1}{N}+L\right) \\
&+ \quad \frac{4m_\pi^2}{f_\pi^2}\Big[-3k_1+\frac{3k_2}{2}+\frac{-k_4}{2}+3k_6-12l_4^r l_6^r \\
&+ \quad \frac{1}{N}\left(-2l_4^r+\frac{31L}{6}+\frac{13}{192}-\frac{181}{48N}\right)+6r_{V1}^r\Big]. \qquad \text{(D.0.14)}
\end{aligned}
$$

In this work, it is too many parameters to fit stably by the NNLO SU(2) ChPT form, and therefore the NNLO SU(2) ChPT analysis is not done.